Instituto Universitário de Lisboa

Department of Information Science and Technology

AGV-RAD: AGV Positioning System for Ports using Microwave Doppler Radar

Lin Ma

A Dissertation presented in partial fulfillment of the Requirements for the Degree of

Master in Telecommunications and Computer Engineering

Supervisor:

Dr. Octavian Adrian Postolache, Associate Professor

ISCTE-IUL

Co-supervisor

Dr. Yongsheng Yang, Full Professor

Shanghai Maritime University

September 2019

Resumo

Automação e inteligência artifical tornaram-se uma tendência inevitável no desenvolvimento dos terminais dos contentores. O posicionamento do VAG (Veículo Autónomo Guiado) é um dos problemas principais para construir as portas automatizadas. Embora a tecnologia RFID de frequência ultra-alta (UHF) existente tenha uma boa precisão e estabilidade de medição no posicionamento VAG dos portos, as etiquetas magnéticas expostas são fáceis de danificar sob a comum carga pesada e o seu habitual custo de construção e manutenção é insuportável para a maioria das portos.

Entre as tecnologias para o posicionamento VAG, o radar Doppler de microondas possui uma forte capacidade de penetração e pode funcionar bem em ambientes complexos (dia, noite, nevoeiro e chuva). Portanto, o sistema de posicionamento VAG baseado em radar Doppler de microondas atraiu muita atenção.

Nesta tese, foi estabelecido um sistema de teste usando a técnica acima mencionada, juntamente com uma plataforma de computação em tempo real, NI myRIO compatível com Wi-Fi. Vários algoritmos de computação foram envolvidos para extrair os valores precisos de distancia e velocidade. O "denoising" de wavelets com a função de limiar adaptado foi utilizado para filtrar o ruído nos sinais de radar. Na análise do domínio da frequência, o algoritmo conjunto FFT e Chirp-Z Transform (CZT) foi proposto para suprimir a influência dos efeitos de resolução e também melhorar o desempenho em tempo real. Além disso, o algoritmo 2D-FFT é usado para calcular a velocidade do VAG. De acordo com o ambiente dos portos, o algoritmo de posicionamento VAG e o método de comunicação adequado baseados em radares Doppler de microondas e NI myRIO-1900s também serão propostos.

A eficiência do sistema proposto foi testada experimentalmente e vários resultados estão descritos nesta dissertação.

Palavras-chave: Posicionamento VAG; Radar Doppler por Microondas; DSP; Radar FMCW

Abstract

Automation and intelligence have become an inevitable trend in the development of container terminals. The AGV (Automated Guided Vehicle) positioning is a primary problem to build the automated ports. Although the existing Ultra-High Frequency(UHF) RFID technology has good measurement accuracy and stability in the port AGV positioning, the exposed magnetic tags are easy to damage under the common heavy load, and its construction and maintenance cost is unbearable to most ports.

Among the candidate technologies for the AGV positioning, microwave Doppler radar has a strong penetrating ability, and can work well in a complex environment (day and night, foggy, rainy). Therefore, the microwave Doppler radar-based AGV positioning system has attracted a lot of attention.

In this thesis, a test system using the above technique was established, together with a NI myRIO real-time Wi-Fi compatible computation platform. Several computation algorithms were implemented to extract the accurate values of range and velocity. Wavelet denoising with the adapted threshold function was considered to filter noise contained in radar signals. In the frequency domain analysis, FFT and Chirp-Z Transform (CZT) joint algorithm was proposed to suppress the influence of fence effects and also improves real-time performance. In addition, 2D-FFT is used to calculate velocity of AGV. According to the port-like environment, the suitable AGV positioning algorithm and communication method based on microwave Doppler radars and NI myRIO-1900s also be proposed.

The effectiveness of the proposed system was experimentally tested and several results are included in this thesis.

Keywords: AGV Positioning; Microwave Doppler Radar; DSP; FMCW Radar

Acknowledgements

At first, I want to express my greatest gratitude to my supervisor, Professor Octavian Postolache, because of his carefulness and patience, as well as tremendous support during the realization of this project.

I would like to express my sincere gratitude to my Shanghai Maritime University supervisors, Professor Yongsheng Yang and Doctor Haiqing Yao. During ISCTE-IUL, they are very concerned about my study and life, and provide assistance to my difficulties in time.

My thanks also goes to my family, especially to my parents, Zhenhe Ma and Meiying Li, and my brother, Shixin Ma, for their support and hard work.

The thanks to my boyfriend, Peiyao Tang, for his constant encouragement, help and care.

Finally, a huge thanks to my colleges, Yongshuang Wang, Dongchen Ni, Yu Jin， Zeyu Ma, Mariana Jacob Rodrigues, and Joao Monge. During the year of studying in Lisbon, we have finished several works and acquired many experiences. And thanks for their help and kind.

Content

List of Figures

List of Tables

List of Acronyms

ADC	Analog-to-Digital Converter
AGV	Automated Guided Vehicle
CW	Continuous Wave
CZT	Chirp-Z Transform
DFT	Discrete Fourier Transform
DSP	Digital Signal Processing
DWT	Discrete Wavelet Transform
ECG	Electrocardiograph
FFT	Fast Fourier Transform
FMCW	Frequency Modulated Continuous Wave
FPGA	Field Programmable Gate Array
FSK	Frequency Shift Keying
IF	Intermediate Frequency
IoT	Internet of Things
IP	Internet Protocol
RCS	Radar Cross Section
RF	Radio Frequency
RFID	Radio Frequency Identification
SNR	Signal-to-Noise Ratio
TCP	Transmission Control Protocol
TEU	Twenty Feet Equivalent Unit
TTL	Transistor-Transistor Logic
UART	Universal Asynchronous Receiver Transmitter
USB	Universal Serial Bus
VCO	Voltage Controlled Oscillator
Wi-Fi	Wireless Fidelity
WLAN	Wireless Local Area Network

Chapter 1. Introduction

1.1 Motivation

According to statistics, the container throughput of Port of Shanghai has reached about 21.54 million TEU in the first half-year of 2019, which has increased 5.02% year on year [1]. Also in this period, the container throughput in Port of Singapore, Port of Rotterdam [2], Port of Antwerp, Port of Hamburg and Port of Los Angeles amounted to 18.03 million TEU, 7.53 million TEU, 5.84 million TEU, 4.66 million TEU, and 4.51 million TEU respectively, which growth rate is 0.06%, 6.36%, 4.85%, 7.62%, and 4.64%. Therefore, the transportation efficiency of the port needs to improve urgently. Otherwise, the backlog of container ships and cargo will have a bad effect on the overall efficiency of the port. AGV is new equipment that occupies an important position in the smart port. It is a fully automatic carrier that transport containers from the quayside to the storage yard. The questions that need to answer regarding AGV operation are: Where am I? Where am I going? How can I get there? Therefore, the most fundamental and critical issue for the AGV system is ‘where am I?’, that is translated to the positioning problem.

At present, Ultra-High Frequency (UHF) RFID (Radio Frequency Identification) technology is the most applied solution for AGV positioning. However, the time response of RFID identification capability is not very short. In addition, it is necessary to lay magnetic tags in the yard in advance, the exposed magnetic tags are easily damaged, so the labor and maintenance costs are extremely high.

To solve and optimize the AGV positioning, the MSc research work proposed a new positioning method that can be applied as a complementary positioning solution for AGV that work in ports.

This project aims to use microwave Doppler radar sensors to achieve AGV positioning system which can detect range and velocity of AGV at the same time. In order to ensure small size and easy installation of the designed system, NI myRIO-1900 which has built-in Wi-Fi (Wireless Fidelity) is used as embedded equipment. LabVIEW software is the main platform using for Digital Signal Processing (DSP). In addition, the positioning interface can display real-time AGV location and path information for the administrator of the port to facilitate scheduling and decision making in time.

1.2 Objectives

This MSc thesis presents a developed hardware and software platform for AGV positioning system based on microwave Doppler radar sensors.

Develop DSP components associated with microwave radar intermediary frequency signals to extract useful information related to the target.

Develop measurement algorithms to extract accurate range and velocity information of AGV. Develop data fusion method, positioning algorithm.

A graphical user interface that presents the AGV location and path information that can be accessed by the administrator of the port in real-time.

1.3 Structure of the Dissertation

Chapter 2 – includes the state of art for remote positioning systems (RFID, LIDAR, microwave Doppler radar and ultrasonic radar). Also the literature review on AGV, FMCW (Frequency Modulated Continuous Wave) radar, and signal processing.

Chapter 3 – presents the reason for the selection of each device and software, then describes the AGV positioning system based on microwave Doppler radar.

Chapter 4 – presents a reasonable processing method for the noise contained in the radar signal, and gives the simulation results to verify its feasibility.

Chapter 5 – is the range and velocity measurement based on the principle of radar beat signal.

Chapter 6 – is the algorithm of AGV positioning method. It mainly includes AGV positioning algorithm, data fusion, error processing. In addition, the experimental results under the simulated port environment are contained in this chapter.

The last chapter is the conclusion, discussions, summarizes and future work of the full text.

Chapter 2. State of the art

2.1 Automated Guided Vehicle (AGV)

As advanced automatic handling equipment, AGV is an equipment that is the key to smart ports providing a high level of automation and unified scheduling. In the last decade, the AGV has been gradually applied to the automatic handling of containers in large international ports.

2.1.1. Container Terminal AGV Transport System

Container terminal refers to a clear boundary area that can accommodate a complete container handling operation process. It is a buffering place for containers when it is converted and transported. Therefore, the container terminal plays an important role in the whole container transportation process.

As mentioned above, with the rapid increase in container throughput, the emergence of automated handling equipment has become inevitable. The AGV is a new device for horizontal transportation in smart ports and takes on the task of moving goods from the quayside to the storage yard in the port operation. AGV is small in size, lightweight and has a large carrying capacity, it is capable of handling containers of two standard sizes: twenty-footer (one TEU) or forty-footer (two TEUs). An AGV may carry a box of one TEU or two TEUs, or carry 2 boxes of one TEU each.

When a ship arrives at the container terminal for transshipment, containers are first discharged from the ship onto the AGV by quay cranes. The AGV then transports the containers to specific storage locations in the yard area, at last, the container is dismounted from the AGV by yard cranes, the floor plan of the port as shown in Figure 2.1 [3].

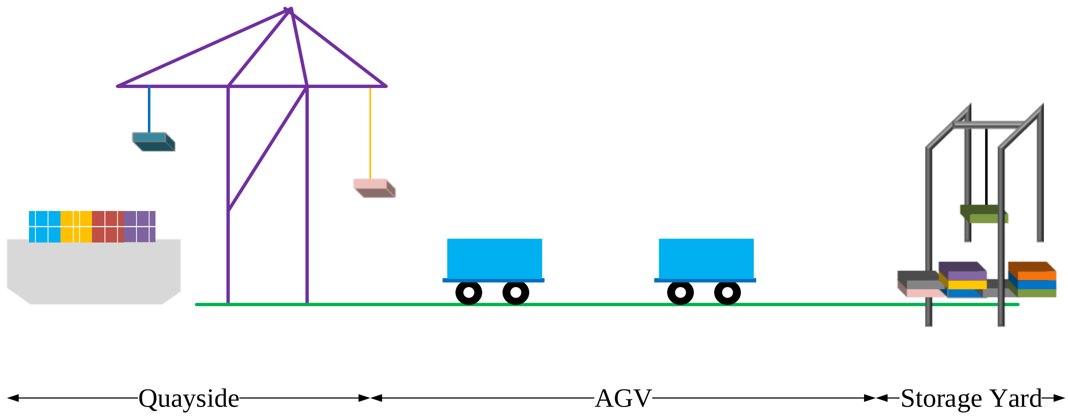

Figure 2.1 - Work Area of AGV in the Port

2.1.2. AGV characteristics

The AGV dimension made by Gottwald from Germany is 14.8m*3.0m*1.9m, and the maximum velocity is 1.67km/h or 2.22km/h. And the AGV dimension of Shanghai Zhenhua Heavy Industries Company Limited is 15m*3.1m*2m, the maximum velocity is 1.67km/h, as shown in Figure 2.2.

Figure 2.2 - AGV (Left: from Gottwald; Right: from Shanghai Zhenhua Heavy Industries Company)

2.2 Microwave Doppler Radar

The basic application of microwave Doppler radar can be traced back to the 1930s, especially during the Second World War, the microwave Doppler radars were widely developed and applied for military defense, target detection, and so on.

The modern applications of radar are highly diverse, including vital sign induction [4], air and ground traffic control [5-7], radar astronomy, air defense system, anti-missile system, marine radars for locating landmark and collision avoidance system, marine surveillance system, meteorological precipitation monitoring, altimetry and flight control system [8], missile target location system and ground-penetrating radars for geological observation.

2.2.1. The Advantages of Microwave Doppler Radar

There have three common solutions that can be considered for AGV positioning in this case: ultrasonic sensor, laser sensor, and microwave radar sensor, these sensors have different characteristics, as shown in Table 2.1.

(1) Ultrasonic sensor: The propagation speed of ultrasonic is obviously affected by temperature. Measurement errors will generate when the ultrasonic instrument is applied in complex and variable fields. In addition, ultrasonic energy decays quadratically with distance, this characteristic leads to bad long-ranging ability [9].

(2) Laser sensor: The laser sensor-based solution is very sensitive to light intensity and air quality in the environment [10].

(3) UHF RFID: The exposed magnetic tags are easy to damage under the common heavy load, and its construction and maintenance costs are unbearable to most ports.

(4) Microwave Doppler radar sensor：Compared to either infrared or visible light, the microwave has greater penetration capability, which has a unique advantage to many civilian and military applications [11].

Table 2.1 - Contradistinction of Microwave Sensor, Laser Sensor, Ultrasonic Sensor and HF RFID

	Microwave Sensor	**Laser sensor**	**Ultrasonic sensor**	**UHF RFID**
Darkness Penetration Ability	Strong	Strong	Weak	Strong
Weather Effect	Small	Large	Small	Small
Temperature Effect	Small	Small	Large	Small
False Alarm Probability	Small	Large	Large	Small
Resolution Capability	Strong	Weak	Weak	Weak
Hardware Cost	Medium	Medium	Low	High
Technical Requirement	High	Medium	Low	Low

Therefore, the microwave Doppler radar sensor has characteristics of strong anti-interference ability, small volume, high resolution, low power consumption, strong ability to penetrate smoke, fog, and dust. It can measure the range and velocity of the target at the same time. Based on its advantages, using microwave Doppler radar to achieve AGV positioning is a novel idea.

2.2.2. Radar frequency band and microwave penetration

The type of radar is divided by the radar band and wavelength. An important indicator in radar transmitters is the radar wavelength. The standard letter designations for radar-frequency bands as Table 2.2, according to IEEE Standard 521-2002,

Table 2.2 - Standard Letter Designations for Radar-Frequency Bands

Band Name	Frequency Range	Wavelength Range	Note
HF	3–30 MHz	10–100 m	Over-the-horizon radar (OTH) radars; 'High Frequency'
VHF	30–300 MHz	1–10 m	Very long range; 'very high frequency'
P	< 300 MHz	> 1 m	Essentially HF + VHF
UHF	300–1000 MHz	0.3–1 m	Very long range (e.g. ballistic missile early warning); 'Ultra High Frequency'
L	1–2 GHz	15–30 cm	Long range (e.g. air traffic control and surveillance); 'L' for 'long'
S	2–4 GHz	7.5–15 cm	Marine radar; 'S' for 'short'
C	4–8 GHz	3.75–7.5 cm	Satellite transponders; a compromise (hence 'C') between X and S bands;
X	8–12 GHz	2.5–3.75 cm	Missile guidance; Named X band because the frequency was a secret during WW2.
K_u	12–18 GHz	1.67–2.5 cm	High-resolution, also used for satellite transponders, frequency under K band (hence 'u')
K	18–24 GHz	1.11–1.67 cm	From German kurz, meaning 'short'; Detecting clouds by meteorologists;
K_a	24–40 GHz	0.75–1.11 cm	Mapping, short range, airport surveillance; frequency just above K band (hence 'a')
mm	40–300 GHz	1.0–7.5 mm	The frequency ranges depend on waveguide size.
V	40–75 GHz	4.0–7.5 mm	Very strongly absorbed by atmospheric oxygen, which resonates at 60 GHz.
W	75–110 GHz	2.7–4.0 mm	Used as a visual sensor for experimental autonomous vehicles.

The frequency is between 300MHz and 3000GHz, and the wavelength is between 0.1mm-1m (excluding 1m) is divided into microwaves. Microwaves, like ordinary electromagnetic waves, usually exhibit three characteristics: penetration, reflection, and absorption. As shown in Table 2.3, microwave energy can penetrate more and more materials, so that the radar can be covered under the cover of a certain material to avoid damage to the radar in the exposed environment. This advantage makes the radar popular.

Table 2.3 - Microwave Penetration of Material

metal	Not at all, full reflection
Water	Almost not at all, full absorption
Chemical foams	Very well, very little attenuation
Clothing	Dry- well Wet-losses up to 20dB
Rain	Well-but up to 6dB attenuation
Plastic	Very well – 0.5 to 3 dB loss with optimized thickness and correct spacing
Human being	Not really, but fraction, absorption and reflection
Wood	Dry- good Wet – losses up to 10 dB
Ice	Up to 10dB attenuation

2.2.3. Radar Architecture

Figure 2.3 shows the Radio Frequency (RF) front end of microwave Doppler receiver [12].

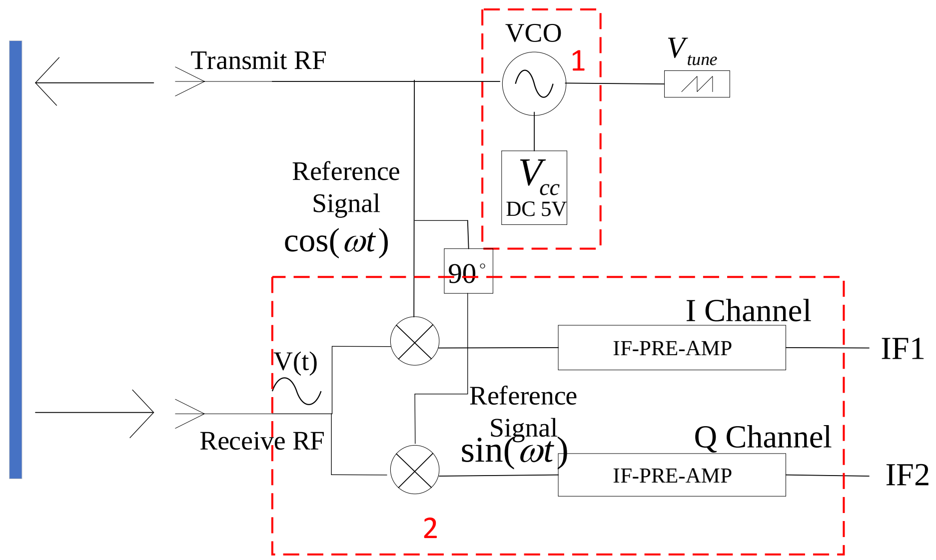

Fig. 2.3 - Radar Front End Block Diagram

Microwave Doppler radar transmits signal by using the transmitting antenna, the receiving antenna receives reflected signal after signal meets obstacles. The Voltage Controlled Oscillator (VCO) receives modulated signal and outputs signals through the transmitted antenna. After directional coupling, most of the signals are transmitted through the transmitted antenna, another small part is divided into two parts and output to the mixer as the local oscillator signal. The signal of the Q channel needs to be phase-shifted by 90°before mixing. The obtained mixed signal is subjected to filtering and amplifying processing, and finally, two Intermediate Frequency (IF) signals of IF1 and IF2 are obtained. The distance can be calculated according to the IF signal, those are, the beat signals.

Microwave radar signals are usually a function of frequency modulation [13]. The received waveform $r(t)$ of a single target has the following form,

$$r(t) = A(t)sin[\Omega t + \theta(t)] \tag{2-1}$$

There, the amplitude $A(t)$ only represents the envelope of Pulse. The main function of the receiver processing is to transform the part of the radar signal which carried the information to the baseband, at the same time measure phase $\theta(t)$. Fig. 2.4 shows a conventional method for the classic radar receiver design.

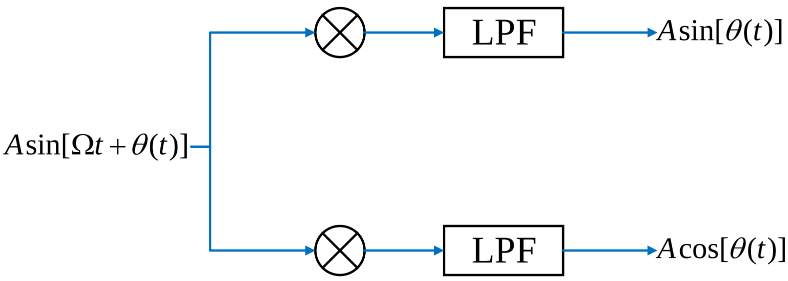

Figure 2.4 - Receiver Model

In Figure 2.4, the following branch is called the co-channel or I channel of the receiver, in which the received signal and an oscillator signal are mixed. The oscillator frequency is the same as the radar frequency. This mixing produces sum and difference components,

$$\begin{aligned} &2\,sin(\Omega t)\,A(t)\,sin[\Omega t + \theta(t)] \\ &\quad = A(t)\,cos[\theta(t)] + A(t)cos[2\Omega t + \theta(t)] \end{aligned} \tag{2-2}$$

The sum frequency component is filtered by the low pass filter, leaving only the modulation component $A(t)cos[\theta(t)]$. In the Q channel, the received signal is also mixed with the local oscillator signal, but the local oscillator signal before mixing is phase shifted by 90°. The mixing output of the Q channel is,

$$\begin{aligned} &2\,cos(\Omega t)\,A(t)\,sin[\Omega t + \theta(t)] \\ &\quad = A(t)\,sin[\theta(t)] + A(t)sin[2\Omega t + \theta(t)] \end{aligned} \tag{2-3}$$

Similarly, only the modulation component $A(t)sin[\theta(t)]$ is left, which is the beat signal.

2.2.4. Antenna System

One of the important components of a microwave Doppler radar system is the antenna, which determines the sensitivity and range resolution of the radar. Gain, beamwidth and side-lobe levels are the most important features of the antenna [14].

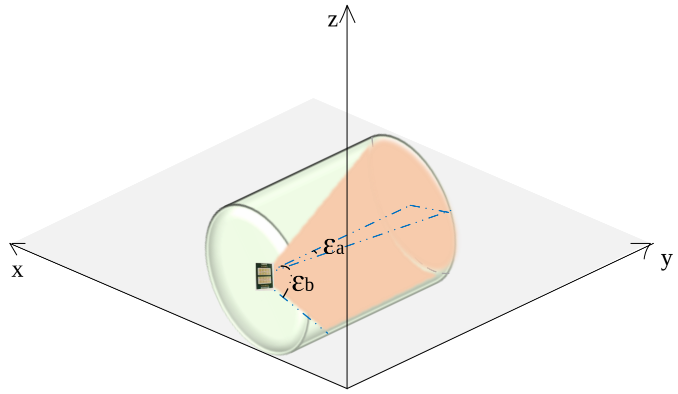

Figure 2.5 - Detection Range of Microwave Doppler Radar

The characteristic of the antenna system determines the detection range of the microwave Doppler radar. As shown in Figure 2.5, ε_a represents the full beamwidth of the antenna azimuth, ε_b represents the full beamwidth of the antenna elevation. The shaded portion represents the approximate detection range of the radar. Different types of radar will have different parameters of ε_a and ε_b.

2.3 Physical Basics- Radar Equation

The radar equation is used to analyze the composition of the beat signal and provides the theoretical basis for the following chapter simulation.

2.3.1. Reflection

One of the characteristics of microwaves is that the wavelength is shorter (that is, 12 mm or 4.7 inches at 24 GHz), which is similar to light and has effects such as scattering, diffraction, reflection, divergence, and interference. Therefore, the microwave Doppler radar emits electromagnetic waves in a scattered manner, and at least a part of its energy is reflected to the point of emission.

The "radar equation" represents the strength of the radar received signal after being reflected by the object. Its mathematical description is as follows,

$$\frac{P_E}{P_S} = \frac{g^2 \cdot \lambda^2 \cdot \sigma}{(4\pi)^2 \cdot D^4} \tag{2.2}$$

There, P_E is the received signal power, P_S is the transmitted power, λ is the wavelength of transmitted signal (12mm at 24GHz), D is the range between microwave Doppler radar sensor and the object.

From the above equation, it can be seen easily that the received signal power has the following phenomenon,

(1) Reverse proportional to the 4.power of the range;

(2) Directly proportional to the Radar Cross Section (RCS) of an object.

2.3.2. Radar Cross Section

Under radar wave radiation, the physical quantity of the target echo intensity is represented by RCS. It is the imaginary area of the target, represented by the projected area of the equivalent reflector which each direction is uniform. The equivalent reflector has the same echo power at the unit stereo angle of received direction with a defined target. In fact, the RCS of the same target is different because the different viewing angles of the target have different radar reflection frequencies.

The approximate RCS of an object at the frequency of 24GHz for [15],

Table 2.4 - Approximate RCS for an Object

An Object	**RCS**
A Human Being	Abt. 0.5 m^2
A Coke Can	0.5 m^2
An Automobile Depending on Angle of Arrival	1-5 m^2
A Metal Sheet of 1 m^2	A few 100 m^2

In summary, a target with bigger RCS is a more good radar target.

2.4 Frequency Modulation

The radar can be divided into two types: Continuous Wave (CW) radar and pulse radar, according to the electromagnetic energy radiation characteristics. The principle of ranging of pulse radar is to obtain the distance information of the target based on the time difference between the transmitted and received pulse signals. The CW radar is a radar system that obtains target information based on transmitted and received CW signals. According to the different forms of radar transmission, CW radar can be divided into non-FMCW wave radar and FMCW radar. The former can measure the velocity of targets within a certain range, but can't obtain the range information. FMCW radar can get both range and velocity information at the same time.

2.4.1. Pulse Radar

The pulse radar is a solution that measures only the range of the target. The waveform generator generates a short-time pulse to modulate the radar waveform. The delay is measured by the time difference of transmitting pulse and receiving pulse, as shown in Fig. 2.6.

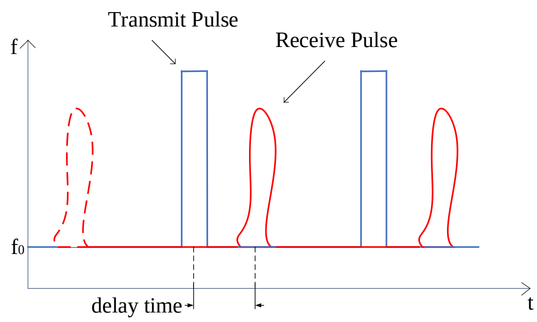

Figure 2.6 - Principle of Pulse Radar

However, since the pulse frequency modulation method can only measure the range of targets, the velocity can only be roughly calculated from the ds/dt. Therefore in the expectation of obtaining accurate range and velocity information, other solutions need to be considered.

2.4.2. Continuous Wave Doppler Radar

The principle of CW radar is based on the Doppler effect. The difference frequency can be extracted, which is the Doppler frequency [16]. In simple terms, the Doppler effect is the change in the frequency or wavelength of a wave as it moves relative to the wave source. The most common example of the Doppler effect is when the whistling train passes by a standing observer, the tones that the observer hears are different during the process of approaching and moving away from the train. Compared to the transmitted frequency of the wave source, the received frequency is higher during the approach, and lower during the recession. That’s because as the source of the wave moves toward the static target, each successive peak is transmitted from a position closer to the observer than the peak of the previous wave. Therefore, compared with the previous wave, it costs less time for each wave reaches to the target, and this phenomenon will increase the frequency received. Conversely, if the wave source is far from the static target, each wave is emitted from a position farther away from the target than the previous wave, so the arrival time between successive waves increases, thereby reducing the frequency.

As shown in Figure 2.7, when the AGV is far from the radar, the frequency observed by the AGV becomes larger than the actual radar's transmission frequency; when the AGV is close to the radar, the frequency observed by the AGV becomes relatively smaller.

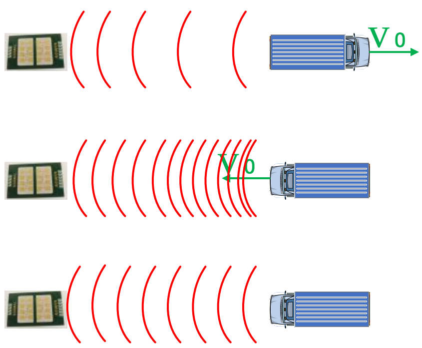

Figure 2.7- Doppler Effect diagram

The frequency relationship between the observer and the source is given by the following relation,

$$f' = \left(\frac{v \pm v_0}{v \mp v_s}\right) f \tag{2.3}$$

It means, f' is the observed frequency, f is the original transmission frequency from the medium. v is the original transmission velocity of the wave in the medium, v_0 is the moving speed of the observer relative to the medium. If it is close to the emission source, the front operation symbol is +, otherwise, it is -. v_s is the source relative to the medium. If the emission source is close to the observer, the front operation symbol is -, otherwise it is +.

In the case where the radar stationary relative to the AGV, the derived process of velocity is shown as follows:

Suppose the target is away from the radar which the initial distance is R_0 at a radial velocity v_0 ($v_0 > 0$), then,

$$\mathrm{R} = R_0 + v_0 t \tag{2.4}$$

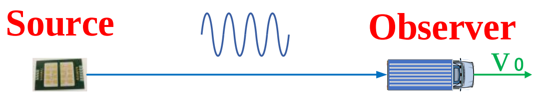

Figure 2.8 - The Radar Transmits Waves and Meets Target

When the radar transmits electromagnetic waves to the target, as shown in Fig. 2.8, the radar is the source of the microwaves, therefore the target is the observer.

$$f_1 = \frac{c - v_0}{c} f \tag{2.5}$$

Here, c is the speed of light, f_1 is the frequency observed by the target, and f is the transmission frequency of the radar.

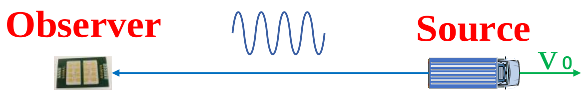

Figure 2.9 - The Microwave back to Radar form Target

When electromagnetic waves are reflected from the target to the radar, like Fig. 2.9, then,

$$f_2 = \frac{c}{c + v_0} f_1 \tag{2.6}$$

Combined with formula (2.5), then,

$$f_2 = f - \frac{2v_0 \cdot f}{c + v_0} \tag{2.7}$$

Because of $v_0 \ll c$, the formula (2.7) can be simplified to,

$$f_2 = f - \frac{2v_0 \cdot f}{c} \tag{2.8}$$

So the resulting Doppler shift $f_{doppler}$ can be expressed as,

$$f_{doppler} = -\frac{2 \cdot v_0}{c} \cdot f \tag{2.9}$$

Therefore, the CW radar can only detect the radial velocity of the target based on the detected Doppler shift, which is not suitable for use in the positioning system.

2.4.3. Frequency Modulated Continuous Wave Radar

FMCW radar is mainly used for ranging and velocity measurement, such as radar altimeter, car collision avoidance and so on. The FMCW radar, which modulates the transmission frequency to obtain the target range and velocity information, has a development history almost as long as the history of the radar itself.

Since the 1980s, the research work of radar systems has received extensive attention. Due to the continuous improvement of related technology and theory, radar has been rapidly developed, and its application fields have been extended to military and civilian such as missile guidance, object imaging, and meteorological observation. L.P.Lighthart et al. [17] analyzed the theory of linear radar. At the same time, RB Chadwick et al. [18] researched problems such as distance crosstalk caused by the coupling of side-lobe, velocity, and distance in linear radar. P.Jones and S.Osterrieder et al. [19] used linear radar to explore the display problem of dynamic targets; W.Knapp and L.P.Lighthart [20] performed suppression research of near-field clutter.

The working principle of the FMCW system radar is to modulate and transmit the carrier frequency signal. Then the beat signal contained with range and velocity information is received through by RF end. Frequency analysis is used for the beat signal can calculate range and velocity values. Frequency modulation commonly has triangle wave modulation, sawtooth wave modulation, and sine wave modulation. The purpose of frequency modulation is change range and velocity information of target to frequency or phase shift, which is more convenient to process.

At present, FMCW radar has been widely used in various fields, such as industrial measurement, military navigation, and security system. Compared with traditional radar systems, the advantages of FMCW radar are mainly shown as follows,

(1) The sensitivity of the FMCW radar receiver is much higher than the traditional radar with the same bandwidth. Therefore, FMCW radar has a higher range resolution and better anti-interference ability in engineering applications.

(2) The bandwidth of the beat signal (the unit is generally KHz) is much smaller than the bandwidth of the transmitted signal (the unit is generally GHz). The radar is receiving signal while transmitting signal, therefore, there is no blind area of FMCW radar.

(3) The beat signal of FMCW radar is mainly processed by FFT which is relatively easy and simple.

(4) The operating current of the FMCW radar system is relatively small, the whole system is small in size, light in weight and simple in structure.

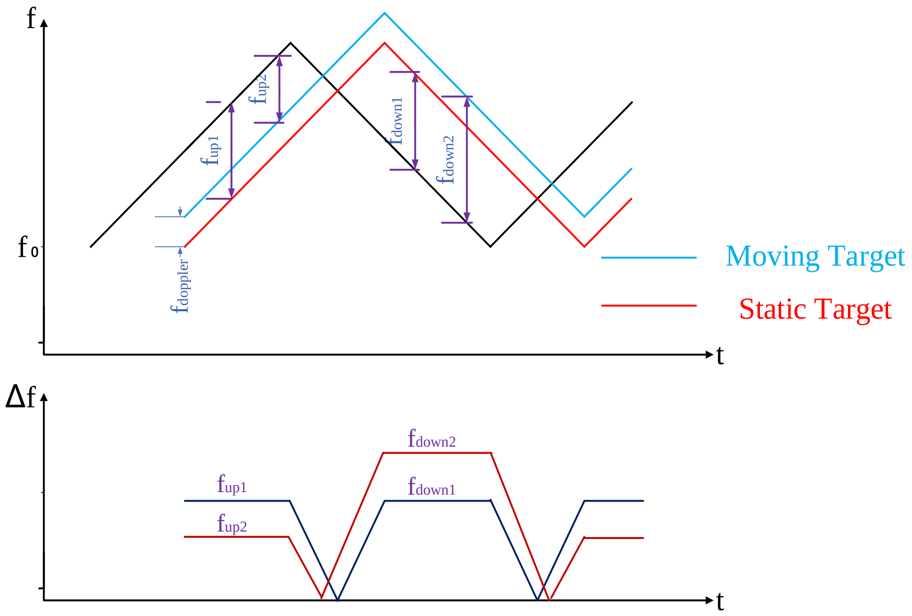

Figure 2.10 - Principle of Triangle Wave Modulation of FMCW Radar

The principle of triangle wave modulation is as Fig. 2.10. For a static target, the source of the beat signal is only based on the time delay between the transmitted signal and the received signal, so the frequency of the difference signal generated in the rising edge and in the falling edge of the triangular wave are equal. For moving targets, the Doppler Effect also produces a frequency shift in the received signal, therefore,

$$f_{up2} = f_{up1} - f_{doppler} \tag{2.10}$$

$$f_{down2} = f_{down1} + f_{doppler} \tag{2.11}$$

In practical applications, it is very difficult to accurately distinguish f_{down} and f_{up}. Although the transmitted signal can be modulated by triangle wave together with CW, the extremely high requirements for the hardware would cause the price very high [21].

Another solution is using the sawtooth wave to modulate the transmitted signal. The principle of sawtooth wave modulation of FMCW radar as shown in Fig. 2.11.

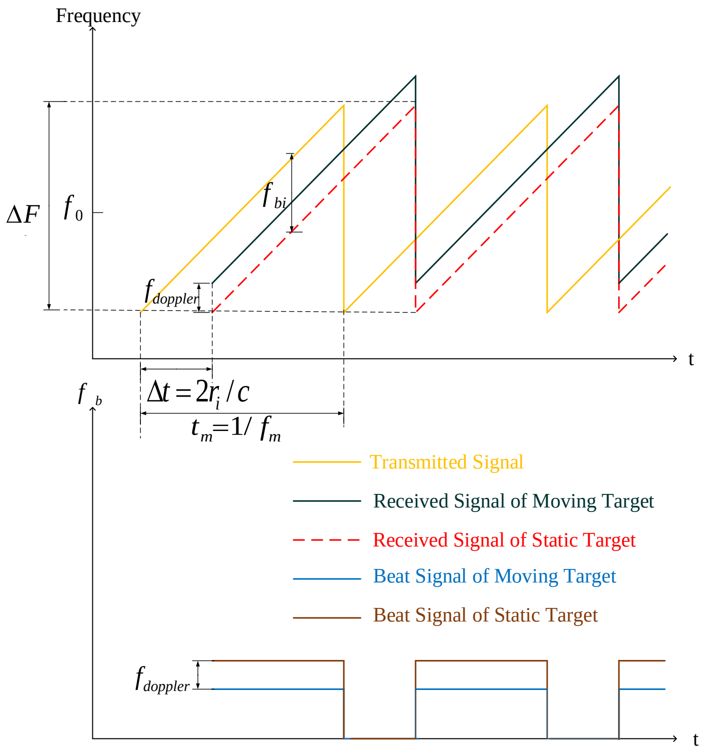

Figure 2.11- Principle of Sawtooth Wave Modulation of FMCW Radar

Assume a static configuration between radar and the object, in other words, there are static radar and static target. The period of the sawtooth wave is $t_m = 1/f_m$. The bandwidth ΔF depends on the voltage of the modulated signal and centers on transmitted frequency f_0. In this case, radar sends a bunch modulated wave to target i, and accept echo from i.

Range r_i can be expressed as time delay Δt between the transmitted signal and the received signal, that is,

$$\Delta t = 2r_i/c \tag{2-12}$$

Under the situation of static radar and moving targets, the Intermediate Frequency (IF) is different from the static configuration because of the Doppler shift. The Doppler shift can be calculated from the phase contained in the signal. Detailed calculation process in Chapter 5.

2.5 Wavelet Denoising

In general, the range and velocity information of the target is extracted by measure the frequency of the IF signal. The IF signal is inevitably affected by various noises during the propagation process, which will cause interference and affect the accuracy of the ranging result, to the IF signal [22]. Hence it is necessary to analyze and filter noise contained in the IF signal. In practical applications, the signal spectrum and noise spectrum of the IF signal are arbitrarily overlapping, however, the traditional filtering method cannot achieve the ideal denoising effect [23].

Wavelet denoising has good characteristics of time domain, frequency domain localization and multi-resolution analysis, which is suitable for the dynamic, non-stationary and abrupt signal. Wavelet denoising has wide applications such as image processing [24-25] and ECG signal [26-27].

Donoho et al. [28] discussed and found a method to remove white noise by using wavelet in 1900. The wavelet transform uses a function with fast decay and oscillation - mother wavelet. Stretching and translating the mother wavelet to get wavelet basis functions. The basic idea of the wavelet transform is to use wavelet basis functions to represent or approximate a function or signal. Wavelet transform is suitable for analyzing the abrupt signal and non-stationary signal. In addition, the wavelet transform has the characteristics of multi-resolution analysis and a bandpass filter and can be implemented by a fast algorithm, so it is often used for filtering and denoising.

There's a lot of related work related to using wavelet transform for denoising. SR Messer [29] proved that wavelet denoising can be used to remove white noise in heart sounds. Giaouris, D. et al. [30] used the wavelet transform to distinguish noise in the actual current signal and modulate motor speed. Yi Hu et.al [31] proposed the use of low-variance spectral estimators based on wavelet thresholding the multiple spectra for speech enhancement to suppress "musical noise". Debin et al. [32] identified weak characteristic signals in the gearbox vibration signals by using a local adaptive algorithm based on wavelet. Madhur Srivastava et al. [33] proposed a new threshold formula to denoise 1-D experimental signals, which can increase the SNR by more than 32dB without distorting the signal. CUI Hua et al. [34] posed a new threshold function, simulation experimental results indicated that the new method gave better SNR gains than hard and soft thresholding methods.

Chapter 3. System Description

3.1 Hardware Platform

The used microwaves Doppler radars are expressed as microwave FMCW Doppler radar sensor IVS-162 and microwave Doppler radar Nano SP25. The radars are mounted in order to detect AGV position and AGV velocity where AGV materialize the target.

Then based on the range and velocity of the target (AGV), designing a suitable positioning method, it is a complete technical chain. The function of IVS-162 is used for parameter adjustment, technical preparation, and experimental support. The SP25 can provide range and velocity information directly in the form of a message, which is easy to be used to validate the hardware system based on IVS-162.

3.1.1. Microwave Radar Sensor IVS-162

The IVS-162, as shown in Fig. 3.1, is the 24GHz K-Band VCO radar transceiver from Innosent. Because of the structure of the planar microstrip antenna, the IVS-162 microwave radar sensor is very compact and energy-saving during operation.

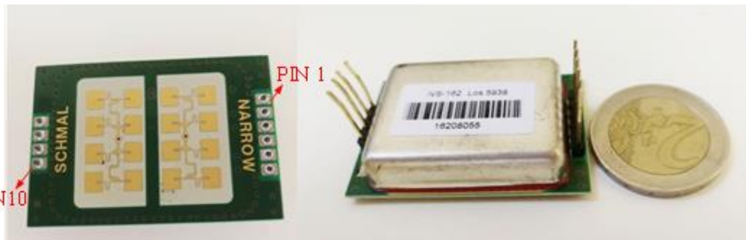

Figure 3.1- Microwave Radar Sensor IVS-162

The functions of the IVS-162 are diverse, including the measurement movement, velocity, presence, and distance of targets. The IVS-162 radar sensor is especially suitable for target information detection, and its antenna angle and beam coverage are wide. Therefore, its application field mainly involves automatic control, electronic security, and many other fields.

The IVS-162 is very easy to integrate with the user's back-end design, with good compatibility. The specific characteristics are as follows:

(1) VCO-Transceiver centered @24GHz

(2) FMCW/CW/FSK capable; therefore measurement of distance as well as recognition of stationary objects possible (depending on modulation)

(3) Split transmit and receive path for maximum gain

(4) Stereo (dual channel) operation for direction of motion indirection

(5) IF-pre-amplifier, bandwidth limited for lowest noise performance

Fig. 3.2 shows the antenna orientation and the relationship between output and angle of the IVS-162. The actual antenna system pattern of IVS-162 as shown in Table 3.1.

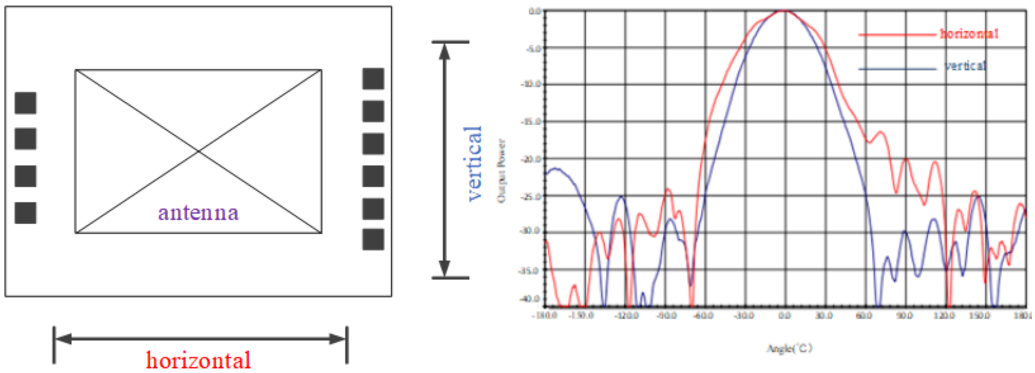

Figure 3.2 - Antenna Direction and Output Power of IVS-162

Table 3.1- Antenna System Pattern

Parameter	Symbol	TYP	Units
Full beam width @-3dB	horizontal	45	°
	vertical	38	°
Side-lobe suppression	horizontal	15	dB
	vertical	20	dB

The data sheet of IVS-162 as shown in Table 3.2, each pin in Fig. 3.1 is connected according to the data sheet.

Table 3.2 - Data Sheet of IVS-162

PARAMETER	CONDITIONS	SYMBOL	MIN	TYP	MAX	UNITS
Transmitter						
Transmit frequencies	Depending on V_{tune}	f		24.000-24.250		GHz
Freq @V_{tune} 5.0V	@25℃	$f_{5.0V}$	24.100	24.125	24.150	GHz
Varactor tuning voltage		V_{tune}	0.5		10	V
Modulation input					150	kHz
Power supply						
supply voltage		V_{cc}	4.75	5.00	5.25	V
supply current	IF-amp included	I_{cc}		35	50	mA
Environment						
operating temperature		T_{op}	-20		+60	℃
Mechanical Outlines						
outline dimensions	compare drawing	height length width		8.3 (19) 44.0 30.0		mm

And the function of each pin is described in Table 3.3,

Table 3.3- PINs of IVS-162

PIN	NAME	Input/ Output	INSTRUCTIONS
1	V_{tune}	Input	Varactor tuning voltage (0.5-10V)
2	enable	Input	Active low
3	V_{cc}	Input	Supply voltage (+5V)
4	GND	Input	Analog ground
5	IF1	Output	Signal I
6	IF2	Output	Signal Q
7	GND	Input	Analog ground
8	GND	Input	Analog ground

3.1.2. Microwave Radar System Nano SP25

The microwave radar system SP25, shown in Fig. 3.3, is a K-Band radar operating in the 24GHz-ISM band as same as the IVS-162, and it can also accurately detect the distance and speed of target at the same time. However, it was chosen because its horizontal detection angle met the positioning needs, as shown in Table 3.4.

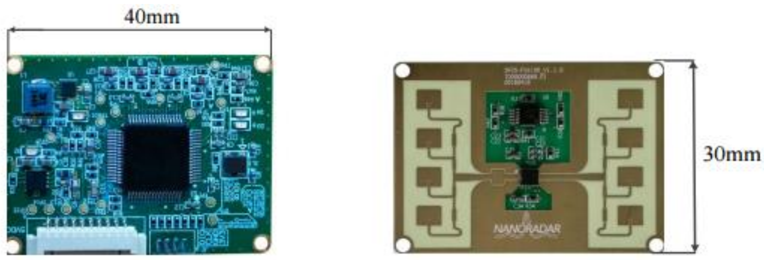

Figure 3.3 - SP25

Because its full beamwidth of antenna azimuth is wider, SP25 can be applied for electronic security, AGV automatic collision avoidance system and so on. Similar to the principle of electronic security, that is, be aware of the direction and position of the target in time, the sp25 is suitable for positioning system for AGV in the port.

Table 3.4 - Radar Parameters of SP25

<table>
<tr><th colspan="3">Range and Velocity Detection</th></tr>
<tr><td colspan="2">Refresh Rate (Hz)</td><td>50</td></tr>
<tr><td colspan="2">Range (m)</td><td>30</td></tr>
<tr><td colspan="2">Distance Accuracy (m)</td><td>0.1</td></tr>
<tr><td colspan="2">Speed Range (m/s)</td><td>±70</td></tr>
<tr><td colspan="2">Speed Accuracy (m/s)</td><td>1.2</td></tr>
<tr><td colspan="2">Range Resolution (m)</td><td>0.75</td></tr>
<tr><td colspan="2">Speed Resolution (m/s)</td><td>2.4</td></tr>
<tr><th colspan="3">Antenna characteristics</th></tr>
<tr><td rowspan="2">Full beam width @-3dB</td><td>Horizontal</td><td>100</td></tr>
<tr><td>Vertical</td><td>38</td></tr>
</table>

The SP25 radar sensor uses a UART-TTL interface, the definition of each PIN is shown in Table 3.5. With a default transfer rate of 115200 baud, with each data message has a start sequence (0xAAAA) and a termination sequence (0x5555), the system status and target output status message of SP25 will be output. If the target is detected, the target number of the target output status message is 1 and the output target status message will be followed by the output target information. The target information message contains parameters such as the distance and speed of the target. In addition, LabVIEW configures the SP25 at the same message format.

Table 3.5- PIN Interface Definition of SP25

PIN	Definition	Range
1	POWER IN	4~6V DC
2	\	\
3	GND	\
4	\	\
5	TTL USART_RX	0~3.3V DC
6	TTL USART_TX	0~3.3V DC
7	\	\
8	\	\
9	\	\
10	\	\

The complete data of UART-TTL communication has 14 bytes, each byte of data is unsigned8-bit, the data range is 0~255 (0~0xFF) and the format as shown in Table 3.6. Each data message contains a message ID to distinguish different types of messages.

Table 3.6 -Target Information

Byte\Bit	7	6	5	4	3	2	1	0
0	Start Sequence (2×Uint8)							
1								
2	Message ID (2×Uint8)							
3								
4	Data Payload (8×Uint8)							
5								
6								
7								
8								
9								
10								
11								
12	End Sequence (2×Uint8)							
13								

The format of the SP25 Target Output Information Message is shown in Table 3.7. The starting sequence (0xAAAA) and the termination sequence (0x5555) have been omitted from the table. When the radar sensor works normally and the target is detected, the System Status Message is the first output, then the Target Output Status Message is outputted. Finally, the Target Output Information Message is outputted.

Table 3.7- The Format of SP25 Target Output Information message

Message ID 0x70C					
Signal Name	Bit	Resolution	Interval	Type	Comment
Index	0..7	1	0…255	u8	Target ID
RCS	8..15	1	0…255	u8	RCS
RangeH	16..23	1m	0…255	u8	Target Distance High 8 Bits
RangeL	24..31	1m	0…255	u8	Target Distance Low 8 Bits
Rsvdl	32..39	-	-	u8	-
VrelH	40..42	1m/s	0..7	u3	Target Velocity High 3 Bits
Rsvsl	43..45	1	1	u3	-
RollCount	46..47	1	-	u2	SP25 is fixed to 0
VrelL	48..55	1m/s	0..255	u3	Target Velocity Low 8 Bits
SNR	56..63	1m/s	0..255	u3	SNR

The value of each field is not the true value of the target information, and the true value of the target information is calculated by the following relationship:

-Indxe	=	IndexValue	//	Target ID, according to Track information
-RCS	=	RcsValue*0.5-50	//	Factory test reserved value, no output
-Range	=	(RangeHValue*256+RangeLValue)*0.01	//	m
-RollCount	=	RollCountValue	//	Count bit
-Verl	=	(VerlHValue*256+VerlValue)*0.05-35	//	Target Speed (m/s)
-SNR	=	Value-127	//	Factory test reserved value, no output

3.1.3. NI myRIO-1900

NI myRIO-1900, as shown in Fig. 3.4, is an embedded system development platform with the functions of real-time processing of the data and Wi-Fi communication capabilities, which is produced by National Instruments (NI). The myRIO-1900 has 34 pins in total, each having different functionality. At the same time, the myRIO-1900 has two ports named port A and port B that can process different tasks respectively. MyRIO-1900 also has four onboard LED’s. At the bottom side of the myRIO-1900, there is a power pin, PC connection point, and USB port. A Xilinx Zynq chip is embedded in NI myRIO-1900, which can use the real-time performance of the dual-core ARM Cortex-A9 and customizable I/O with Xilinx FPGAs. The hardware block diagram of NI myRIO-1900 is shown in Fig. 3.5.

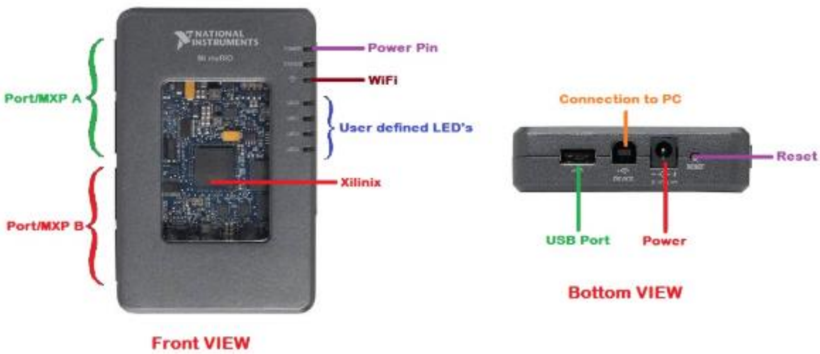

Figure 3.4- NI myRIO-1900 Guide Diagram

One of the advantages of myRIO is that its FPGA supports the development and design of real systems to solve problems faster. Compared to other microcontrollers, with FPGA support, myRIO-1900 avoids the complex syntax used in C and many other languages. Because the using process of myRIO-1900 only creates programming logic, so the complexity can be reduced when designing complex systems. The myRIO-1900 is much faster than a standard microcontroller, so it can be easily used in efficient systems that require fast output response. It also supports different languages such as C, C++, or Graphical Language (FPGA).

For many embedded applications, it is also desirable to view the current operating state of the embedded system or perform parameter and data interaction through the upper computer. NI myRIO-1900 can be connected to the upper computer through Wi-Fi. The upper computer program can be written in the same LabVIEW project, and the data can be interacted in the upper computer and NI myRIO-1900 by sharing network variables or TCP/IP. In this way, the system can be developed entirely under the same software environment LabVIEW.

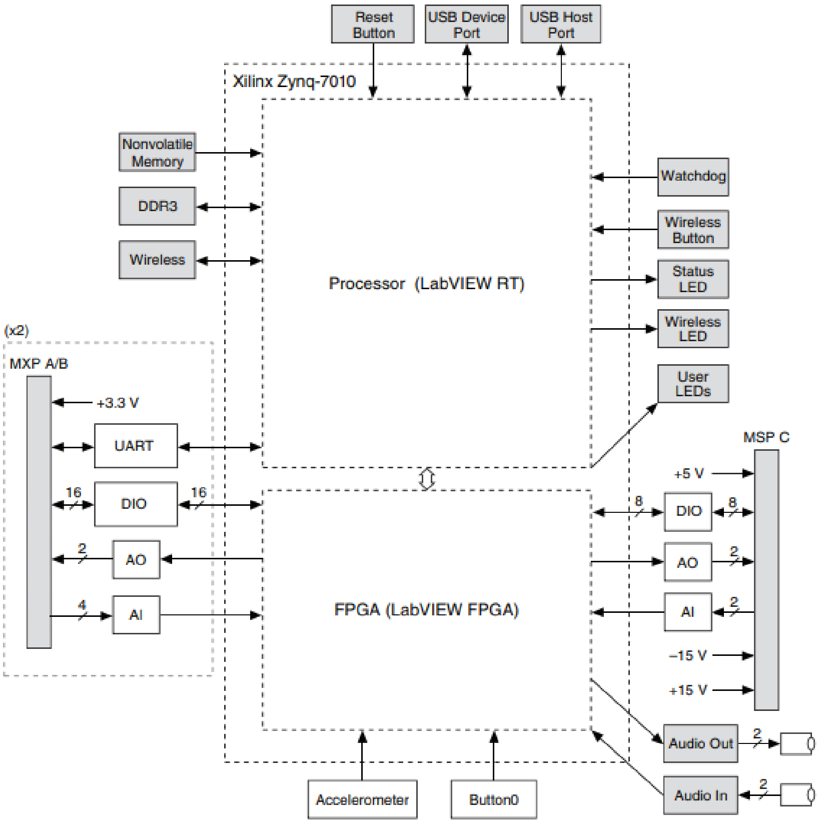

Figure 3.5- NI myRIO-1900 Hardware Block Diagram

3.2 Wireless Communication Protocols- Wi-Fi

As mentioned earlier, the NI myRIO-1900 comes with a built-in Wi-Fi shield. For projects that require a quick connection between the device and the Internet, Wi-Fi is the ideal protocol. Therefore, NI myRIO is chosen in this project because of embedded in Wi-Fi which can be used for fast data transfer and has the ability to process large amounts of data. The main features of Wi-Fi are shown in Table 3.8. In principle, Wi-Fi is a Wireless Local Area Network (WLAN) technology created in the IEEE 802.11 standard. Wi-Fi essentially uses an infrastructure network that also supports ad hoc networks in infrastructure mode [35]. The range of Wi-Fi depends on the version of Wi-Fi, it is larger in open spaces than in rooms with walls or other interfering objects [36]. For example, IEEE 802.11a has a range of 120 meters, while IEEE 802.11b has a range of up to 300 meters. The advantages and disadvantages of the Wi-Fi protocol are described in Table 3.9.

Table 3.8- Main Features of Wi-Fi

Feature	Wi-Fi
IEEE standard	IEEE 802.11
Max Signal Rate	54 Mbps
Frequency	2.4 GHz; 5 GHz
Range	250 m
Nodes	Unlimited (ad hoc); 2007 (infrastructure)
Typical Power Consumption	100 - 350 mA
Complexity	High

Table 3.9- Advantages and Disadvantages of the Wi-Fi Protocol

Advantages	**Disadvantages**
- Decent coverage and outreach and can penetrate walls and other obstacles on the way - Adding or removing devices from a Wi-Fi network is a simple process	- High energy consumption - Radio waves in the network may interfere with other equipment

3.3 Implementation of Hardware Platform

At first, the implement of the hardware platform is based on IVS-162. The main equipment of the hardware platform is shown in Fig. 3.6.

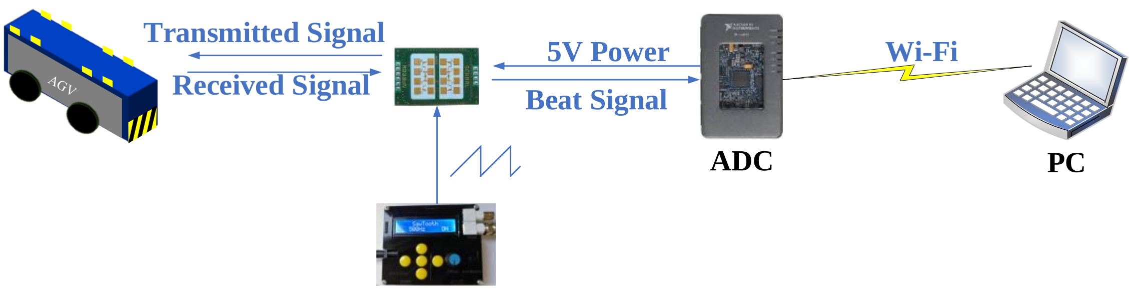

Figure 3.6- Equipment of Hardware Platform

In this case, NI myRIO-1900 supplies electricity to microwave Doppler radar sensor IVS-162 and has the function of ADC. To sample the IF signal of IVS-162 and transmit it to PC, it is important to configure parameters of the radar sensor by using NI myRIO-1900.

3.3.1 Data Acquisition

The acquisition of the IF signal is the first step of signal processing. It refers to converting the analog IF signal output from the IVS-162 radar sensor into the digital signal. The signal acquisition has a basic parameter - the sampling frequency.

In theory, the higher the sampling frequency, the more accurately the acquired digital signal recovers its analog signal. However, too high sampling frequency has two disadvantages, one is subject to the limitations of the actual ADC device. Second, the larger the amount of data sampled in a certain period of time, the higher the requirements for the storage and processing of the digital signal processor. According to the Nyquist sampling theorem, when the sampling frequency is greater than twice the highest frequency of the signal, the digital signal obtained can completely recover its analog signal. Therefore, considering some non-ideal characteristics of the actual system, engineering applications generally select the sampling frequency to be 3-5 times the highest frequency of the signal [37].

Since the positioning system requires a fast response time to the target, the data acquisition and data analysis time of the radar is also needed to be fast, so it is necessary to use high-speed data acquisition and high-speed data processing for the beat signal. The block diagram of the data acquisition system is shown in Fig. 3.7.

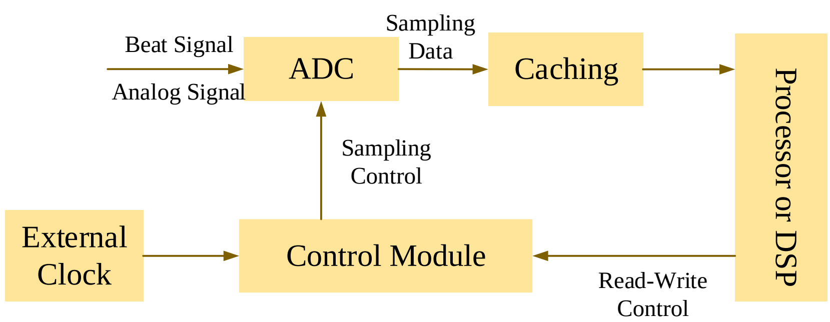

Figure 3.7- Data Acquisition System Diagram

3.3.2 Generation of Sawtooth Wave Signal

The sawtooth wave generator that used in this project is the DDS Function Signal Generator as shown in Fig. 3.8. The specifications of the DDS Function Signal Generator is shown in follows,

Table 3.10- Specifications of DDS Function Signal Generator

Specifications of DDS Function Signal Generator:
Lightweight and compact, it can reduce the size and weight of the positioning system;
Use the 1602 LCD menu to easily view the set parameters;
Intuitive keyboard, the power automatically restore the last used configuration;
Signal amplitude of the offset amount can be adjusted separately by two potentiometers;
Can achieve sawtooth wave, triangle wave, sine wave and so on easily, and frequency range is between 1Hz to 65534Hz;
Operating voltage is only DC 9V.

There, NI myRIO-1900, as shown in Fig. 3.8, is only used to adjust the voltage of the signal generator. The test result is shown in Fig. 3.9.

Figure 3.8- DDS Function Signal Generator and Adjust Output voltage

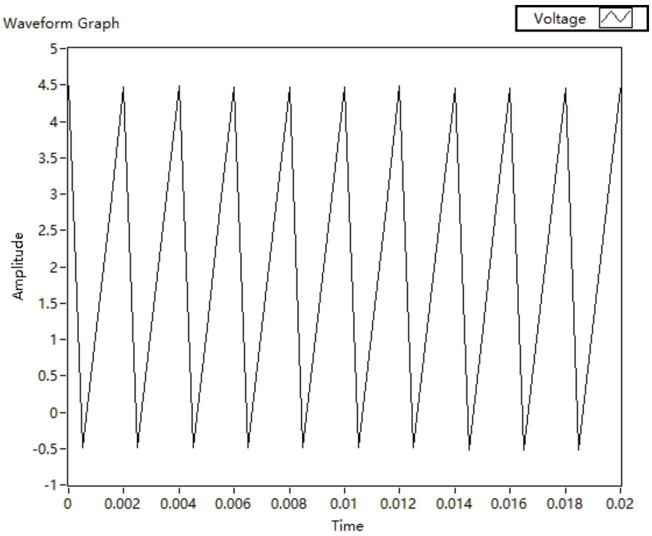

Figure 3.9- Result of Sawtooth Wave with 5V and 500Hz

Form Figure 3.9, it can be observed that the DDS Function Signal Generator can generate stability sawtooth wave with 5V voltage and a period of 500Hz.

3.3.3 The Connection Method of SP25

Since the SP25 requires TTL to USB serial port adapted to read the message generated by SP25, the TX and RX pins of myRIO-1900 are selected to be cross-connected with the TX and RX pins of SP25, as shown in Fig. 3.10.

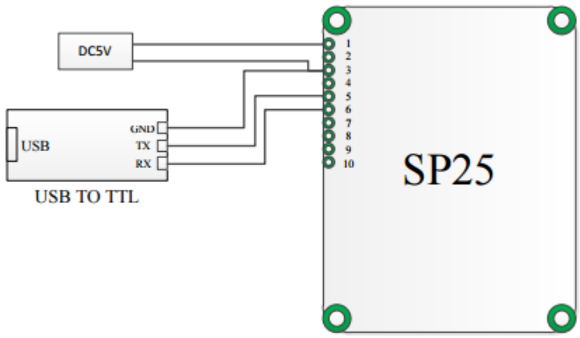

Figure 3.10- Connection of SP25 ports

The power of the SP25 is also supported by NI myRIO. If all the configuration is successful, the message can be read by the PC.

3.4 Developed Software

3.4.1 Description of LabVIEW software

LabVIEW is a program development environment from National Instruments (NI). The most important reason for its widespread use is that it uses a graphical editing language ‘G’ to write programs, and the resulting programs are in the form of block diagrams. LabVIEW uses data flow programming. The data flow between nodes in the block diagram determines the execution order of VIs and functions. VI refers to a virtual instrument and is a program module of LabVIEW.

LabVIEW software is at the heart of the NI design platform and is ideal for developing measurement or control systems. Like C and BASIC, LabVIEW has a large database that can perform any programming task, including data acquisition, GPIB, serial port control, data analysis, data display, and data storage. In addition, LabVIEW also has traditional program debugging tools, such as displaying the results of data and its subroutines (subVI) in an animated form, setting breakpoints, single-stepping, etc., to facilitate program debugging.

LabVIEW controls have many panels like traditional instruments (such as oscilloscopes, multimeters) that can be used to create highly visualized user interfaces. The user interface is referred to as the 'front panel'. Users can use icons and wires to control the controls on the front panel as needed. This is the graphics source code - the 'G' code. Also known as block diagram code.

3.4.2 NI myRIO-1900 Required Software

There are several additional software required for NI myRIO-1900 as shown in Table 3.11. The NI MAX can be used to configure the network and operating status of my RIO. LabVIEW Development System, Real-Time Module and myRIO Toolkit are necessary modules for creating myRIO Project. The project needs to call the script of ‘m’ file written by MATLAB in LabVIEW, so MathScript RT was installed. Similarly, if the user doesn’t need to call the MATLAB script in myRIO Project, it is not necessary to download MathScript RT.

Table 3.11- Required Software of myRIO-1900

Sr. No	Software
1	NI MAX
2	LabVIEW Development System
3	LabVIEW Real-Time Module
4	LabVIEW myRIO Toolkit
5	MathScript RT

3.4.3 MATLAB software

MATLAB (from MathWorks) is an advanced technical computing language and interactive environment for algorithm development, data visualization, data analysis, and numerical computing.

The reason why this thesis selected MATLAB for signal noise was that it has an appropriate wavelet processing library and the algorithm used has undergone various optimization and fault-tolerant processing. Normally, the user can use it instead of the underlying programming language. With the same computational requirements, the amount of work required to program with MATLAB is greatly reduced.

In this project, MATLAB is used to implement some more complex algorithms, and it is embedded in LabVIEW software using MATLAB script functionalities.

Chapter 4. Beat Signal of Microwave Radar Sensor Denoising

4.1 Noise Sources

The echo of the target is always in a certain clutter, and the task of the target detection is to extract the target signal from the clutter. In order to improve the detection capability of the target, the necessary clutter processing should be performed before the target detection. The task of clutter processing is to reduce the clutter power, improve the SNR and find the probability of the target as high as possible.

4.1.1 SNR

The SNR is the ratio of signal (meaningful information) to noise (unwanted signal) in an electronic device or electronic system. The signal refers to the electronic signal that needs to be processed outside the device. The noise is the irregular extra signal (or information) that does not exist in the original signal, and the noise does not change as original signal changes [38].

The SNR is expressed as the ratio of the average power of the signal to the average power of the noise, that is,

$$\mathrm{SNR} = \frac{P_{signal}}{P_{noise}} \tag{4-1}$$

If the signal and noise are measured at the same impedance, the SNR can be obtained by calculating the square of the amplitude ratio,

$$\mathrm{SNR} = \left(\frac{A_{signal}}{A_{noise}}\right)^2 \tag{4-2}$$

Where A is the Root Mean Square (RMS) amplitude, for example, RMS voltage.

The signals are often expressed using the logarithmic decibel scale. Based upon the definition of decibel, signal and noise may be expressed in decibels (dB) as,

$$P_{signal,dB} = 10\log_{10}(P_{signal}) \tag{4-3}$$

In addition,

$$P_{noise,dB} = 10\log_{10}(P_{noise}) \tag{4-4}$$

In a similar manner, SNR can be expressed in decibels as,

$$SNR_{dB} = 10\log_{10}(\frac{P_{signal}}{P_{noise}}) \tag{4-5}$$

However, when the signal and noise are measured in volts (V) or amperes (A), which are measures of amplitude, they must first be squared to obtain a quantity proportional to power, as shown below,

$$SNR_{dB} = 10\log_{10}[\left(\frac{A_{signal}}{A_{noise}}\right)]^2 = 20\log_{10}(\frac{A_{signal}}{A_{noise}}) \tag{4-6}$$

4.1.2 Noise Sources Analysis

When the positioning system based on microwave radar sensor works in the actual environment, it will encounter a variety of interferences, such as from the reflected echo from a non-target (for example overhead cranes), the noise generated for the rain and the wind, and the noise from multipath interference and the radar itself. The echo received by the received antenna of microwave Doppler must have various noise and clutter. Therefore, in the process starting from when the signal is transmitted until it is received, noise could enter the microwave radar from each component.

The noise here can be classified into two types according to their source, the external noise and the internal noise [39]. The external noise is incited by external interference factors and noise signals enter the components of radar through the receiving antenna. The internal noise mainly includes weather interference and industrial interference. Both the external noise and internal noise in the radar system can as described to the undulating noise. As a common type of noise, it is necessary to filter noise in time-domain analysis and frequency domain analysis. The entire noise signal is random, and the amplitude and phase are always changing in a random manner, although its waveform is continuous in the time domain. In the actual analysis, it often regarded as Gaussian noise. It is well known that the power spectral density of Gaussian white noise is uniformly distributed, and its amplitude is subject to a Gaussian distribution. If the SNR is low, the following situation may occur: the amplitude of the noise signal is much higher than the maximum value be pre-set, but at this point, the system treats it as a target, which produces a false target. Therefore, it is necessary to perform denoising processing on the beat signal, and after filtering and denoising, a purer beat signal can be obtained. In the next section, the wavelet transform will be selected to process noise in the beat signal.

4.2 Theory of Wavelet Transform

A wavelet is simply a small wave that has a tool for the analysis of transient, nonstationary or time-varying phenomena. Discrete Wavelet Transform (DWT) was used to materialize the noise filtering algorithm.

4.2.1 Discrete Wavelet Transform

When reconstructing a signal using the wavelet transform, it is necessary to discretize the wavelet and use a discretized wavelet transform.

As usually, the discretized formula of the scale parameter a and the translation parameter b are $a = a_0^j$ and $b = ka_0^j b_0$ respectively. In practice, the most commonly used is dyadic wavelet, that is, the parameters are $a_0 = 2,\ b_0 = 1$. And discretized wavelet can be expressed as,

$$\psi_{j,k}(t) = 2^{\frac{j}{2}}\psi\left(2^j t - k\right), j, k \in Z \tag{4-7}$$

So, the Discrete Wavelet Transform (DWT) is [40],

$$c_{j,k} = WT_f(j,k) = \int_{-\infty}^{+\infty} f(t)\psi^*(t)dt \tag{4-8}$$

There, $c_{j,k}$ is the coefficient of DWT.

4.2.2 Mallat Algorithm

French scientist S.Mallat introduced the multi-resolution analysis theory in the field of computer vision into wavelet analysis and derived the corresponding fast algorithm in 1987, that is, Mallat algorithm [41]. The role of the Mallat algorithm in the multi-resolution analysis is similar to the role of the FFT algorithm in Fourier analysis.

Assuming that $\{V_j\}$ is the integrated multiresolution analysis, φ and ψ are corresponding scale function and wavelet function respectively, and $f \in V_{J_1}$ (J_1 is a fixed integer). So,

$$f(t) = A_{J_1} f(t) = \sum_k c_{J_1,k} \varphi_{J_1,k}(t) \tag{4-9}$$

Here, $f(t)$ can be decomposed into the component $A_{J_1+1} f(t)$ in V_{J_1+1} and the component $D_{J_1+1} f(t)$ in W_{J_1+1},

$$f(t) = A_{J_1} f(t) = A_{J_1+1} f(t) + D_{J_1+1} f(t) \tag{410}$$

Among them,

$$A_{J_1+1} f(t) = \sum_k c_{J_1+1,k} \varphi_{J_1+1,k}(t) \tag{4-11}$$

$$D_{J_1+1} f(t) = \sum_k d_{J_1+1,k} \psi_{J_1+1,k}(t) \tag{4-12}$$

And D_{J_1+1} is called the mapping of W_{J_1+1} space.

Because of,

$$< \varphi_{J_1,m}, \varphi_{J_1+1,k} >= \bar{h}_{m-2k} \tag{4-13}$$

$$< \varphi_{J_1,m}, \psi_{J_1+1,k} >= \bar{g}_{m-2k} \tag{4-14}$$

So,

$$c_{J_1+1,k} = \sum_m \bar{h}_{m-2k} c_{J_1,m} \tag{4-15}$$

$$d_{J_1+1,k} = \sum_m \bar{g}_{m-2k} c_{J_1,m} \tag{4-16}$$

Introducing operators *H* and *G*,

$$(H_\sigma)_k = \sum_m \bar{h}_{m-2k} a_m \tag{4-17}$$

$$(G_\sigma)_k = \sum_m \bar{g}_{m-2k} a_m \tag{4-18}$$

So formulas (4-19) and (4-20) can be expressed as,

$$c_{J_1+1} = Hc_{J_1} \tag{4-19}$$

$$d_{J_1+1} = Gc_{J_1} \tag{4-20}$$

Similarly,

$$f(t) = A_{J_2}f(t) + \sum_{j=J_1+1}^{J_2} D_j f(t) \tag{4-21}$$

Among them,

$$A_j f(t) = \sum_k c_{j,k}\varphi_{j,k}(t) \tag{4-22}$$

$$D_j f(t) = \sum_k d_{j,k}\psi_{j,k}(t) \tag{4-23}$$

That is,

$$\begin{cases} c_{j+1} = Hc_j \\ d_{j+1} = Gd_j \end{cases} \quad \mathrm{j} = J_1, J_1+1, \cdots, J_2 - 1 \tag{4-24}$$

The formula (4-24) is the famous tower decomposition algorithm of Mallat. It can also call $A_j f(t)$ as the continuous approximation of $f(t)$ at resolution 2^j. $D_j f(t)$ is the continuous detail of $f(t)$ at resolution 2^j. And the corresponding series c_j and d_j are discrete approximations and discrete details respectively. The decomposition flow chart of the Mallat algorithm as shown in Fig.4.1.

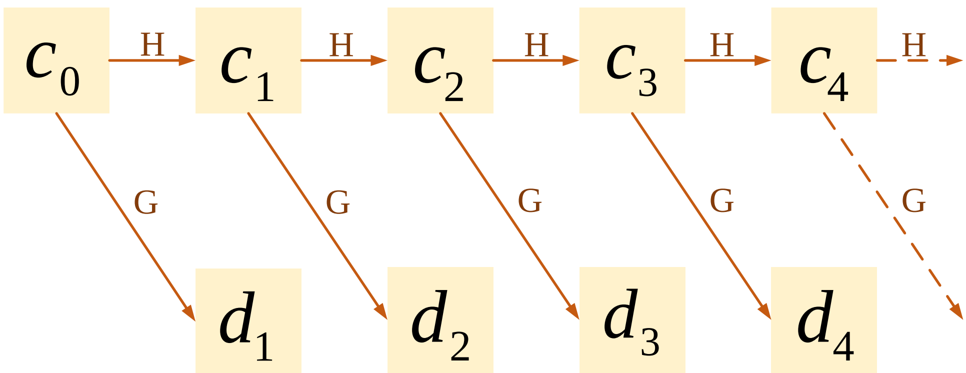

Figure 4.1- Signal Decomposition Flow Chart of Mallat Algorithm

Corresponding to the Mallat tower decomposition algorithm, the following reconstruction algorithm can be obtained.

$$c_{j,k} = \sum_{m} h_{k-2m} c_{j+1,m} + \sum_{m} g_{k-2m} d_{j+1,m} \tag{4-25}$$

Let H^* and G^* are the adjoint operators of H and G, respectively.

$$(H_a^*)_k = \sum_{m} h_{k-2m} a_m \tag{4-26}$$

$$(G_a^*)_k = \sum_{m} g_{k-2m} a_m \tag{4-27}$$

So the formula (4-25) can be written as,

$$c_j = H^* c_{j+1} + G^* d_{j+1} \quad \mathrm{j} = J_2 - 1, \cdots, J_1 \tag{4-28}$$

The signal reconstruction flowchart of the Mallat algorithm is shown in Fig. 4.2,

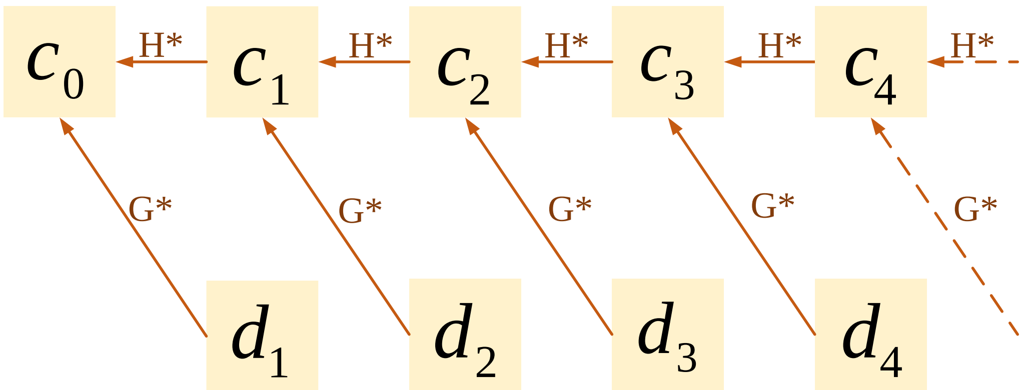

Figure 4.2- Signal Reconstruction Flow Chart of Mallat Algorithm

4.3 Threshold Denoising

Assume the following observed signal is,

$$f(k) = s(k) + n(k) \tag{4-29}$$

Here, $s(k)$ is the pure signal, $n(k)$ is the additive random noise. The wavelet transform of observed signal is,

$$\omega(k) = \theta(k) + z(k) \tag{4-30}$$

In the formula, ω, θ, and z are the wavelet coefficients of the observed signal, the pure signal, and the noise signal, respectively.

The wavelet denoising method is to set a threshold (obtained by prior knowledge). The wavelet coefficient larger than the threshold is considered to be generated by the signal. The wavelet coefficient smaller than the threshold is considered to be generated by noise. Deleting the coefficient generated by noise is the purpose of denoising.

The method of wavelet threshold denoising includes the following three steps:

(1) Calculate the wavelet transform of the observed signal contained with noise. Select the appropriate wavelet and wavelet decomposition layer j, and decompose the observed signal to the *j* layer to obtain the corresponding wavelet decomposition coefficient.

(2) The wavelet coefficients obtained by the decomposition are processed by the threshold to obtain the estimated values of the pure signal wavelet coefficients.

(3) Perform an inverse wavelet transform on these estimated values to obtain a reconstructed signal.

4.3.1 Mother Wavelets

In Table 4.1 [42], there are common wavelets that can support DWT and suit for actual signal denoising. Figure 4.3 shows the characteristic of wavelets. *N* is the vanishing moment of wavelet.

Table 4.1- Wavelets

Name	Representation	Orthogonality	Symmetry
Haar	haar	√	√
Daubechies	dbN	√	Approximate
Coiflets	coifN	√	Approximate
Symlets	symN	√	Approximate

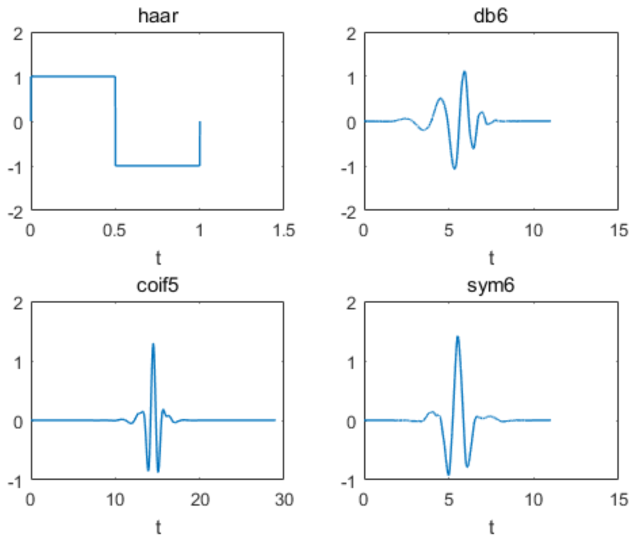

Figure 4.3- Wavelets

To verify which mother wavelet is suitable, in Part 4.4, the simulation results will help to choose the most satisfying mother wavelet in this project.

4.3.2 Decomposition Layer *J*

In wavelet decomposition, the larger the number of *J* decomposition layer, the more distinct the characteristics of noise and signal performance, and the better the separation of the two; on the other hand, the reconstructed signal distortion will be larger in a certain extent. It will also affect the effect of denoising. In the real application, it must pay special attention to the contradiction between noise and signal, then choose a suitable layer decomposition.

Wavelet decomposition layers are selected from 3-5 in the situation of IF signal denoising [43-44].

4.3.3 Threshold λ

The first step of threshold denoising based on wavelet transform is to determine the appropriate threshold because the choice of threshold directly affects the quality of denoising.

Assuming that noisy signal $f(t)$ in scale of 1 to m $(1<m<J)$ acquires the summary of wavelet coefficient is n through wavelet decomposition. J is the Binary scale parameter, the standard deviation of additional noise is σ, so the universal threshold is,

$$\lambda = \sigma\sqrt{2ln(N_j)} \tag{4-31}$$

There, j is present decomposition layer, N_j is the length of wavelet coefficient, σ is standard deviation of signal, and σ needs to estimate from the noisy signal,

$$\sigma = median(|d_{j,k}|)/0.6475 \tag{4-32}$$

The principle of this method is, N_j standard Gaussian variables have the characteristic of independent identical distribution, the probability that the maximum value is less than λ tends to *1* as *N* increases.

If the measured signal contains independent and identical distributed noise, after wavelet transform, the wavelet coefficients of the noise part are also independently and identically distributed. If the noise with independent and identical distribution is decomposed by wavelet, its coefficient sequence length *N* is large. According to the above theory, the probability that the maximum value of the wavelet coefficients is less than λ approaches 1, that is, there has a threshold λ, such that all wavelet coefficients of the sequence are smaller than λ. With the increasing of the decomposition layer number, the length of the wavelet coefficients is shorter. According to the calculation formula of λ, the threshold is also smaller. Therefore, threshold can be set simply in the case that the noise has the characteristic of independent and identical distribution to achieve denoising.

4.3.4 Hard Threshold Function and Soft Threshold Function

There are two methods can achieve threshold processing generally, hard threshold estimation and soft threshold estimation, their estimation formulas can be expressed as follows,

$$d'_{j,k} = \begin{cases} d_{j,k}, |d_{j,k}| \geq \lambda \\ 0, |d_{j,k}| < 0 \end{cases} \tag{4-33}$$

$$d'_{j,k} = \begin{cases} sign(d_{j,k}) \cdot (|d_{j,k}| - \lambda), |d_{j,k}| \geq \lambda \\ 0, |d_{j,k}| < \lambda \end{cases} \tag{4-34}$$

The formula (4.33) is hard threshold estimation function, (4.34) is soft threshold estimation function. In above two formulas, $d_{j,k}$ is wavelet transform coefficient of noisy observation signal, λ is threshold, $d'_{j,k}$ is wavelet transform estimation value of pure signal. The hard threshold function and soft threshold function of estimation wavelet coefficient are shown in Fig.4.4.

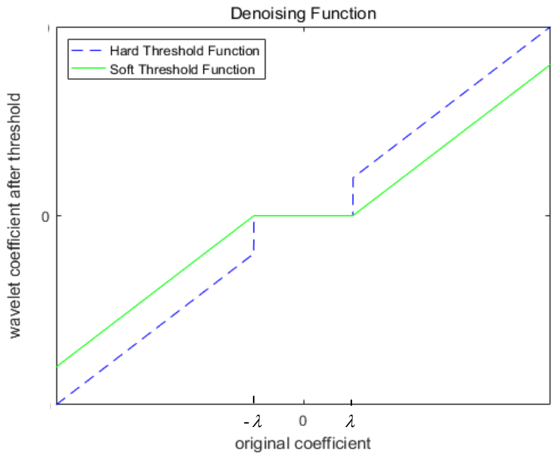

Figure 4.4- Hard Threshold Function and Soft Threshold Function

4.3.5 Adapted Threshold Function

In the previous section, this paper discussed soft and hard threshold denoising methods. Although these two methods are widely used in practice, they all have some shortcomings [45]. The hard threshold is discontinuous in the whole wavelet domain and there are interrupted points in the place of $\pm\lambda$, as shown in Figure 4.4. So the signal $f'(k)$ which has been reconstructed by $d'_{j,k}$ may appear some oscillation. In the soft thresholding function, there is a constant deviation between $d'_{j,k}$ and $d_{j,k}$ when $|d_{j,k}| \geq \lambda$. This will causes a deviation between the reconstructed signal $f'(k)$ and the real signal [46].

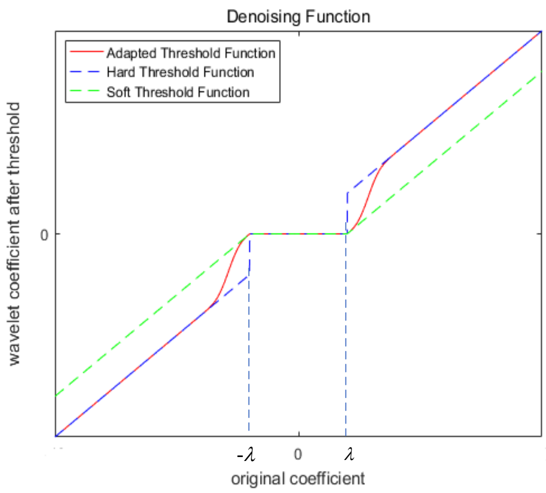

Figure 4.5- Adapted Threshold Function and Compering with Classic Functions

Thus, an adapted threshold function is proposed in this thesis. And this function as shown in Fig. 4.5.

$$d'_{j,k} = \begin{cases} sign(d_{j,k})(|d_{j,k}| - \dfrac{3 \cdot thr(j)}{3 + e^{\sqrt{(\frac{d_{j,k}}{thr(j)})^2 - 1}}}), |d_{j,k}| \geq \lambda \\ 0, |d_{j,k}| < \lambda \end{cases} \tag{4-35}$$

From Figure 4.5, it can be seen obviously that the adapted threshold function has improved compared with the hard threshold function and the soft threshold function in terms of hopping and fixed difference. The flow chart of wavelet denoising based on the adapted threshold function is shown in Fig. 4.6.

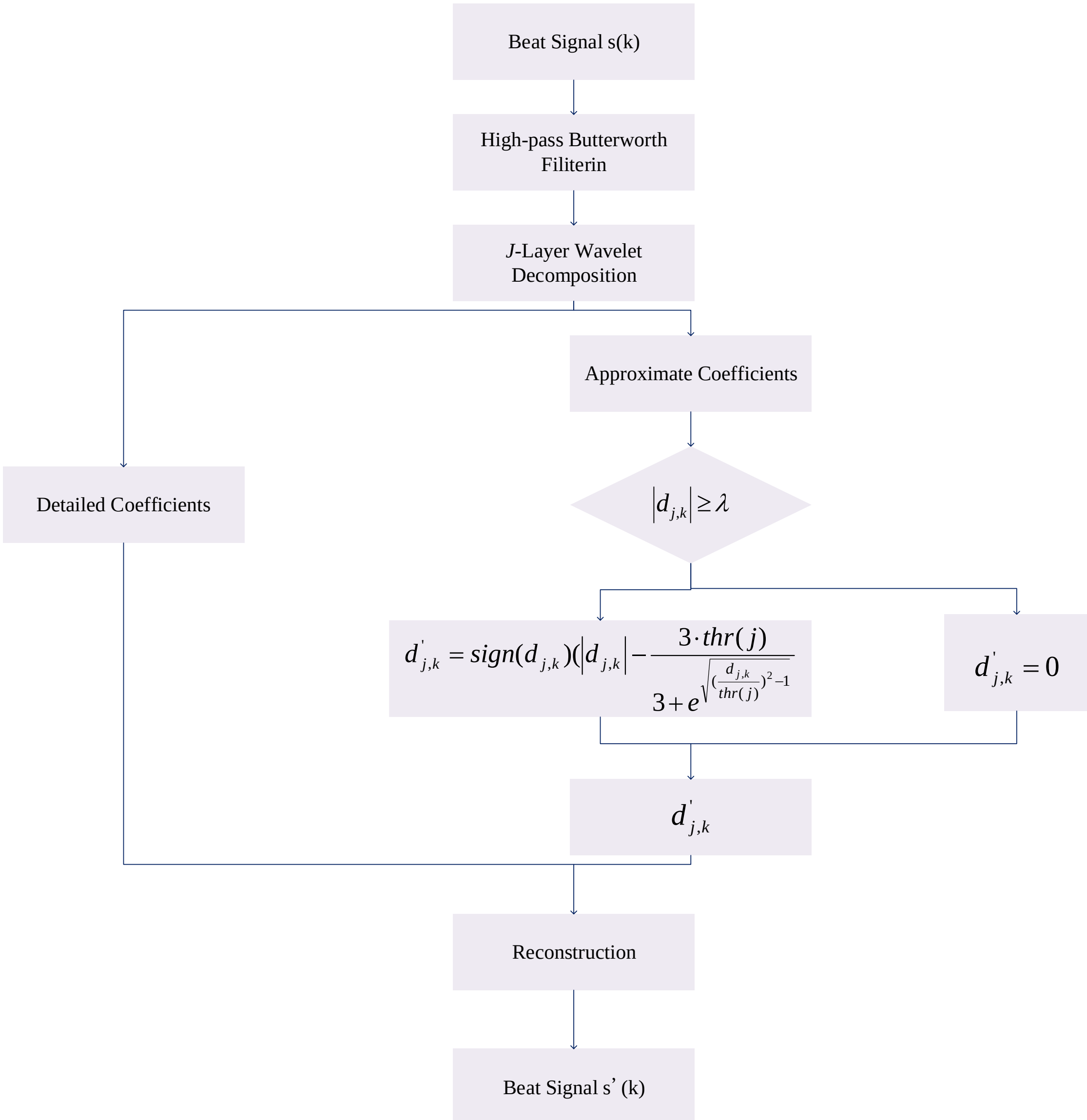

Figure 4.6- The Flow Chart of Wavelet Denoising based on Adapted Threshold Function

The procedure of wavelet denoising based on the adapted threshold function is shown in the Figure 4.7. The simulation experiments were conducted by MATLAB. After verifying the effectiveness of the proposed algorithm, in order to achieve it in NI myRIO which is using LabVIEW, the wavelet denoising is called as LabVIEW Script.

```
NAME='sym6';
lev=4;
[C,L]=wavedec(Y,lev,NAME);
a=appcoef(C,L,NAME,lev);
d1=detcoef(C,L,4);
d2=detcoef(C,L,3);
d3=detcoef(C,L,2);
d4=detcoef(C,L,1);
length1=length(d1);
length2=length(d2);
length3=length(d3);
length4=length(d4);
thr1=median(abs(d1),2)/0.6475*(2*log(length1))^(1/2);
thr2=median(abs(d2),2)/0.6475*(2*log(length2))^(1/2);
thr3=median(abs(d3),2)/0.6475*(2*log(length3))^(1/2);
thr4=median(abs(d4),2)/0.6475*(2*log(length4))^(1/2);
for i1=1:1:length1
   if abs(d1(i1))>=thr1
      d1(i1)=sign(d1(i1))*(abs(d1(i1))-thr1/exp((d1(i1)-thr1)^3));
   else d1(i1)=0;
   end
end
for i2=1:1:length2
   if abs(d2(i2))>=thr2
      d2(i2)=sign(d2(i2))*(abs(d2(i2))-thr2/exp((d2(i2)-thr2)^3));
   else d2(i2)=0;
   end
end
for i3=1:1:length3
  if abs(d3(i3))>=thr3
      d3(i3)=sign(d3(i3))*(abs(d3(i3))-thr3/exp((d3(i3)-thr3)^3));
   else d3(i3)=0;
   end
end
for i4=1:1:length4
   if abs(d4(i4))>=thr4
      d4(i4)=sign(d4(i4))*(abs(d4(i4))-thr4/exp((d4(i4)-thr4)^3));
   else d4(i4)=0;
   end
end
h=[a d1 d2 d3 d4];
p=waverec(h,L,NAME);
```

Figure 4.7 – Implemented MATLAB Script of Wavelet Denoising with Adapted Threshold Function

4.4 Simulation Results

The simulations were carried out in MATLAB. Assuming that a pure beat signal, which sample time *3ms*, sample frequency *50kHz*, modulated frequency *500Hz*, as shown in Fig 4.8, and set SNR to *25dB*, *20dB*, and *15dB respectively*. Fig. 4.9 and Fig. 4.10 are the examples of wavelet denoising by using a hard threshold function, a soft threshold function and the adapted threshold function respectively, in addition, the wavelet using in this example is '*sym6*'.

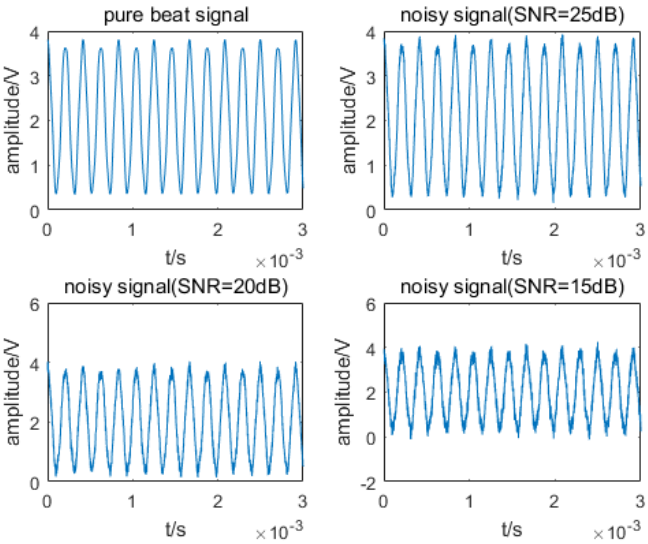

Figure 4.8- Beat signal and noisy beat signal

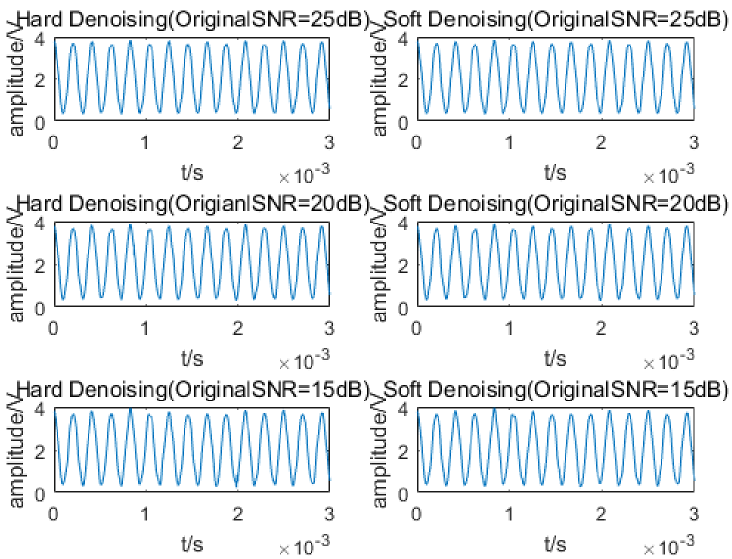

Figure 4.9- Hard Threshold Denoising and Soft Threshold Denoising

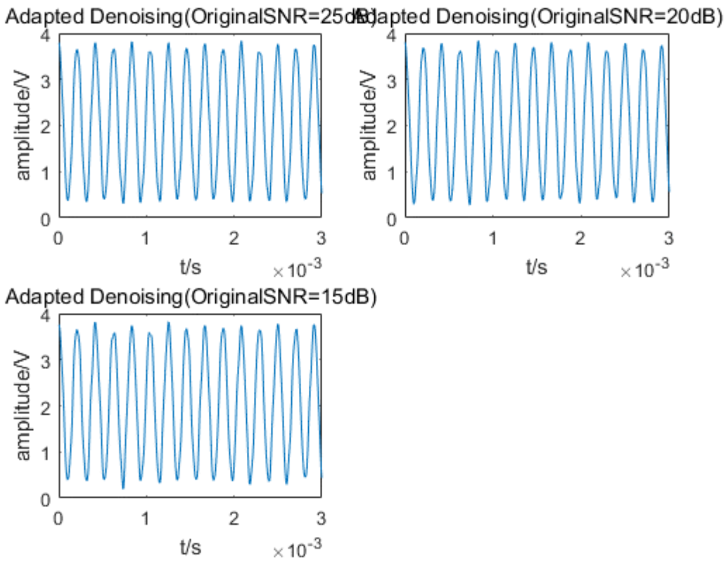

Figure 4.10- Adapted Threshold Denoising

For a more intuitive view of the denoising results, use a table to represent the SNR of the different decomposition layers and wavelet. Table 4.2 is the results of wavelet denoising based on hard threshold function, Table 4.3 is the results of wavelet denoising based on soft threshold function and Table 4.4 is the results of wavelet denoising based on adapted threshold function.

Table 4.2- Wavelet Denoising based on Hard Threshold Function

wavelet	**N**		**Level =3**	**Level =4**	**Level =5**		**Level =3**	**Level =4**	**Level =5**		**Level =3**	**Level =4**	**Level =5**
haar		**SNR =25**	19.57	13.67	7.87	**SNR =20**	19.27	13.64	7.87	**SNR =15**	18.56	13.53	7.83
coif N	**1**		32.30	24.18	13.69		29.17	23.77	13.67		24.64	22.81	13.59
	2		34.69	31.27	20.64		30.29	29.58	20.51		24.42	26.91	20.12
	3		34.90	32.40	23.30		29.67	30.22	23.07		24.29	27.59	22.49
	4		35.10	32.86	24.32		30.46	30.35	24.10		25.29	26.81	23.43
	5		35.06	33.93	24.23		30.29	30.94	24.07		25.13	27.30	23.49
sym N	**2**		32.21	23.77	13.58		28.72	23.36	13.56		24.68	22.30	13.48
	3		34.55	29.27	17.29		29.85	27.94	17.28		24.64	25.62	17.02

	4		34.91	30.99	20.32		29.99	29.22	20.21		24.96	26.22	19.97
	5		34.45	31.23	21.82		29.88	29.64	22.60		24.61	25.67	22.15
	6		34.89	32.15	23.45		29.97	29.65	23.26		24.63	26.55	22.71
	7		35.24	32.09	24.06		30.37	29.98	23.84		24.94	26.50	23.22
	8		34.58	32.88	24.01		30.08	30.46	24.04		25.00	26.20	23.26
dbN	**2**		32.11	23.75	13.56		28.46	23.35	13.54		24.49	22.31	13.50
	4		34.83	30.87	20.18		30.11	29.11	20.08		24.57	26.11	19.81
	6		35.57	32.25	23.54		29.80	30.05	23.37		24.78	26.23	22.71
	8		34.97	32.86	24.54		30.03	30.83	24.34		24.72	27.06	23.61

Table 4.3- Wavelet Denoising based on Soft Threshold Function

wavelet	**N**		**Level =3**	**Level =4**	**Level =5**		**Level =3**	**Level =4**	**Level =5**		**Level =3**	**Level =4**	**Level =5**
haar		SNR =25	19.23	13.67	7.87	SNR =20	19.27	13.64	7.87	SNR =15	18.56	13.55	7.83
coif N	1		32.30	24.18	13.69		29.17	23.77	13.67		25.03	22.81	13.59
	2		34.69	31.34	20.64		30.29	29.58	20.54		24.42	26.91	20.21
	3		35.11	32.40	23.29		29.67	30.41	23.05		24.62	27.59	22.58
	4		35.09	32.85	24.26		30.40	30.91	24.12		25.29	26.87	23.43
	5		35.06	33.70	24.38		30.29	31.26	24.17		25.13	27.56	23.67
sym N	2		32.21	23.77	13.58		29.09	23.42	13.56		24.68	22.34	13.48
	3		34.68	29.27	17.29		30.61	28.30	17.28		24.81	25.76	17.03
	4		34.91	31.00	20.33		30.11	29.34	20.26		24.96	26.22	20.02
	5		34.70	31.36	22.80		29.96	29.85	22.68		24.82	26.18	22.27
	6		34.98	32.20	23.49		29.97	30.19	23.30		24.96	26.87	22.85
	7		35.23	32.18	24.05		30.37	30.13	23.84		25.19	26.76	23.22
	8		34.58	33.04	24.22		30.09	30.68	24.08		24.43	26.79	23.38

dbN	2		32.11	23.75	13.57		28.68	23.40	13.55		24.74	22.57	13. 50
	4		35.06	30.87	20.17		30.34	29.28	20.08		24.74	26.45	19.87
	6		35.38	32.37	23.55		30.37	30.52	23.42		24.78	26.84	22.70
	8		34.97	32.86	24.57		30.03	30.83	24.38		24.65	27.06	23.75

Table 4.4- Wavelet Denoising based on Adapted Threshold Function

wavelet	**N**		**Level =3**	**Level =4**	**Level =5**		**Level =3**	**Level =4**	**Level =5**		**Level =3**	**Level =4**	**Level =5**
haar		SNR =25	19.57	13.67	7.85	SNR =20	19.31	14.35	8.14	SNR =15	18.75	13.55	7.83
coif N	1		32.99	24.18	13.70		29.87	24.35	14.08		25.62	22.81	13.62
	2		35.35	31.34	20.67		30.86	30.47	20.96		25.33	26.91	20.48
	3		35.58	32.40	23.44		30.64	30.42	23.35		25.80	27.59	23.02
	4		35.95	33.34	24.32		30.95	31.26	24.73		25.75	27.06	23.75
	5		35.82	34.36	24.44		31.05	31.72	24.24		25.64	28.06	23.94
sym N	2		32.53	23.81	13.58		29.26	23.51	13.97		25.37	22.90	13.50
	3		35.89	29.39	17.32		30.62	28.59	17.60		25.57	26.48	17.20
	4		35.63	31.19	20.37		30.21	30.08	20.30		25.62	27.06	20.11
	5		35.97	31.80	22.85		30.38	30.13	22.79		26.73	27.91	22.37
	6		35.55	32.60	23.50		30.30	30.79	23.37		26.28	27.83	23.00
	7		35.91	32.49	24.09		30.92	30.97	23.96		25.74	27.48	23.51
	8		36.08	33.28	24.33		30.71	31.09	24.78		25.26	28.27	23.83
dbN	2		32.49	23.79	13.58		29.51	23.55	13.97		25.17	22.80	13.50
	4		35.76	31.04	20.19		30.73	29.79	21.12		25.49	27.41	19.99
	6		35.87	32.45	23.60		31.01	30.65	24.55		25.80	27.62	23.03
	8		35.62	33.07	24.61		30.75	31.30	25.47		25.66	27.74	24.96

Taking the noisy signal with SNR=20 as an example, the SNR after wavelet denoising based on hard threshold function, soft threshold function and adapted threshold function respectively are extracted and compered with each other. The result is shown in Fig. 4.11, Fig. 4.12 and Fig. 4.13.

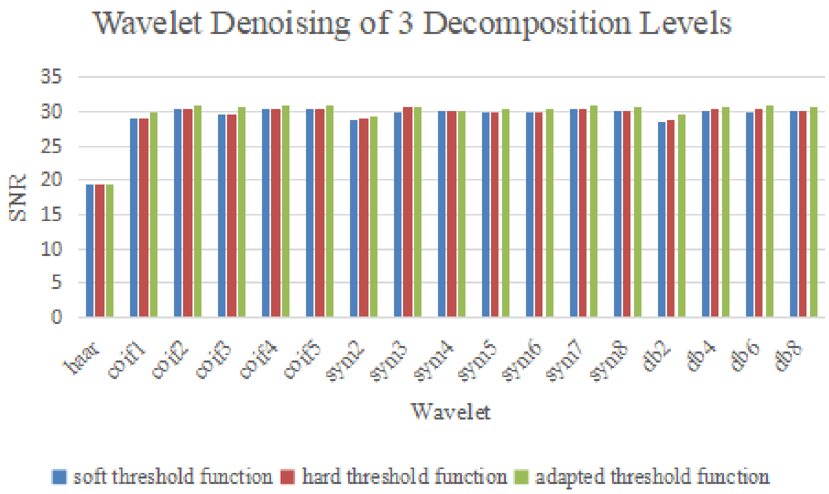

Figure 4.11- Wavelet Denoising of 3 Decomposition Levels

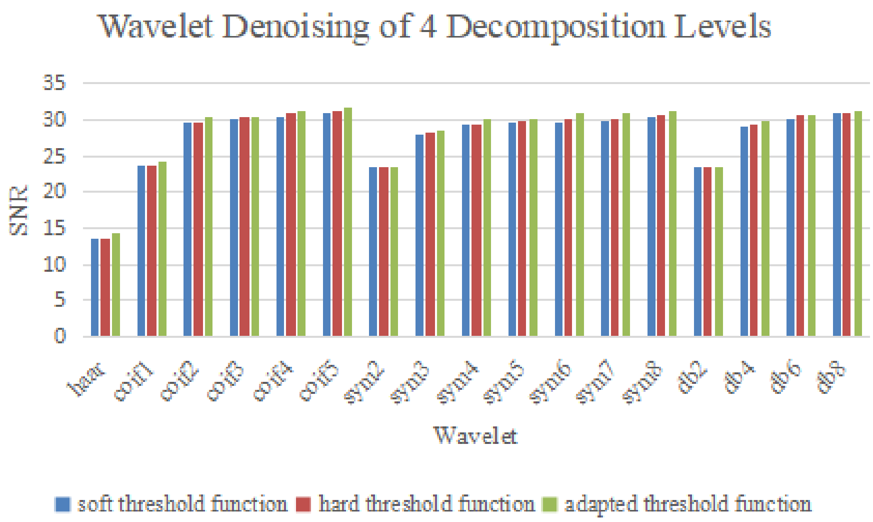

Figure 4.12- Wavelet Denoising of 4 Decomposition Levels

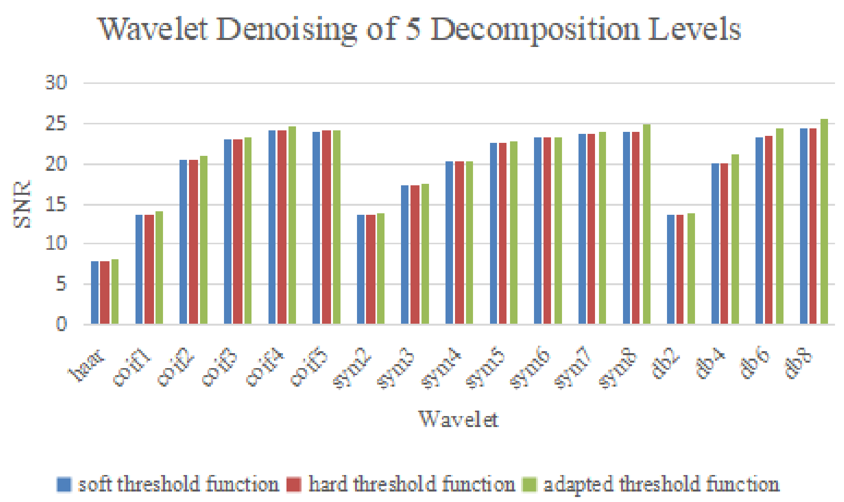

Figure 4.13- Wavelet Denoising of 5 Decomposition Levels

From above figures, it can be seen clearly that the adapted threshold function compared with the hard threshold function denoising and soft threshold function denoising has been improved. Therefore, the proposed adapted threshold function denoising is feasible and can be selected for positioning system. Then choose the appropriate decomposition layers according to the SNR after wavelet denoising based on adapted threshold function. Fig. 4.14, Fig. 4.15 and Fig. 4.16 show the comparison of different decomposition layers under the original SNR of 25, 20 and 15 respectively.

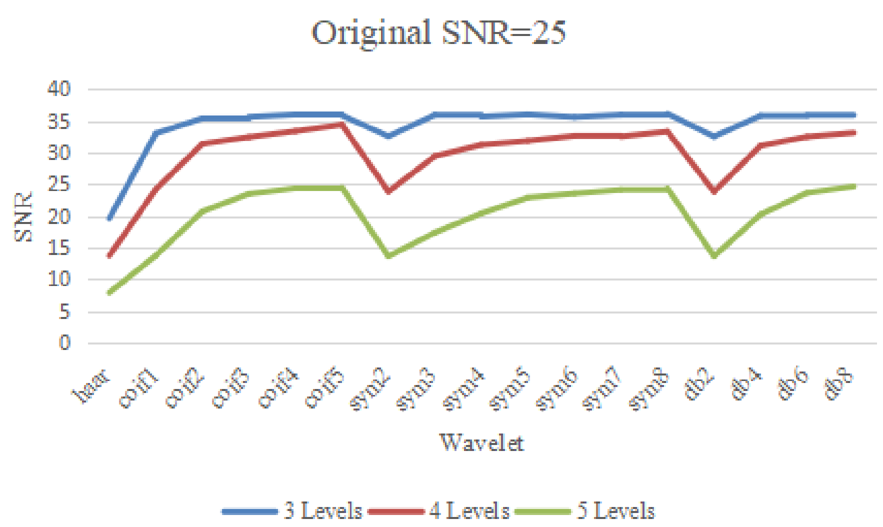

Figure 4.14- Wavelet Denoising based on Adapted Threshold Function of Original SNR=25

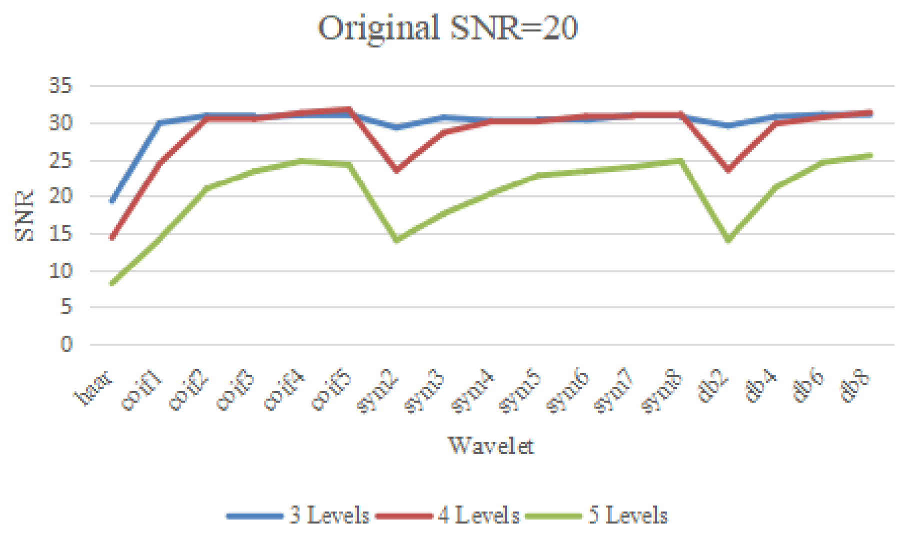

Figure 4.15- Wavelet Denoising based on Adapted Threshold Function of Original SNR=20

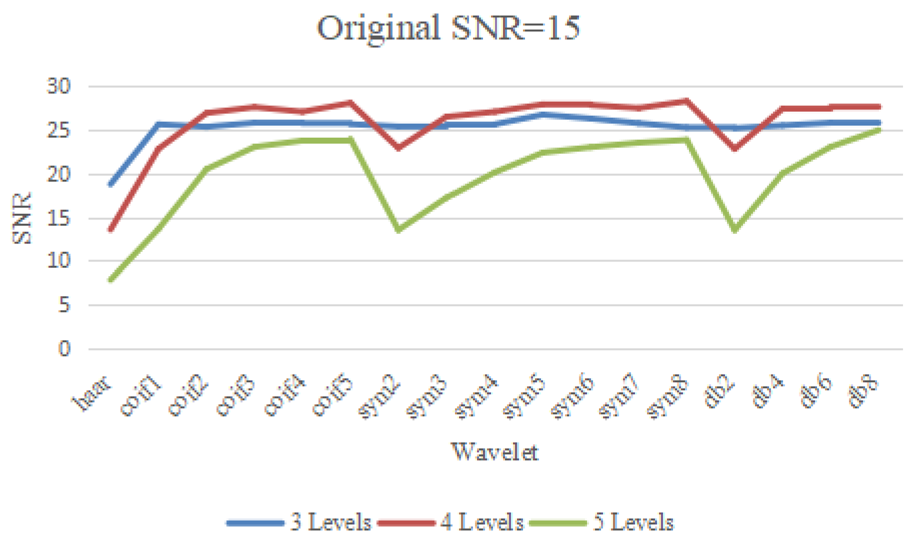

Figure 4.16- Wavelet Denoising based on Adapted Threshold Function of Original SNR=15

From Fig. 4.14, Fig. 4.15 and Fig. 4.16, it can be seen that when the number of decomposition layers is 3 or 4, the SNR is high and the reduction degree of useful signal is ideal. However, 4 layer decomposition exhibits better reduction degree than the 3 layer decomposition, because the higher number of decomposition has a better elimination on noise, but there is a higher possibility of distortion. Therefore, this project uses 4 decomposition levels, and the wavelet is '*sym6*'.

Chapter 5. Range and Velocity Detection

The range detection and velocity detection of the target expressed by AGV, using microwave radar is an important part of the whole positioning system. The technologies and experimental verification were conducted by microwave radar sensor IVS-162.

5.1 Detection Principle

It can be known from the Chapter 2 that FMCW is appropriate to detect range and velocity at the same time. The IF signal received by the received antenna is an echo that the transmitted signal reflects through the spatial propagation and encounters the target. Ideally, the received signal is a transmitted signal with a certain delay, and the delay is related with the propagation speed of the signal in the medium and the distance of target and antenna.

The task of signal processing is to analyze the IF signal obtained by filtering the high-frequency part through the low pass filter. After filtering the noise by using wavelet denoising with the adapted threshold function as mentioned in Chapter 4, the IF signal is processed to calculate the distance of the transmitting antenna-target-receiving antenna.

5.1.1 Static Target

For a static scenario, static microwave Doppler radar and static target, for a transmitted signal which is modulated by Sawtooth wave with the period of $t_m = 1/f_m$. The bandwidth ΔF depends on the modulated signal, and its central point is the transmitted center frequency f_0.

The equation of IF signal $S_b(t)$ is [47],

$$S_b(t) = k \sum_i a_t \, a_{ri} \cos(2\pi \left(2\Delta F \cdot f_m \frac{r_i}{c}\right) t + \emptyset_i) \tag{5-1}$$

So the range of target i can be expressed as,

$$r_i = \frac{c \cdot f_{bi}}{2\Delta F \cdot f_m} \tag{5-3}$$

There, $\emptyset_i$ can be expressed as,

$$\emptyset_i = 2\pi f_{bi} \frac{2r_i}{c} \tag{5-4}$$

Therefore, the phase $\emptyset_i$ of IF signal is only related with the differential frequency and the time delay of the transmitted signal and received signal.

5.1.2 Range Resolution

Range resolution is defined as the ability of microwave Doppler radar to distinguish two rather near targets. From (5-1), frequency component is proportional to range of target i. In this case, assuming that range resolution is equal to frequency resolution.

$$\delta f = \frac{1}{t_m} = f_m \tag{5-5}$$

The frequency is related to the range resolution, so the range resolution δr is,

$$\delta r = \delta f \frac{c}{2\Delta F \cdot f_m} = \frac{c}{2\Delta F} \tag{5-6}$$

As it can be observed from (5-6), the minimum detection range of microwave Doppler radar only depends on band width ΔF. Range resolution can be changed by adjusting the ΔF. The higher range resolution can be obtained by increasing the bandwidth.

5.1.3 Moving Target

When detecting the moving target by using microwave Doppler radar which is modulated by Sawtooth wave, the radial velocity causes the FMCW to produce the Doppler shift. Assuming that the direction of the moving target away from the microwave radar is positive, according to the Doppler shift, the IF signal $S_b(t)$ is represented as,

$$S_b(t) = k \sum_i a_t \, a_{ri} \cos(2\pi \left(2\Delta F \cdot f_m \frac{r_i}{c} + 2f_0 \frac{v_{ri}}{c}\right) t + \emptyset_i \tag{5-7}$$

Where, f_0 is the center frequency of the transmitted signal. For each specific target i, f_{bi} is,

$$f_{bi} = 2\Delta F \cdot f_m \frac{r_i}{c} + 2f_0 \frac{v_{ri}}{c} \tag{5-8}$$

The velocity of the moving target can be expressed as,

$$v = -\frac{c \cdot f_{doppler}}{2f_0} \tag{5-9}$$

In addition, the main expression of phase $\emptyset_i$ is the same as (5-4),

$$\emptyset_i = 2\pi f_{bi} \frac{2r_i}{c} \tag{5-10}$$

5.2 Range Measurement Algorithm

5.2.1 FFT

From above description, the range and velocity of the target is contained in IF signal. The purpose of spectrum analysis is to extract the range and velocity information contained in IF signal. Among the many spectrum analysis algorithms, Fast Fourier Transform (FFT) is one of the most widely used methods, because this method is mature in theory, easy to implement, high in reliability, and strong in real-time. The FFT is not a new spectrum analysis method, it is a fast calculation algorithm for Discrete Fourier Transform (DFT). DFT is appropriate for analyzing the spectrum of discrete signals.

The DFT is a discrete form of continuous Fourier transform, and the continuous time Fourier transform (or spectrum) of the analog signal $x(t)$ can be expressed as [48],

$$X(\omega) = \int_{-\infty}^{+\infty} x(t)e^{-j\omega t}dt \tag{5-11}$$

There, $x(t)$ is sampled as $x(nT)$, T is sampling interval. The Fourier transform of discrete signal $x(nT)$ can be described as,

$$X(k) = \sum_{n=0}^{N-1} x(n)W_N^{nk}, k = 0,1,\cdots,N-1 \tag{5-12}$$

Where, $W_N = e^{-j2\pi/N}$. The phase factor W_N has periodicity and symmetry, that is,

$$\text{Symmetry: } W_N^{k+N/2} = -W_N^k \tag{5-13}$$

$$\text{Periodicity: } W_N^{k+N} = W_N^k \tag{5-14}$$

The (5-12) is N-point DFT, N represents the length of the DFT and should satisfy $N \geq M$.

According to equation (5-12), calculating N-size discrete Fourier transform once needs $(N-1)$ complex addition and N complex multiplication. Calculating M-size

DFT calculation, it needs to calculate $M(M-1)$ complex addition and M^2 complex multiplication. It means that when using 1024-point DFT for sequence, that is, *N=1024*, the calculation of complex addition and complex multiplication is about 1 million times, which will seriously affect the real-time and performance of the system.

The emergence of FFT makes up for this deficiency of DFT. The FFT firstly divides the N-point sequence $x(n)$ into two sub-sequences $x_1(r)$ and $x_2(r)$ of N/2 points according to the parity rule, then DFT is applied for $x_1(r)$ and $x_2(r)$ respectively,

$$X_1(k) = \sum_{r=0}^{\frac{N}{2}-1} x_1(r) W_{\frac{N}{2}}^{kr} = DFT[x_1(r)], k = 0,1,\cdots,\frac{N}{2}-1 \tag{5-15}$$

$$X_2(k) = \sum_{r=0}^{\frac{N}{2}-1} x_2(r) W_{\frac{N}{2}}^{kr} = DFT[x_2(r)], k = 0,1,\cdots,\frac{N}{2}-1 \tag{5-16}$$

According to the characteristic of $W_N = e^{-j2\pi/N}$, the DFT after the first split can be divided into,

$$X(k) = X_1(k) + W_N^k X_2(k), k = 0,1,\cdots,\frac{N}{2}-1 \tag{5-17}$$

$$X\left(k+\frac{N}{2}\right) = X_1(k) - W_N^k X_2(k), k = 0,1,\cdots,\frac{N}{2}-1 \tag{5-18}$$

From (5-17) and (5-18), it can be observed that there have public items $X_1(k)$, W_N^k and $X_2(k)$. Therefore, the (5-17) and (5-18) can be applied to butterfly computation. Then, after a number of splits, the calculation of an N-point DFT requires $2(\frac{N}{2})^2 + \frac{N}{2} = \frac{N(N+1)}{2} \approx \frac{N^2}{2}$ $(N \geq 1)$ times complex multiplication and $\mathrm{N}\left(\frac{\mathrm{N}}{2}-1\right)+\frac{2\mathrm{N}}{2} = N^2/2$ times complex addition. Compared to processing directly with DFT, the amount of computation is reduced by half after only one decomposition.

5.2.2 Meaningful of refine the spectrum

From the perspective of spectrum analysis, the discrete spectrum of the IF signal is obtained by calculating the difference frequency in a finite time range, so the distance resolution of the radar not only depends on the distance resolution affected by the bandwidth ΔF but depends on the sampling interval on the spectrum.

The fence effect is generated because the result of the N-point FFT is limited to *N* sample points, and the spectral value between the two-point sampling interval is indistinguishable. Therefore, the target distance obtained by the discrete spectrum is also discontinuous and discrete. The estimated distance is a certain ΔR integer relationship with the distance resolution, but the actual distance is not necessarily an integer multiple of the distance resolution. The fence effect has a bad impact on the accuracy of the radar system. In order to ensure the accuracy of the positioning, it is necessary to find ways to improve the accuracy of the radar.

As mentioned above, increasing the number of sampling points of the FFT will inevitably increase the computational complexity of the FFT, that is, increases the operation time, thereby reducing the real-time performance of the system. Therefore, when the FFT is used to process the radar signal, the real-time performance of the radar is contradictory to the accuracy of the ranging. The traditional FFT needed to be improved to resolve this contradiction.

In this project, the algorithm which is FFT combined with Chirp-Z Transform (CZT) is proposed. It is well known that the DFT can be seen as a uniform sampling of the signal along the unit circle on the Z-domain, but in practical applications, not the spectrum on the entire unit circle is meaningful. CZT can be used to calculate the transformation on any curve on the unit circle [49]. Therefore, the FFT and CZT joint algorithm is a method of 'from coarse to fine' of the spectrum, that is, the frequency estimation is divided into two steps of coarse estimation and fine estimation.

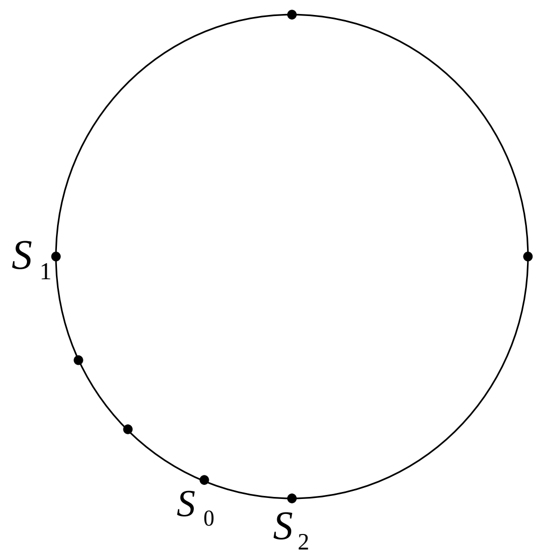

Figure 5.1- The description of FFT and CZT joint algorithm

For example, as shown in Fig. 5.1, the coarse estimation is applied to find the location of the spectrum peak in the circular arc S_1 to S_2. Then CTZ is used to estimate the accurate frequency within the interval $[S_1, S_2]$. It can be observed clearly that 4-point FFT and 4-point CZT joint algorithm can achieve the estimated frequency accuracy as same as 16-point FFT. It is futile to subdivide outside of the arc S_1 to S_2 which will add unnecessary computation. So theoretically FFT and CZT joint algorithm can reduce the amount of computation while maintaining the same accuracy.

5.2.3 Chirp-Z Transform

In order to better understand CZT, its definition and calculation method is described in detail. The Z transformation of the sequence $x(n)$ is [50],

$$X(z) = \sum_{n=0}^{+\infty} x(n) z^{-n} \tag{5-19}$$

Let z be sampled at z_k,

$$z_k = AW^{-k}, k = 0,1,\cdots,M-1 \tag{5-20}$$

There, M is the number of points to analyze the complex spectrum, A and W are arbitrary complex numbers, which can be expressed as follows,

$$A = A_0 e^{j\theta_0} \tag{5-21}$$
$$W = W_0 e^{-j\varphi_0} \tag{5-22}$$

Where A is the complex starting point of sampling contour, W is the ratio of points on sampling contour, A_0 is the vector radius of the sampling starting point, W_0 control contour to bend inward or outward. If $W_0 > 1$, the helical line inwardly contracts; if $W_0 < 1$, the helical line outwardly stretches, if $A_0 = W_0 = 1$, the transformation path of CZT is a section of arc on the unit circle. θ_0 is the phase angle of the initial sample point, φ_0 is the angular frequency difference of adjacent sample points.

For a sequence $x(n)$ of length N, the CZT of M point on unit circle can be expressed as,

$$X(z_k) = \sum_{n=0}^{N-1} x(n) A^{-n} W^{kn}, k = 0,1,\cdots,M-1 \tag{5-23}$$

Similar to DFT if calculating (5-23) directly, it needs $N \cdot M$ complex multiplications and $(N-1) \cdot M$ complex additions. If M, N is large, the computational complexity is very large, which limits the computational speed.

Rabiner et al. [51] used the relation to change the product of powers into sums, that is,

$$nk = [n^2 + k^2 - (n-k)^2]/2 \tag{5-24}$$

The CZT then computes *M* transform points from a time series of *N* points, where *M* and *N* are arbitrary. M transform points of CZT for weighting the input samples by $A^{-n}W^{n^2/2}$, performing an *(N+M)* point convolution and weighting the resulting *M* points by $W^{k^2/2}$,$k = 0,1,\cdots M-1$, so, there has,

$$X(z_k) = W^{\frac{k^2}{2}} \sum_{n=0}^{N-1} [x(n)A^{-n}W^{\frac{n^2}{2}}]W^{\frac{-(k-n)^2}{2}}, k = 0,1,\cdots,M-1 \tag{5-25}$$

Order,

$$g(n) = x(n)A^{-n}W^{\frac{n^2}{2}} \tag{5-26}$$

$$h(n) = W^{\frac{-n^2}{2}} \tag{5-27}$$

Hence,

$$X(z_k) = W^{\frac{k^2}{2}} \sum_{n=0}^{N-1} g(n)h(k-n) = W^{\frac{k^2}{2}}[g(k) * h(k), k = 0,1,\cdots,M-1 \tag{5-28}$$

From (5-28), it can be concluded that the *Z* transformation of z_k points can be obtained by solving the linear convolution of $g(k)$ and $h(k)$, then multiplying by $W^{\frac{k^2}{2}}$.

5.2.4 The Procedure of FFT and CZT Joint Algorithm

In the real application in the positioning system, the specific implementation method has four steps, the chart flow as shown as Fig. 5.2.

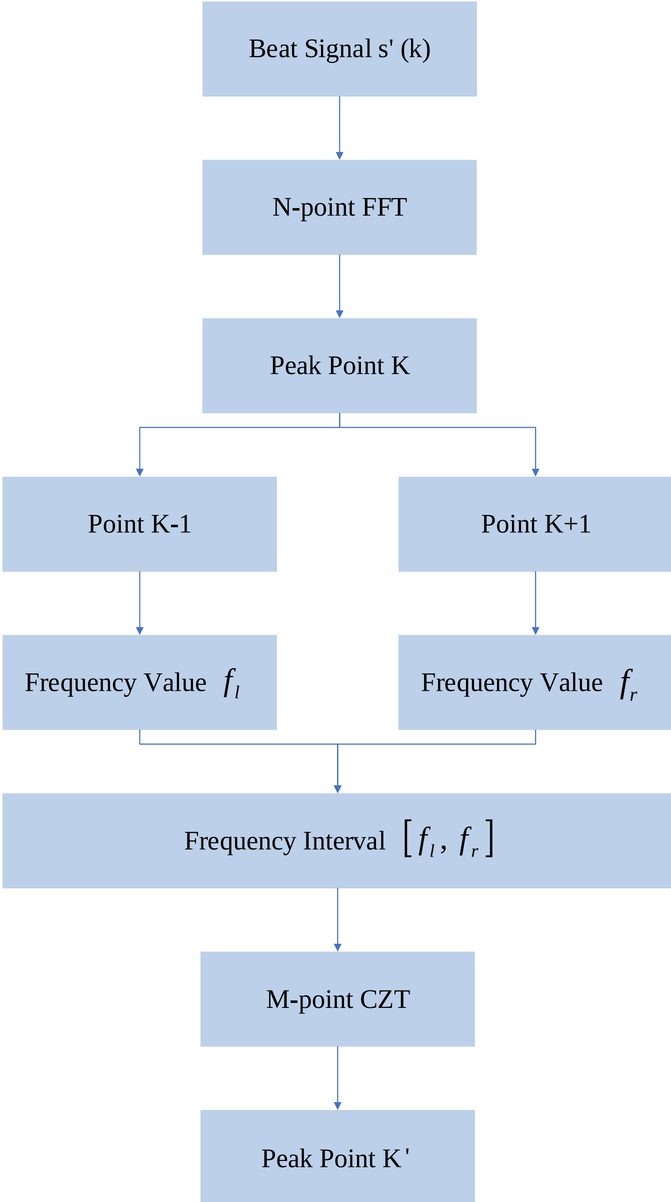

Figure 5.2- The Flow Chart of FFT and CZT Joint Algorithm

(1) The beat signal is calculated by N-point FFT, and the maximum amplitude point K (peak point) is found, then calculating the corresponding frequency value f ;

(2) The frequency values f_l and f_r of two adjacent points (K-1) and (K+1) is calculated;

(3) Maximum value K_{max} and corresponding frequency value f_{Kmax} can be calculated by using M-point CZT during frequency interval $[f_l, f_r]$;

(4) The range information of target can be acquired from f_{Kmax} which corresponding to peak point K'.

The program of FFT and CZT joint algorithm is shown in Figure 5.3. The algorithm is implemented in LabVIEW.

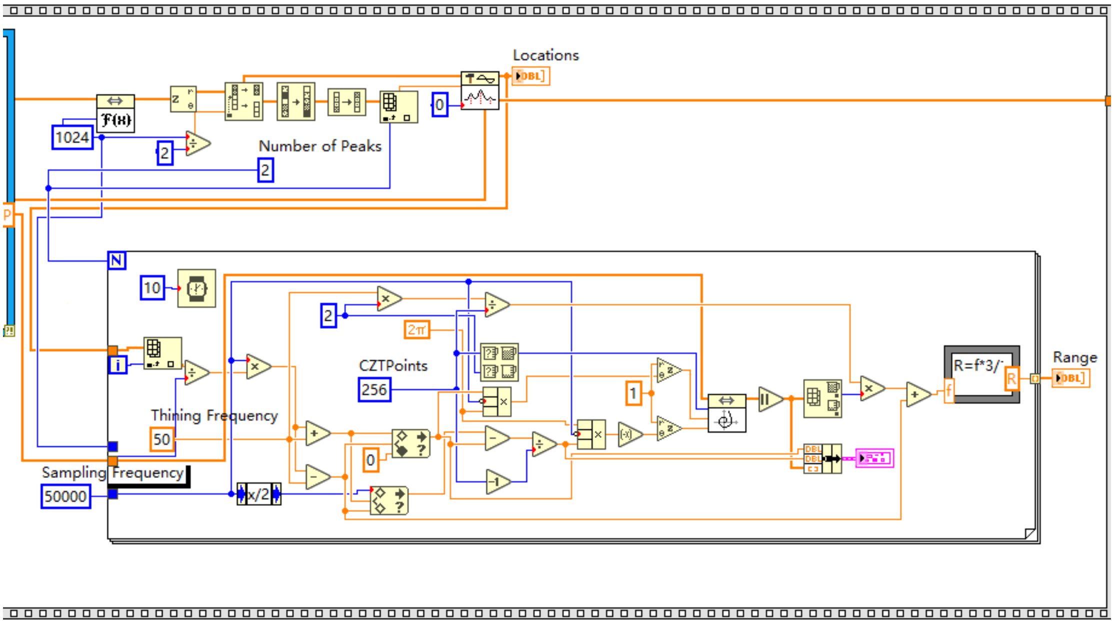

Figure 5.3 - The LabVIEW Program of FFT and CZT Joint Algorithm

5.3 Velocity Calculation Method

The idea of speed calculation is, the transmission time of the radar signal is shorter than the movement time of the target. Therefore, it can be assumed that the range and radial velocity remain constant on all slopes [52-55]. Moreover, the Doppler shift will result in a constant phase change in the ranging frequency, which can be exhibited in one period of a single ramp, as shown in Figure 5.4. Therefore, the distance-speed map can be obtained by extracting the frequency and phase using the 2D-FFT processing.

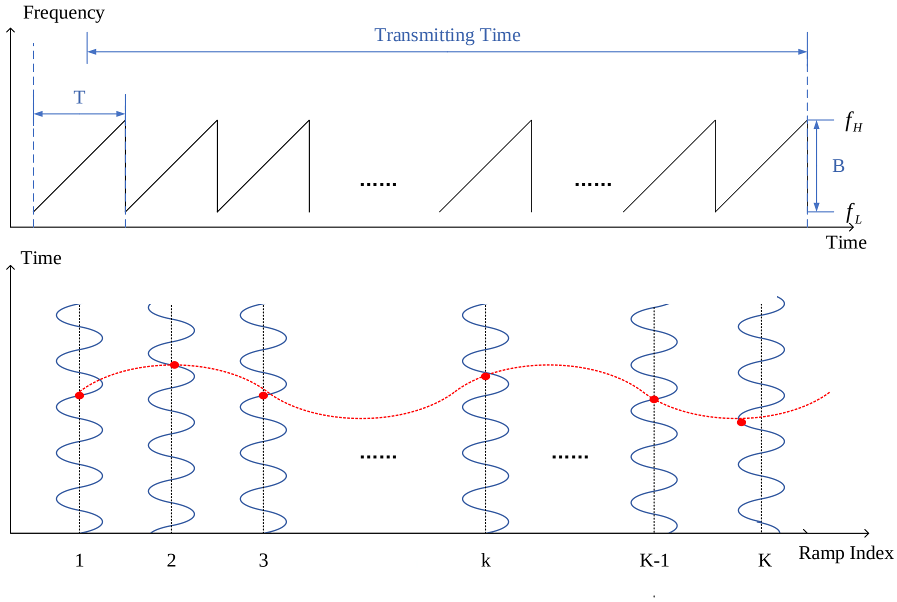

Figure 5.4- Beat Signal for a Single Moving Target in Ramp Index Domain

The Doppler shift of the signal can be found by observing the spectrum of the signal over K consecutive periods $(K \cdot T)$. To calculate velocity value, the FFT algorithm is applied to the outputs of the first FFT. Fig. 5.5 describes this process,

(1) The row-wise FFT is taken on the time samples;

(2) The column-wise FFT is taken on the output of the first FFT;

(3) After two dimensional FFT processing, the range-Doppler map which contains range and velocity information of the target can be obtained.

The 2D FFT program of LabVIEW can be seen in Figure 5.6. In this project, the MATLAB Script is used to transform 1D IF signal to 2D signal according to period *T*. However, according to user requirement, only LabVIEW can also achieve this purpose.

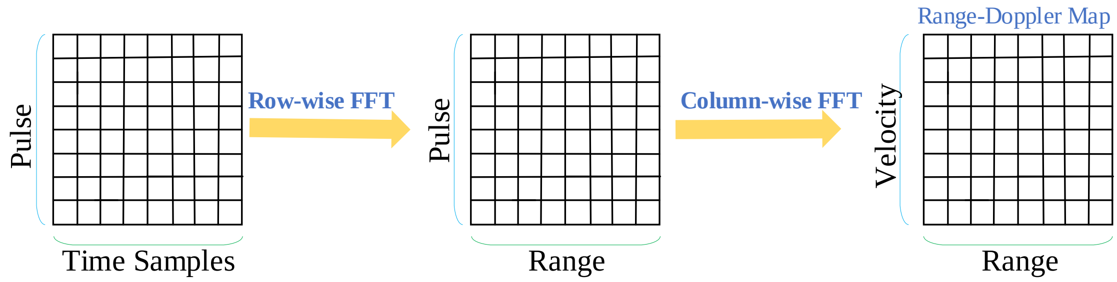

Figure 5.5- Principle of 2D FFT

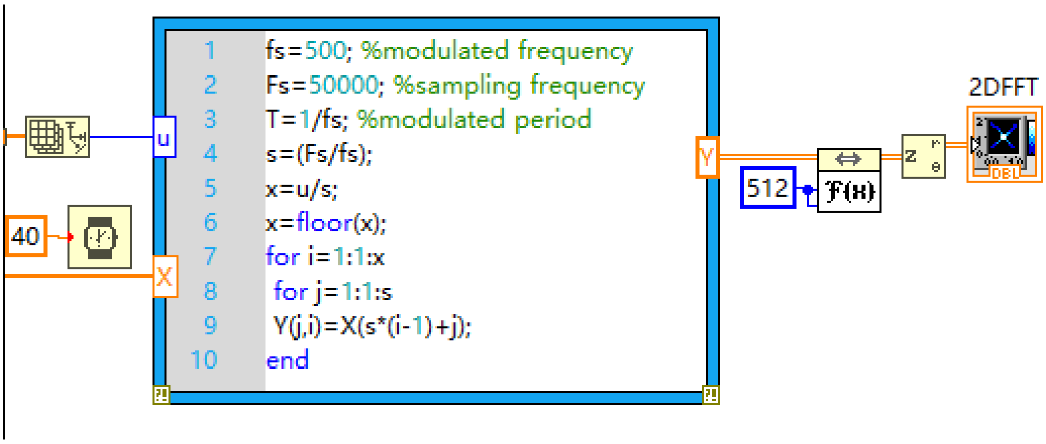

Figure 5.6 - The LabVIEW Program of 2D FFT

5.4 Validation

5.4.1 Parameters and Experimental Setup

From Chapter 2, the maximum velocity of the AGV is 21.6km/h. In addition, considering the actual experimental environment, the maximum range that the radar can detect is 30m. The maximum difference frequency generated by the range is $f_{delay} = 8333.33Hz$. And the maximum Doppler shift generated by the velocity is $f_{doppler} = 962.5Hz$. So for single AGV, the total difference frequency that can be generated is the sum of f_{delay} and $f_{Doppler}$, which is 9295.83Hz.

Hence, the parameters of microwave radar sensor IVS-162 can be set as Table 5.1,

Table 5.1- Parameters of Microwave Radar

Supply Voltage	V_{CC}	5V
Modulated Frequency	f_m	500Hz
Modulated Voltage	V_m	5V
Bandwidth	ΔF	125MHz
Sampling Frequency	f_s	50kHz
Range Resolution	δr	1.25m

The experimental equipment is shown in Fig. 5.7.

Figure 5.7- The System Prototype

The laboratory environment is shown in Fig.5.8. The measurement setup is tested in an open courtyard, the target is a metal board as an alternative to a real AGV for their similar materials. The whole system is placed about 1.7 meters above ground to avoid the interference from ground clutter.

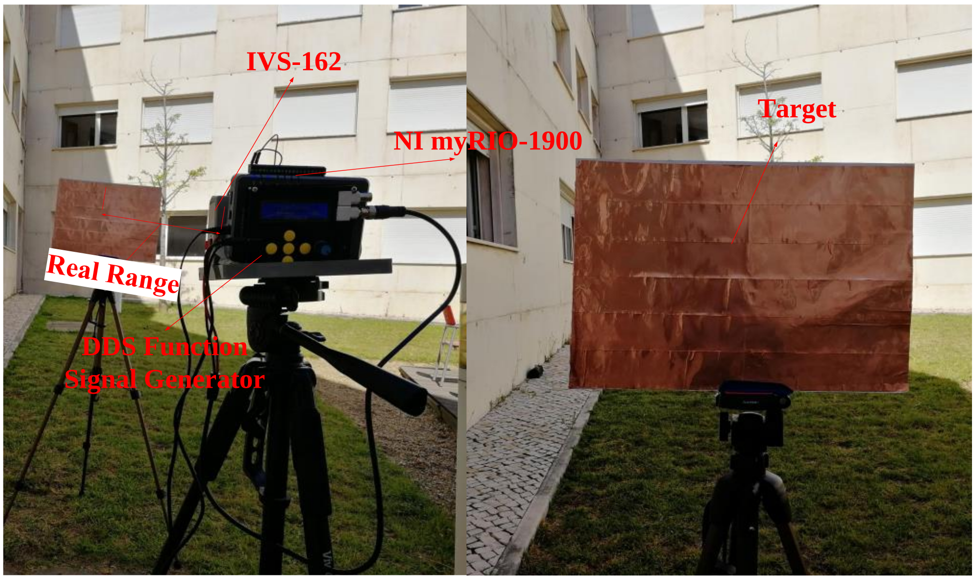

Figure 5.8- Experimental Setup

5.4.2 Experimental Results

Taking into account the limitations of experimental microwave Doppler radar performance, six tests were conducted for the static target, the ranges were 3m, 4m, 5m, 6m, 9m, 11m respectively. In tests, the target is a metal plate. Experimental results only verify the accuracy of ranging.

A 500Hz Butterworth high-pass filter was set to filter low-frequency noise such as modulated signal leakage in the beat signal. The wavelet denoising with adapted threshold function was used to filter high-frequency White Gaussian noise. The DWT used '*sym6*' as wavelet basis function, the level of wavelet decomposition was *4*.

In Fig. 5.9 is presented with the measured beat signal and the beat signal after wavelet denoising of target ranges of 6m and 11m. Comparing the signals can be underlined the capabilities of wavelet denoising with adapted threshold function applied algorithm that reduce the White Gaussian noise and improve the SNR of the beat signal.

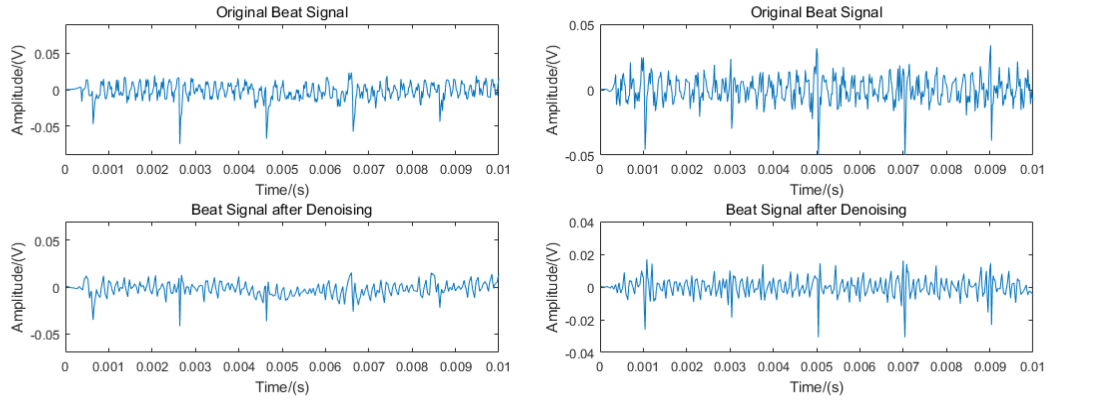

Figure 5.9- Measured Beat Signal and Denoising Beat Signal of 6m (Left) and 11m (Right) Range

After the noise was filtered out, the FFT and CZT joint algorithm is applied for the more pure beat signal to acquire the difference frequency of target mentioned above. The FFT size is chosen as 1024, and the CZT size is 256. The reason for choosing 256-size CZT is the range resolution can reach 0.9mm because of 0.38 Hz frequency resolution. Larger CZT size can also lead to poor real-time performance. Using 1024-point FFT to acquire spectrum.

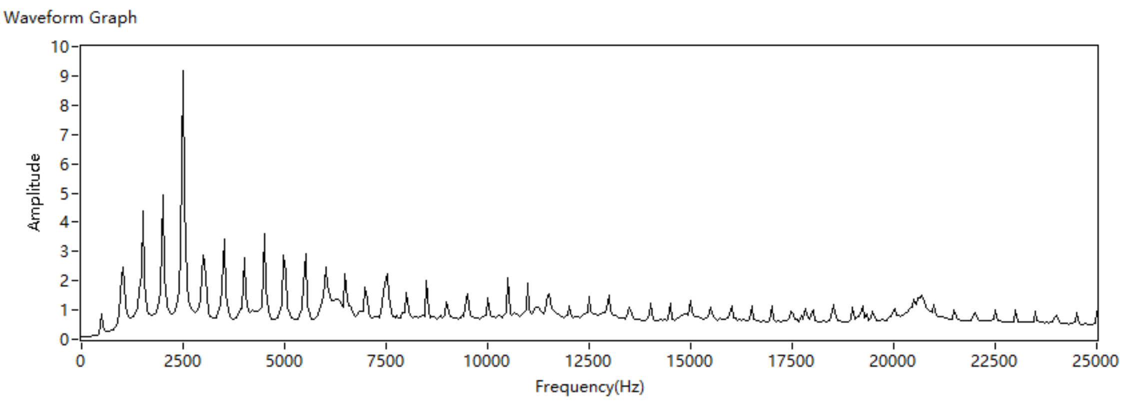

Figure 5.10- FFT Spectrum for 6m

Fig.5.10 describes the FFT spectrum of 6m-range, that is, the distance between radar and target is 6m. There is a peak of 51st point. The frequency of the 50th point is 2441.13Hz and the 52nd point is 2538.64Hz. Processing frequency interval [2441.13, 2538.64] by using 256-point CZT.

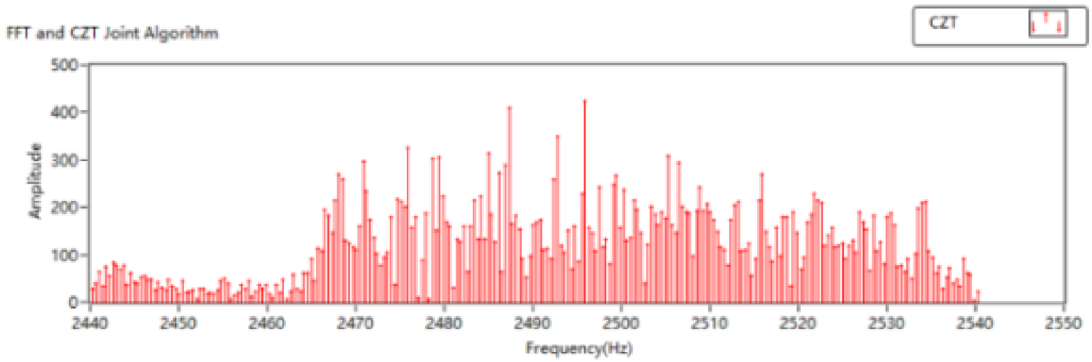

Figure 5.11- CZT Spectrum for 6m

CZT spectrum as shown in Fig.5.11. The 153rd point is the peak of CZT.

The results of the FFT and CZT joint algorithm of 11m as shown in Fig.5.12. Similarly, the 94th point is a peak of FFT and the frequency interval of 93rd points and 95th points is [4541.02, 4638.67]. Within this interval, the 106th point is a peak after 256-point CZT.

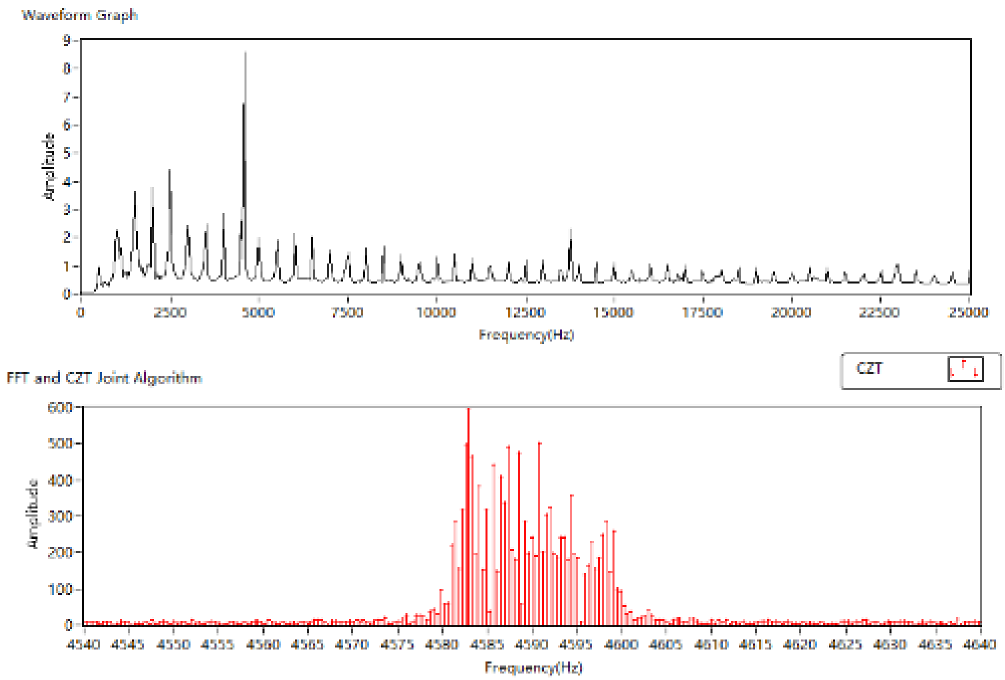

Figure 5.12- FFT and CZT joint Algorithm: FFT Spectrum and CZT Spectrum for 11m

From Fig.5.10, Fig.5.11, and Fig.5.12, it is easy to observe that different ranges of target produce different peak locations in the spectrum after 1024-point FFT. Therefore the frequency interval needed to use 256-point CZT to refine has a significant difference. According to differential frequencies, the ranges can be calculated. The experimental results can be seen in Table 5.2. The result is the mean obtained by repeating 20 times under the same method and experimental conditions.

Table 5.2- Range Measurement Experimental Results

	Real Range (m)	IVS-162			SP25 Result (m)
		Result 1[a] (m)	Result2[b] (m)	Result3[c] (m)	
Test 1	3.00	2.93	2.97	2.99	3.02
Test 2	4.00	3.82	3.89	3.95	3.93
Test 3	5.00	4.80	4.94	5.01	4.97
Test 4	6.00	5.86	5.97	5.99	6.05
Test 5	9.00	9.30	9.24	9.17	8.85
Test 6	11.00	11.25	11.02	10.99	11.03

[a.] Range only based on FFT

[b.] Range based on FFT and CZT Joint Algorithm, without Wavelet Denoisin

[c.] Range based on Wavelet Threshold Denoising and FFT and CZT Joint Algorithm

From the above table we can observe that all the values of Result 2 are closer to the real range than Result 1, and the errors of Result 2 are 1%, 2.75%, 1.2%, 0.5%, 2.67%, and 0.18% respectively. Because the spectrum after CZT reduces the fence effect, a more accurate frequency corresponding to the target can be obtained. Therefore the FFT and CZT Joint Algorithm is feasible in the short-range detection system of FMCW Doppler radar. For most optimization results as shown in Result 3, the errors of range detection accuracy go down to 0.33%, 1.25%, 0.2%, 0.17%, 1.88% and 0.09% respectively. And correspond to the application of wavelet denoising based on adapted threshold function and FFT and CZT joint algorithm at the same time to calculate the range of the target, finally has a satisfactory effect.

In addition, the errors from microwave radar system SP25 are 0.67%, 1.75%, 0.6%, 0.83%, 1.67%, 0.27% respectively. Therefore, comparing the two sets of results generated from two types of radar, they have roughly similar errors. Both range detection accuracy of IVS-162 and SP25 satisfy the requirement of AGV aid positioning in the port.

And five tests were conducted for moving target only to verify the effectiveness of the detected velocity.

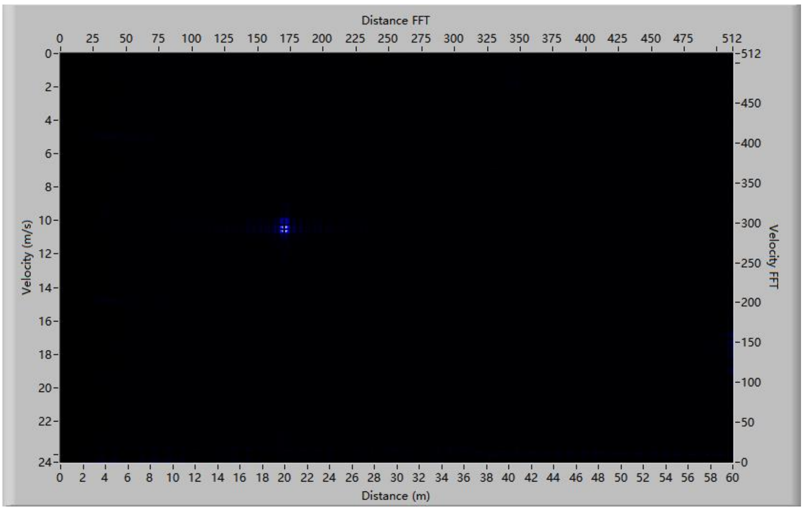

Figure 5.13- The Result 1 with Range is 20m and Velocity is 10m/s of Target

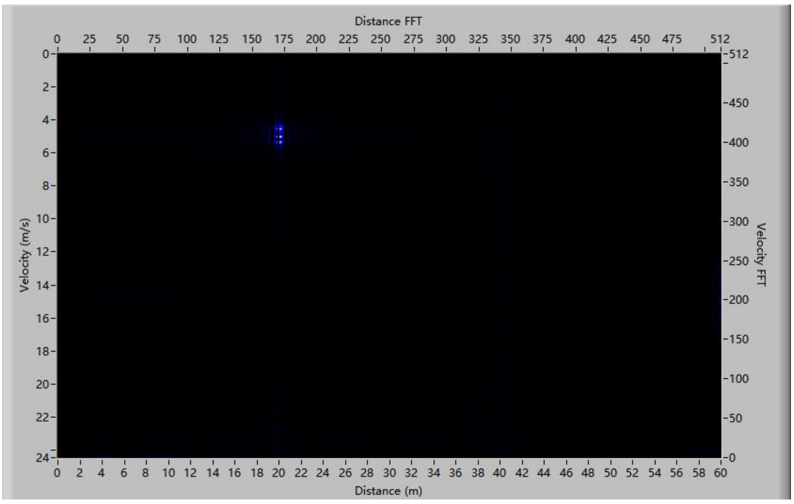

Figure 5.14- The Result 2 with Range is 20m and Velocity is 5m/s of Target

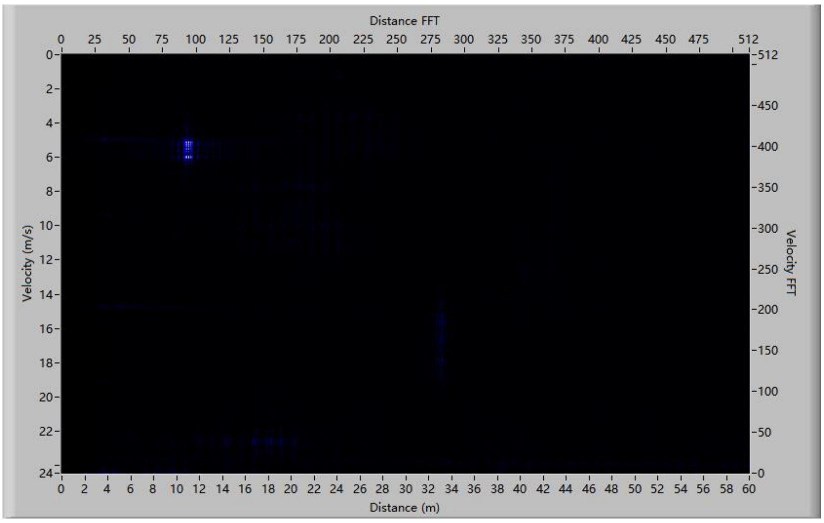

Figure 5.15- The Result 3 with Range is 11m and Velocity is 6m/s of Target

Figure 5.13, Figure 5.14 and Figure 5.15 are the results after 2D FFT. The X-axis (Distance (m)) represents the distance of the target, the Y-axis (Velocity (m/s)) is the velocity of the target. By using 2D FFT to extract the difference frequency and phase of the radar signal, the distance and velocity of the target are presented as blue dots in the resulting graph. The specific values are shown in Table 5.3.

Table 5.3- Velocity Measurement Experimental Results

	Real Distance (m)	Real Velocity (m/s)	IVS-162		SP25	
			Detected Distance (m)	Detected Velocity (m/s)	Detected Distance (m)	Detected Velocity (m/s)
Test 1	20.00	10.00	19.82	10.40	19.98	10.08
Test 2	20.00	5.00	20.14	5.05	19.98	5.10
Test 3	11.00	6.00	11.02	5.87	10.99	6.07
Test 4	8.00	6.00	8.07	6.14	8.01	5.93
Test 5	6.00	3.00	6.01	3.12	5.97	3.06

From Table 5.3, it can be inferred that the 2D FFT achieves good accuracy for speed estimation. In addition, the results of microwave Doppler radar system SP25 are shown in Table 5.3. Comparing the errors of the two types of radars, it can be found that both have accurate detection results.

Chapter 6. Positioning Method

According to the validation in Chapter 5, the IVS-162 and SP25 both have accurate detection results. The positioning system of this project consists of two microwave radar systems SP25s and two NI myRIO-1900s. This is because, as mentioned in Chapter 3, the message generated by SP25 contains the range and velocity information directly, and the horizontal of full-beam width (@-3dB) is 100° which is more suitable for AGV positioning. However, the horizontal of full-beam width (@-3dB) of IVS-162 is only 45°, which does not satisfy the design concept of the positioning system. Hence the positioning system consisting of two SP25s and two NI myRIO is the final step in the whole technology chain.

6.1 Reading Target Information

In order to read target information generated from microwave radar system SP25, it is necessary to parse the message from SP25.

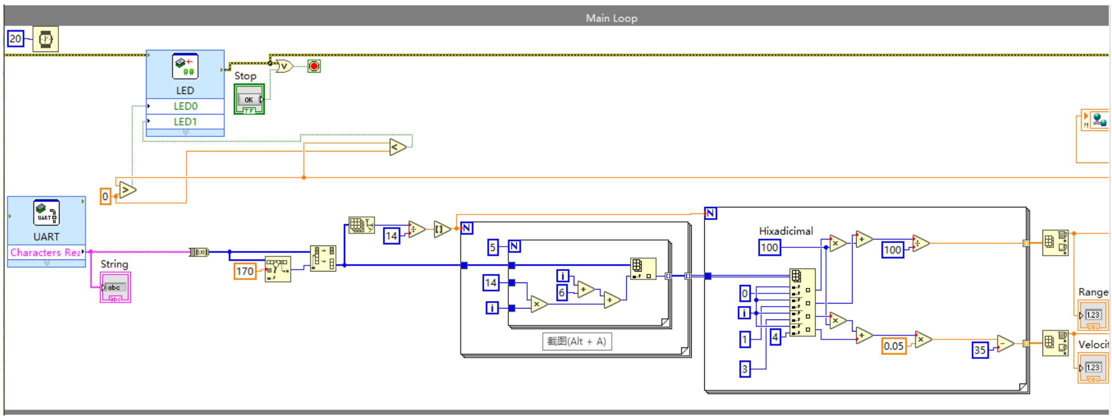

Figure 6.1- Main Program for Reading Target Information of SP25

As described in Chapter 3, after successfully connecting the TX and RX of SP25 with the TX and RX of myRIO, the message can be transmitted to PC via myRIO. The reading program is achieved in one myRIO Project, the programming language is LabVIEW, as shown in Figure 6.1.

To ensure that the message would not be lost, 20 milliseconds of Wait are selected to meet the 50Hz data update rate. In addition, the 'For' loop is set in this program to read the complete 14-bit message from the start sequence (0xAAAA) to terminating sequence (0x5555). The front panel of the reading program and example of the message is shown in Fig. 6.2.

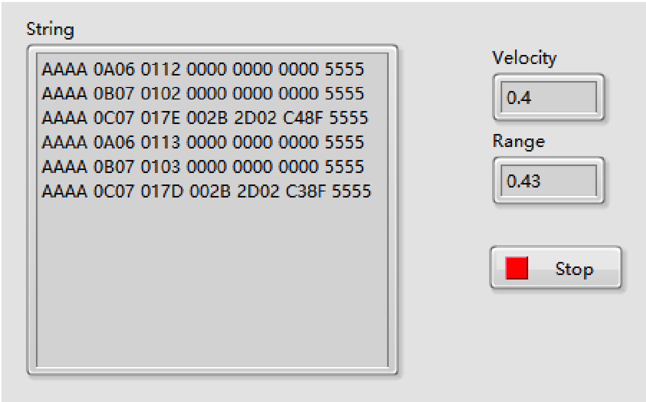

Figure 6.2- The Test of Single SP25 Microwave Radar System

6.2 Positioning Algorithm and Communication Method

In order to detect AGV in a defined area, a simple positioning algorithm is selected, as shown in Figure 6.3.

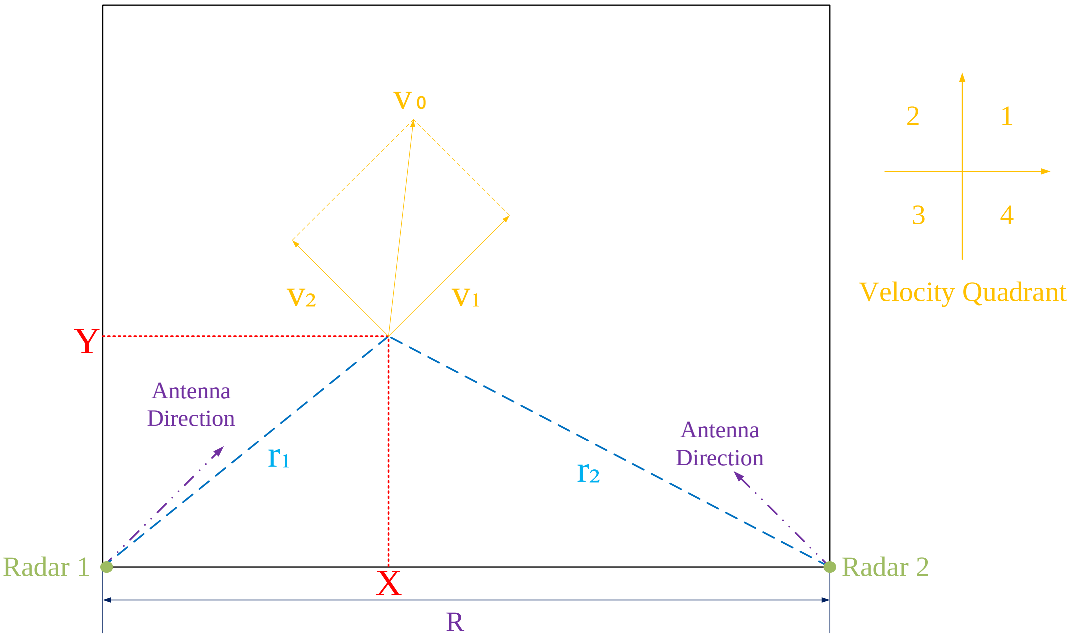

Figure 6.3- Main Positioning Method

It means, that in order for the area to be tested, two radar systems should be fixed in two corners of the area. The direction of the radar antenna is the same as the angle bisector, which can ensure cover for all the detected area. According to the real-time ranges r_1, r_2 and velocity v_1, v_2, the positioning information can be calculated from the triangle principle. The positioning coordinate *[X, Y]* can be calculated from the below equations,

$$X = \frac{r_1^2 - r_2^2 + R^2}{2R} \tag{6-1}$$

$$\mathrm{Y} = \sqrt{r_1^2 - (\frac{r_1^2 - r_2^2 + R^2}{2R})^2} \tag{6-2}$$

The velocity of the target (AGV) is,

$$v_0 = \sqrt{v_1^2 + v_2^2} \tag{6-3}$$

According to analysis, the real target (AGV) velocity is related to the sign of velocity components v_1 and v_2. The '+' sign of v_1 of radar 1 detected indicates that the target is moving away from the radar, the '-' sign is the target is approaching the radar. The v_2 is as same as v_1. In order to more clearly represent the direction of the target (AGV) movement, a velocity-based quadrant was established. If $v_1 > 0$, no matter the sign of v_2 is, the real velocity direction of the target (AGV) is,

$$\theta = \frac{\pi}{4} + arctan\frac{v_2}{v_1}, \theta\epsilon[-\pi, \pi] \tag{6-4}$$

If $v_1 < 0$, no matter the sign of v_2 is, the real velocity direction of the target (AGV) is:

$$\theta = -\frac{3\pi}{4} + arctan\frac{v_2}{v_1}, \theta\epsilon[-\pi, \pi] \tag{6-5}$$

After designing the positioning algorithm, the communication between myRIO to myRIO, myRIO to PC is necessary. As a description in Chapter 3, NI myRIO-1900 can connect with Wi-Fi, and also be a Wi-Fi gateway. When the myRIOs and the PC are under the same Wi-Fi environment, the communication between several myRIOs which under the same 'myRIO Project' can use 'Shared Variables' and Wi-Fi. In addition, the communication between myRIO and PC is using Wi-Fi. This advantage makes myRIO-1900 more popular in practical applications, such as a quadrotor UAV [56], a real-time radiation monitoring system [57], and the mobile robot [58]. The whole system is based on two NI myRIO-1900, as shown in Fig. 6.4. One named 'myRIO 38', the other named 'myRIO 55'. The Project 'New Project' is built under 'myRIO 38', as shown in Fig. 6.5. Then the 'myRIO 55' is searched and added in this Project. The 'myRIO 55' has self-starting and radar (*Radar 1*) signal processing function, then send both the range and velocity values to the 'myRIO 38' by shared variables 'Range01' and 'Velocity02'. At the same time, the 'myRIO 38' processes another radar (*Radar 2*) signal and calculates values of range and velocity for the target (AGV), at the same time receives the information from the ‘myRIO 55’ by Wi-Fi.

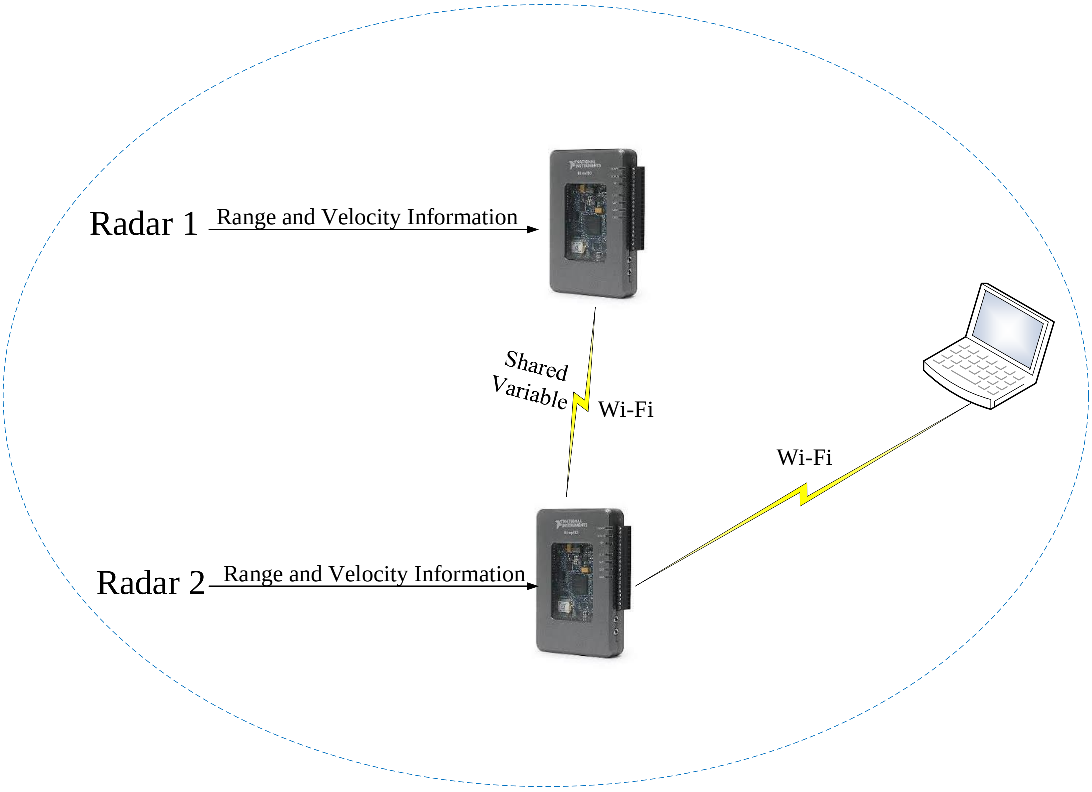

Figure 6.4- Positioning System

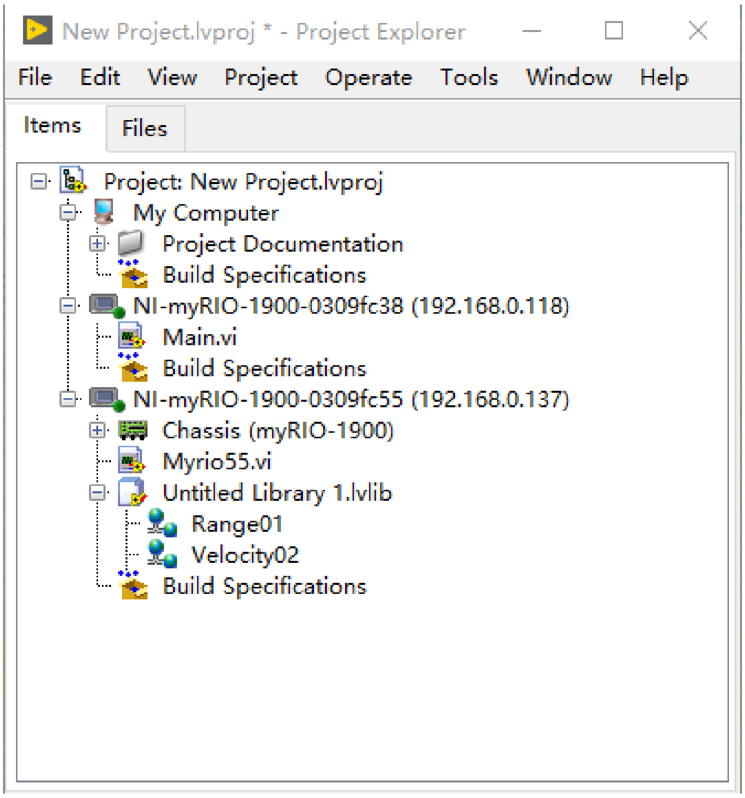

Figure 6.5- NI myRIO Project

6.3 Path of the AGV

In the actual port, the AGV needs to remain working at most of the time. Therefore it is necessary to track the real-time path of the AGV. When an AGV appears in the microwave Doppler radar detected area, each positioning coordinate constitutes the path of the AGV. Considering that how to extract the path of AGV from fixed quay cranes in actual ports and eliminate positioning errors in experiments, several works have been done. Several activities have been done in order to extract the path of the AGV from fixed cranes in actual ports and to eliminate positioning errors in experiments.

6.3.1 Positioning Error

For example, an AGV entered the radar detected area in a straight line, as shown in Fig. 6.6. The positioning errors have several reasons,

(1) Target misjudgment. The presence of known machines, such as overhead cranes and other non-AGV targets in the radar area causes the incoherence of detection points.

(2) Missing positioning information. The main reason for missing positioning information is, one radar detected target but another detected known machines. However, these two range values can't generate positioning information according to the positioning algorithm. Another reason is the loss of information due to system delay. In general, if the system is in a good Wi-Fi environment, the probability of the second reason affecting the system is small.

(3) Locate different targets. The reason is the same as (2).

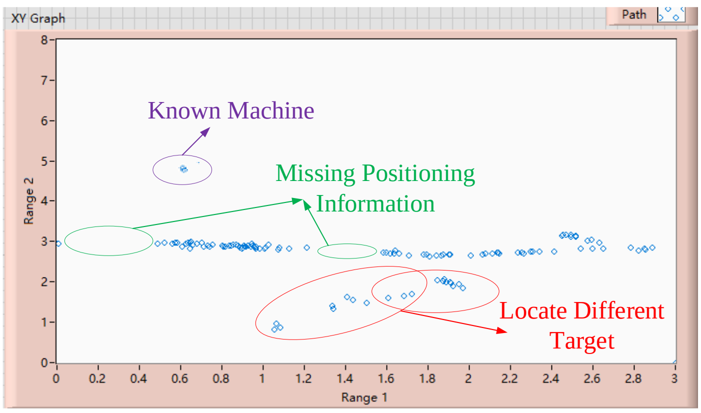

Figure 6.6 - The Errors in Actual Test

6.3.2 Positioning Error Handling

In order to remove the interference of known machines in the environment, these machines can be utilized as static features, and their distance from the antenna does not change over time. Therefore, for the interference of static objects, the positioning system needs to be fixedly placed in the space to be tested before the positioning, thereby all known machines positions appearing in the space to be tested are recorded.

In addition, in order to accurately track the trajectory of the target AGV, it is necessary to correct the error positioning information as described in Chapter 6.3.1.

The processing of path detection as shown in Fig. 6.7. The $[X_t, Y_t]$ is the positioning information of time *t*. If there a new location $[X_t, Y_t]$ appears in the system at time *t*, it can be considered that the AGV appearing in the radar area. In order to remove the wrong location from all locations, it is necessary to process positioning information one by one. f_{update} is the update frequency of positioning values.

In particular, before AGV began operating, the positioning system was put in the detected area. The system recorded the detected several locations which can be seen as the location of the known machines to ensure non-AGV location information would not affect the real AGV path. Set a threshold, if each new location information was smaller than the known location information, the positioning system would remain the dormant state. If not, the system began to record each information at time *t*. At first, the $[X_{t+1}, Y_{t+1}]$ at time *t+1* was compared with $[X_t, Y_t]$ at time *t*, the threshold here was v_{max}/f_{updata}. If the distance between $[X_{t+1}, Y_{t+1}]$ and $[X_t, Y_t]$ was smaller than v_{max}/f_{updata}, both location values can be recorded by the system. If not, calculating the distance between $[X_t, Y_t]$ at time *t* and $[X_{t+2}, Y_{t+2}]$ at time *t+2*, the threshold was set to $2 \times v_{max}/f_{updata}$. If the distance was smaller than $2 \times v_{max}/f_{updata}$, the positioning system saved $[X_t, Y_t]$ and $[X_{t+1}, Y_{t+1}]$, at the same time, gave up $[X_{t+1}, Y_{t+1}]$, if not, the positioning system gave up $[X_t, Y_t]$ and began to compare from $[X_{t+1}, Y_{t+1}]$.

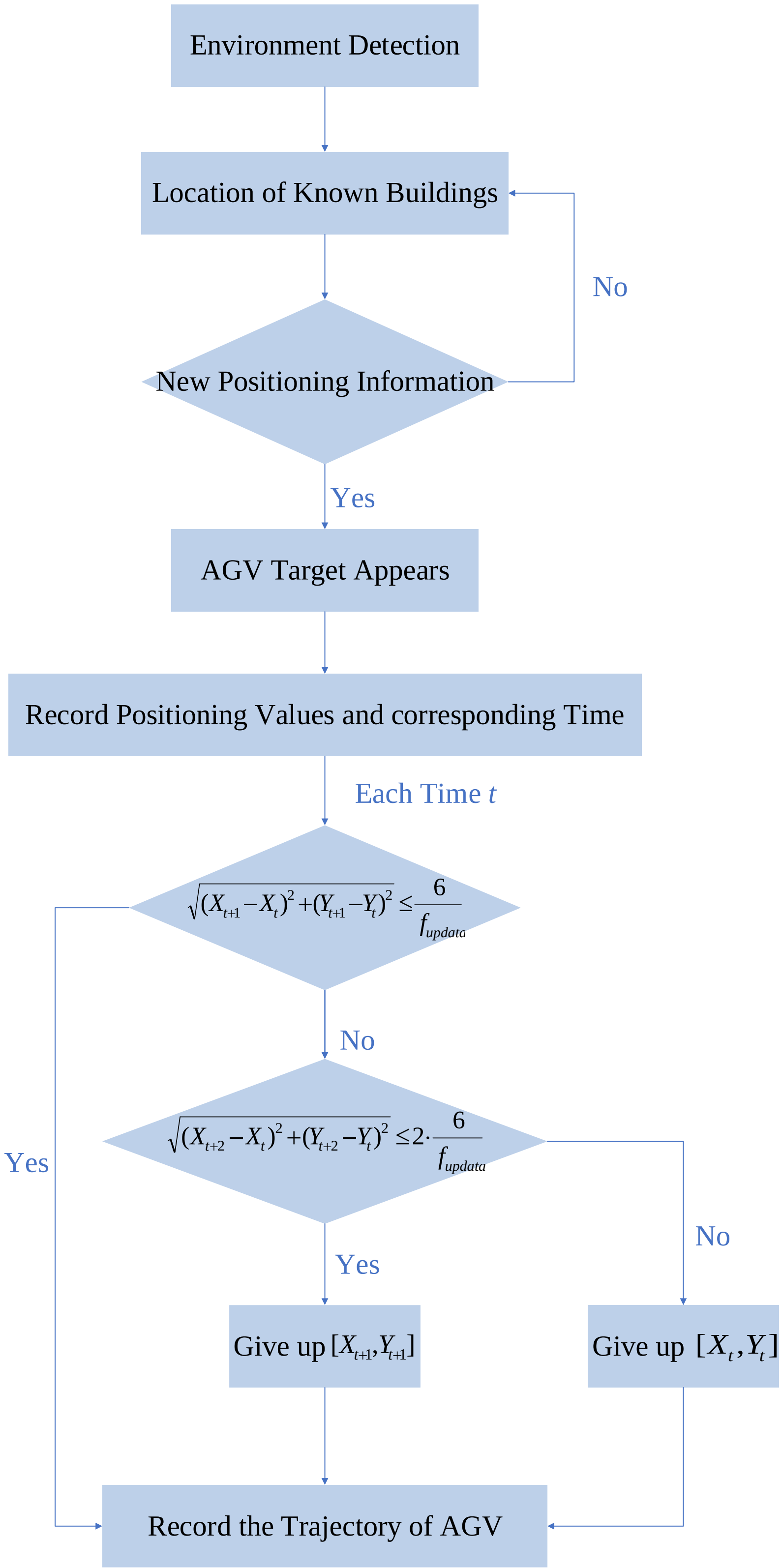

Figure 6.7- The Flow Chart of Path Generation

6.4 Experiment and Result

6.4.1 AGV Experimental Setup

The laboratory environment is the same as Chapter 5. All the positioning setups were tested in an open courtyard. To make the laboratory environment more similar to the real port, the target was a mobile vehicle, which can also drive on a prescribed trajectory like AGV. In addition, the area was $5 \times 5m^2$ which was 8 times smaller than the actual area from the quayside to the storage yard.

The whole positioning system was put as shown in Fig. 6.8. The microwave radar system 1 is set at the origin of coordinate, and it can be seen as [0, 0]. The other microwave system was set at the coordinate of [0, 5]. Each radar system contained a microwave radar system SP25, NI myRIO-1900 and a tripod. To verify the maximum horizontal angle of the detected area and the accuracy of experimental results, each radar system was placed 45 degrees in the same direction of the angle bisector definition.

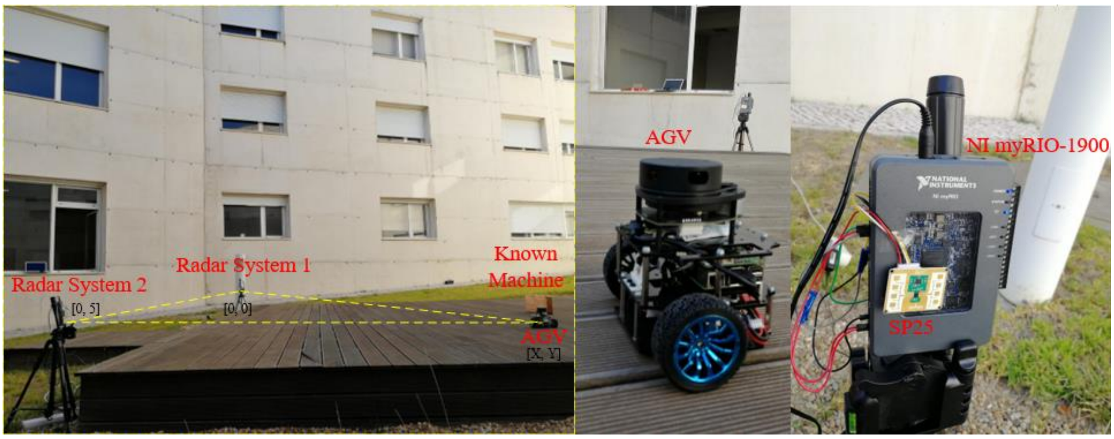

Figure 6.8- Laboratory Environment

6.4.2 Results

At first, the AGV was fixed in the area to detect the accuracy of stationary object positioning. In actual ports, this step can be also used to test environment when there has not any AGV operate, in addition, the software can record the position information and identify AGV to ensure that the AGV path will not go wrong.

The two experiments to detect the fixed target were performed, and their actual coordinates were [2, 2] and [4.3] respectively. Fig. 6.9 and Fig. 6.11 are the results of positioning information of [2, 2] and [4, 3]. The results selected 20 consecutive points from the positioning information and displayed in the figure. In addition, Figure 6.10 and Figure 6.12 are positioning errors. The errors can be calculated according to the equation $\varepsilon = \sqrt{(X - X_0)^2 + (Y - Y_0)^2}$, there, *[X, Y]* was the detected point from the system, $[X_0, Y_0]$ was the real position of the target.

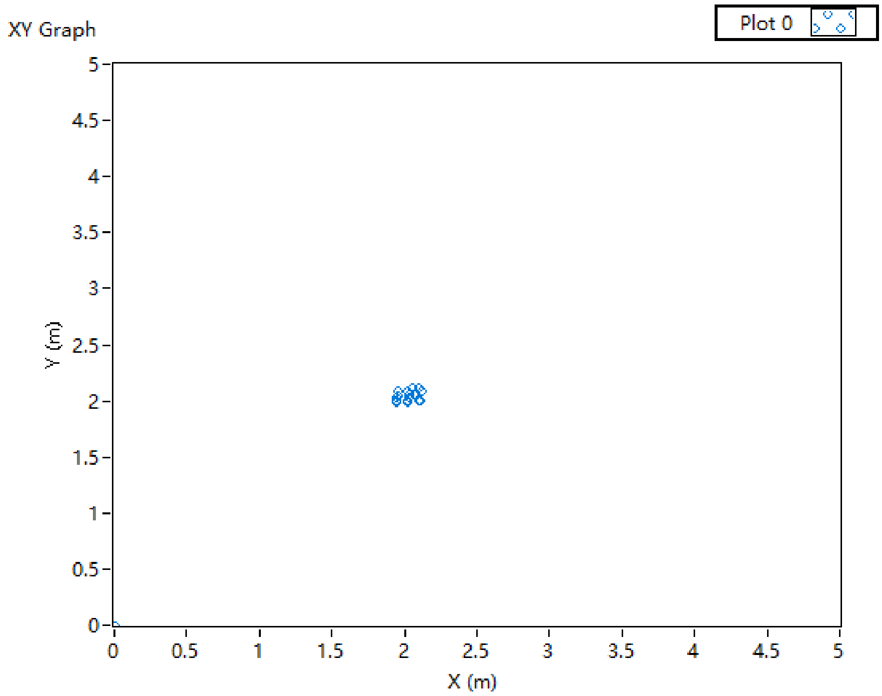

Figure 6.9- The Positioning Result at Point [2, 2]

Figure 6.10- The Absolute Error of Positioning Result at Point [2, 2]

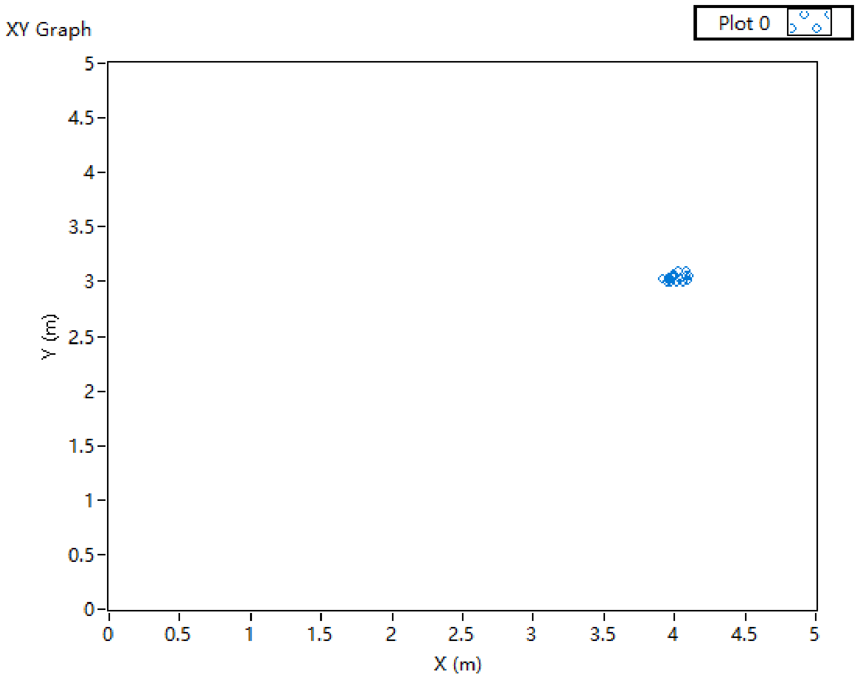

Figure 6.11- The Positioning Result at Point [4, 3]

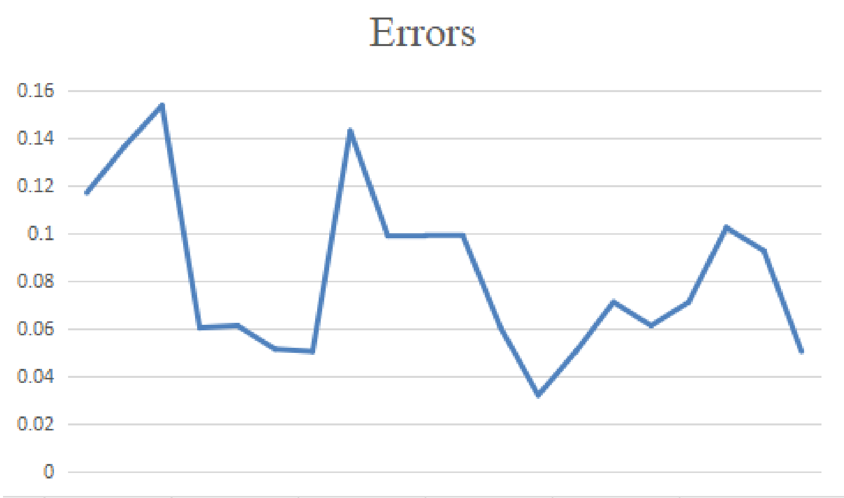

Figure 6.12- The Absolute Error of Positioning Result at Point [4, 3]

Form Figure 6.10 and Figure 6.12, it can be seen easily that the errors are between 2% to 15%, which satisfied the positioning requirements basically.

The next set of experiments was that a metal box, which can be thought about a known machine, was fixed in the detected area. The coordinate of the box was [3.5, 3.5]. AGV moved at a constant speed *v=1m/s* parallel to the X-axis from coordinates [1, 3]. The results without error processing as shown in Figure 6.13, the fixed metal box was easily distinguished from the AGV path.

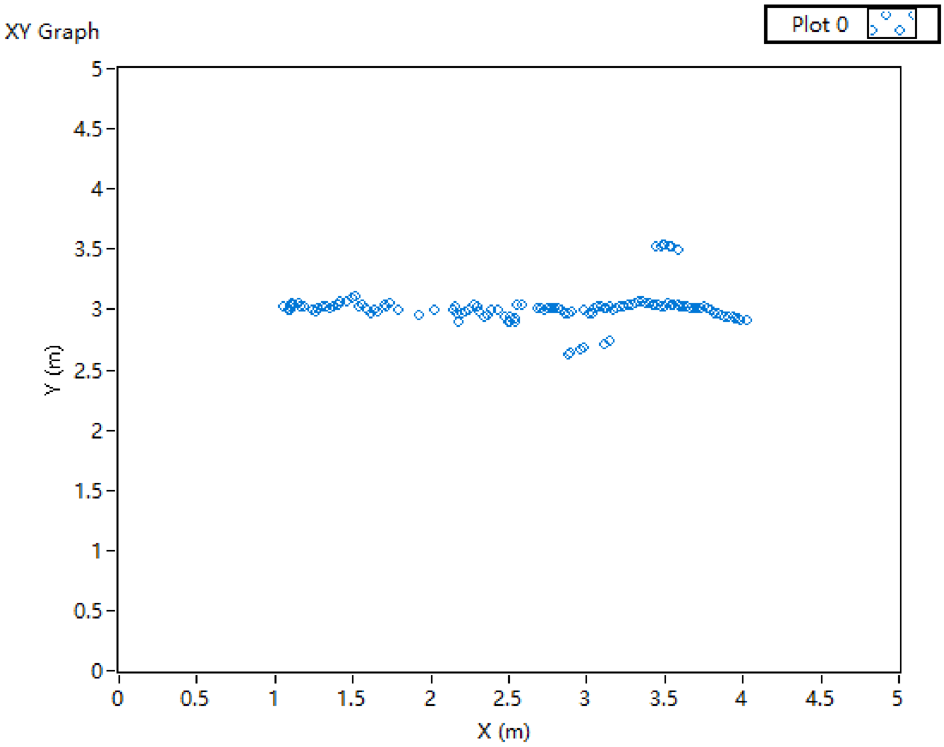

Figure 6.13 - The Test Result without Processing

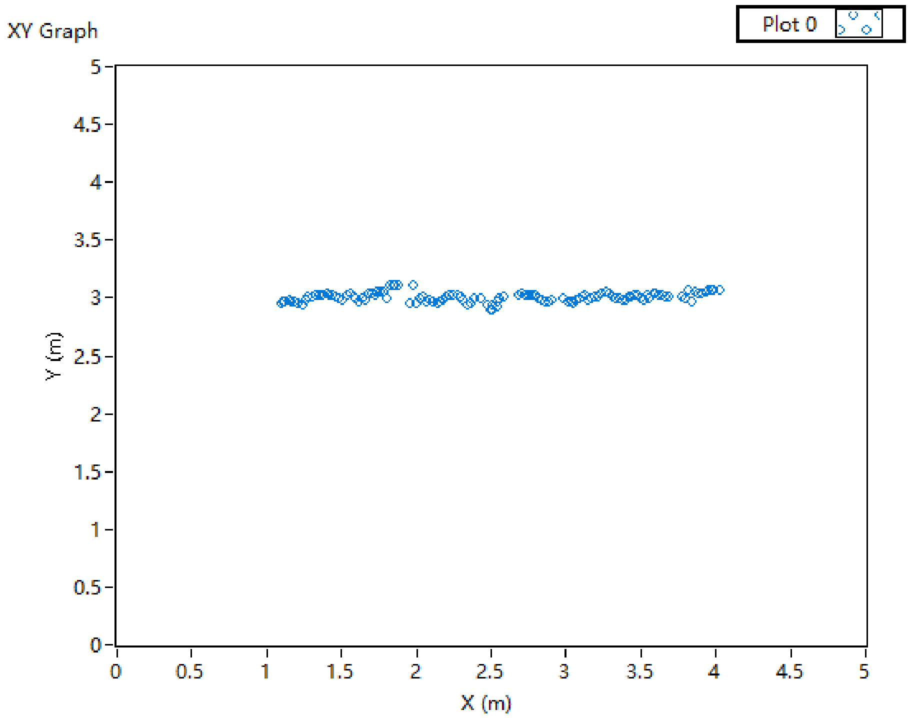

Figure 6.14 - The Test Result with Processing

From Figure 6.14 it can be observed, the method of error processing was useful for AGV path.

The last experiments were that the target moves in a rectangular path at the uniform velocity, and the results were shown in Fig. 6.15 and Fig. 6.16. The simulated AGV moved according to designed trajectory A with a speed of 5m/s. And the simulated AGV moved according to designed trajectory B with a speed of 2m/s.

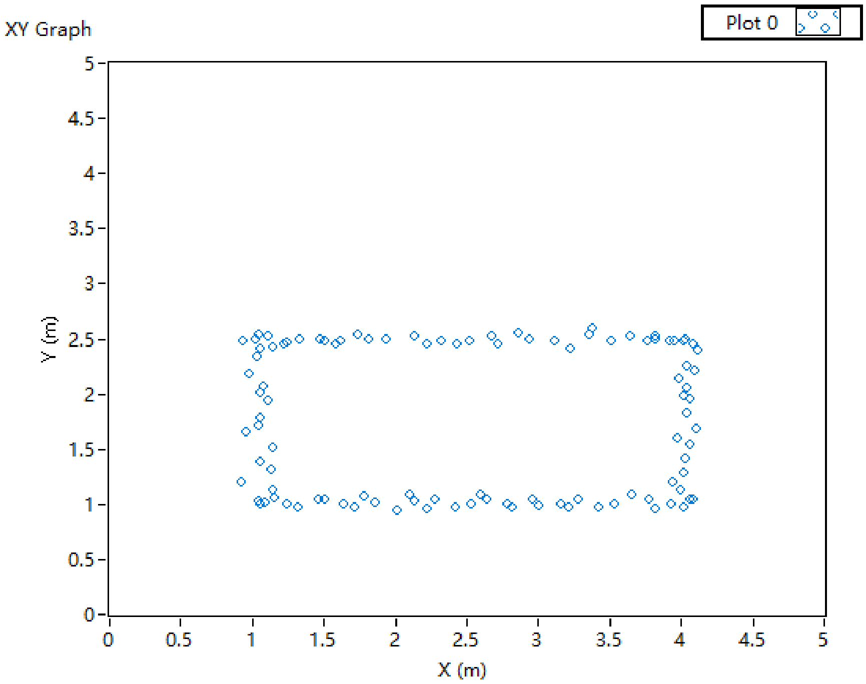

Figure 6.15- Positioning a Rectangular Path *A*

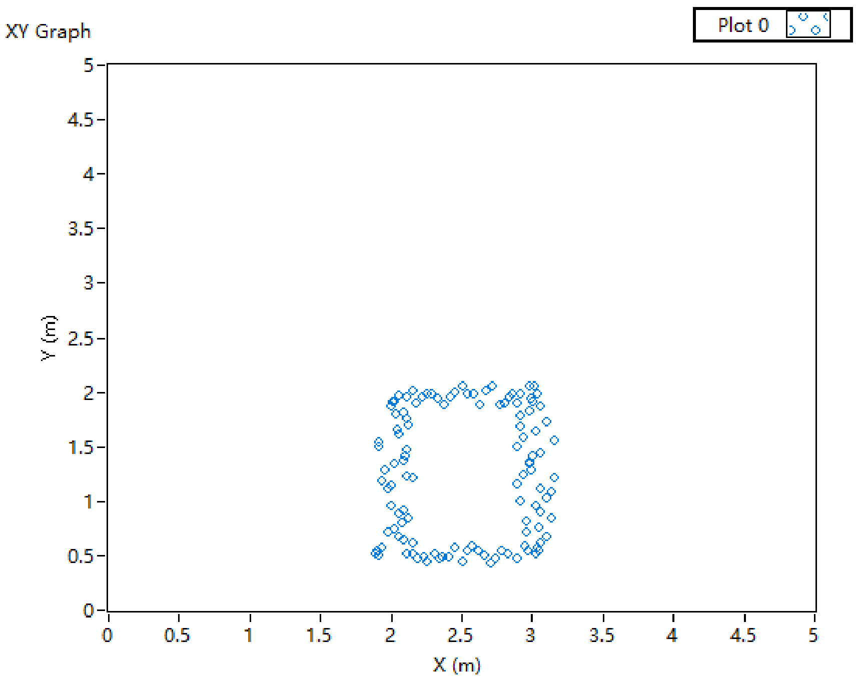

Figure 6.16- Positioning a Rectangular Path *B*

According to calculating, in the port-like environment, when the AGV speed was 5m/s, the absolute error was 11.89%. And when the AGV speed was 2m/s, the absolute error was about 15.71%, which can verify that the above algorithms were useful. In addition, it is feasible to use microwave Doppler radar for port AGV positioning.

Chapter 7. Conclusions and Future Work

7.1 Conclusions

An AGV positioning system based on microwave Doppler radar for the port including the hardware and software were designed and implemented, represent the reached goals of this thesis.

The system is designed as an alternative choice for the existing UHF RFID technology, which is more low cost and labor-saving. The system capabilities were tested and obtained real-time positioning information for AGV. The results can be displayed in the interface based on LabVIEW and monitored by the port management who can dispatch the AGV in time. Thus, the operation efficiency of the port would not be affected by the hostile environment (night, foggy et.al) or period of the RFID tags maintenance.

In order to achieve the light and portability of equipment, NI myRIO-1900 is used as a power source and ADC of microwave Doppler radar. Secondly, because of its built-in Wi-Fi, the wireless communication between myRIO and myRIO, myRIO and PC can be realized.

To achieve the goal of positioning, it is important to acquire distance and velocity information of the AGV in the detected area. Therefore, at first, proposed the wavelet denoising based on the adapted threshold function to filter unwanted noise and extract a more pure radar signal. Then considering that the fence effect brought by FFT and under the situation that will not affect the real-time performance of the whole system, FFT and CZT joint algorithm is selected to calculate the range value of AGV. In addition, 2D FFT is used to get the velocity value. The experimental results of using a microwave radar sensor can verify the validity of the above methods.

According to the parameters of the microwave Doppler radar system, an accurate positioning algorithm for AGV is proposed. The related tests were conducted and the system effectiveness is verified by analyzing the errors of the experimental results.

To summarize, the AGV positioning system based on microwave Doppler radar for the port is a novel idea and the results prove that microwave Doppler radar can be widely applied to the ports in the future.

7.2 Contributions

The Dissertation's main contributions are:

- Design and implementation of wireless AGV positioning system based on microwave Doppler radar for the port;
- A practical approach regarding filtering for radar signal based on wavelet denoising;
- The development and implementation of range and velocity detection for AGV by using spectrum zoom, which can not only improve accuracy but also improve the real-time performance of the whole system;
- Development of a real-time system and appropriate GUI for positioning information display.

The developed work and initial results were included in the article and the poster in Appendix A, which were accepted and presented at the IEEE ISSI 2019 international conference, August 29-30, Lisbon, Portugal. The article will be published in IEEE Xplorer.

Lin Ma, Octavian Adrian Postolache, Haiqing Yao and Yongsheng Yang, "Short-Range Detection Scheme based on Microwave Doppler Radar and Wavelet Denoising with Adapted Threshold Function", ISSI 2019, Lisbon Portugal 2nd International Symposium on Sensing and Instrumentation in IoT Era.

7.3 Future Work

Despite being a fairly complete system, improvements can still be made, both software and hardware. Further testing of the system also may be performed in different situations, such as the more dark or cloudy environment.

The system only implements a single target ranging and it is not suitable for complex environments that have two or more targets. In future work, the target recognition from a known environment will be considered.

It is necessary to implement a central switch to turn on / off all equipment at the same time, which will save energy and be more convenient for the worker in the port.

In the real port environment, depending only on the communication of Wi-Fi will not satisfy the range of detected area, the other communication protocol such as 4G or others will be considered.

Reference

[1] "The Port Group (homeport) Throughput." [Online]. Available: http://http://www.portshanghai.com.cn/jtwbs/webpages/server_teu.html.

[2] "Half-Year Report 2019." [Online]. Available: https://www.portofrotterdam.com/sites/default/files/half-year-report-port-of-rotterdam-authority-2019.pdf?token=6_097xkb. [Accessed: 22-July-2019].

[3] Yang, Yongsheng, et al. "Internet of things for smart ports: Technologies and challenges." *IEEE Instrumentation & Measurement Magazine* 21.1 (2018): 34-43.

[4] Droitcour, Amy, et al. "A microwave radio for Doppler radar sensing of vital signs." *2001 IEEE MTT-S International Microwave Sympsoium Digest (Cat. No. 01CH37157)*. Vol. 1. IEEE, 2001.

[5] Urazghildiiev, I. R., et al. "A vehicle classification system based on microwave radar measurement of height profiles." (2002): 409-413.

[6] Xuan, Yiguang, et al. "A high-range-resolution microwave radar system for traffic flow rate measurement." *Proceedings. 2005 IEEE Intelligent Transportation Systems, 2005.*. IEEE, 2005.

[7] Park, Seongkeun, et al. "Vehicle tracking using a microwave radar for situation awareness." *Control Engineering Practice*18.4 (2010): 383-395.

[8] Zyweck, Anthony, and Robert E. Bogner. "Radar target classification of commercial aircraft." *IEEE Transactions on Aerospace and Electronic systems* 32.2 (1996): 598-606.

[9] Ke Zhang, Guohua Yu and Ganghai Liu. "Research on Processing Method of Ultrasonic Ranging Echo Signal". Diss. 2008.

[10] Rongyi, Ji, Zhao Changming, and Ren Xuecheng. "High precision and high frequency pulse laser ranging system [J]." *Infrared and Laser Engineering* 40.8 (2011): 1461-1464.

[11] Lin, Jenshan, and Changzhi Li. "Wireless non-contact detection of heartbeat and respiration using low-power microwave radar sensor." *2007 Asia-Pacific Microwave Conference*. IEEE, 2007.

[12] Skolnik, Merrill I. "Introduction to radar." *Radar handbook* 2 (1962): 21.

[13] Richards, Mark A. *Fundamentals of radar signal processing*. Tata McGraw-Hill Education, 2005.

[14] Chang K, Schuss J. Computer simulation of radome effects for the Doppler weather radar antenna system[C]//Digest on Antennas and Propagation Society International Symposium. IEEE, 1989: 1542-1545.

[15] Ruck, George T., et al. *Radar cross section handbook*. Vol. 1. New York: Plenum press, 1970.

[16] Gill, T. P. The Doppler Effect, An Introduction to the Theory of the Effect. Logos Press, Limited, 1965

[17] LighthartLP N L R. System aspect solid-state FM-CW weather surveillance radar[J]. Conference Proceeding, 1987, 19(21,112): 115.

[18] Chadwick R.B, Strauch R.G. Processing of FM-CW Doppler radar signals from

Distributed Target[J]. IEEE Trans on AES, 1976, 15(1),185-188
[19] Knapp W, Wigger B. Experiments with near-clutter-suppressing FMCW radar[C]. Conference Proceeding 16th European Microwave Conference, 1986, 329-33.
[20] Lighthart L.P. Fix target clutter Suppression using a polarimetric FMCW radar[C]. Conference Proceeding, 1989, 14-16, 590-595.
[21] Rouveure R , Faure P , Monod M O . PELICAN: Panoramic millimeter-wave radar for perception in mobile robotics applications, Part 1: Principles of FMCW radar and of 2D image construction[J]. Robotics and Autonomous Systems, 2016, 81:1-16.
[22] Ayhan, Serdal, et al. "Impact of frequency ramp nonlinearity, phase noise, and SNR on FMCW radar accuracy." IEEE Transactions on Microwave Theory and Techniques 64.10 (2016): 3290-3301.
[23] CHEN Wenhui, LIU Qin, LIU Xiomin, et al. Application of wavelet threshold denoising method in signal processing of FMCW radar. Computer Engineering and Applications, 2015, 51(8):195-199. (in Chinese)
[24] Chen, Ying, and C. Han. "Adaptive wavelet threshold for image denoising." *Electronics Letters* 41.10 (2005): 586-587.
[25] Chang, S. Grace, Bin Yu, and Martin Vetterli. "Spatially adaptive wavelet thresholding with context modeling for image denoising." *IEEE Transactions on image Processing* 9.9 (2000): 1522-1531.
[26] Alfaouri, Mikhled, and Khaled Daqrouq. "ECG signal denoising by wavelet transform thresholding." *American Journal of applied sciences* 5.3 (2008): 276-281.
[27] Poornachandra, S. "Wavelet-based denoising using subband dependent threshold for ECG signals." *Digital signal processing* 18.1 (2008): 49-55.
[28] Ruskai, Mary Beth. "The World according to wavelets." American Scientist 85.1 (1997): 85-87.
[29] Messer, Sheila R., John Agzarian, and Derek Abbott. "Optimal wavelet denoising for phonocardiograms." *Microelectronics journal* 32.12 (2001): 931-941.
[30] Giaouris, D., and J. W. Finch. "Denoising using wavelets on electric drive applications." Electric Power Systems Research78.4 (2008): 559-565.
[31] Hu, Yi, and Philipos C. Loizou. "Speech enhancement based on wavelet thresholding the multitaper spectrum." IEEE transactions on Speech and Audio processing 12.1 (2004): 59-67.
[32] Debin, CHEN Zhixin XU Jinwu YANG. "New method of extracting weak failure information in gearbox by complex wavelet denoising." Chinese Journal of Mechanical Engineering 21.4 (2008): 87-91.
[33] Srivastava, Madhur, C. Lindsay Anderson, and Jack H. Freed. "A new wavelet denoising method for selecting decomposition levels and noise thresholds." *IEEE Access* 4 (2016): 3862-3877.
[34] Cui, Hua, and Guoxiang Song. "A Kind of Modified Project Based on the Wavelet Treshold Denoising Method [J]." *Modern Electronic Technique* 1 (2005).
[35] J. S. Lee, Y. W. Su, and C. C. Shen, “A comparative study of wireless protocols: Bluetooth, UWB, ZigBee, and Wi-Fi,” IECON Proc. (Industrial Electron. Conf.,

vol. 4, no. 6, pp. 46–51, 2014.

[36] “Connectivity of the Internet of Things.” [Online]. Available: https://learn.sparkfun.com/tutorials/connectivity-of-the-internet-of-things. [Accessed: 12-Jan-2018].

[37] Feifei Zhu. Research on 3D collision prevention algorithm based on millimeter wave radar location. Diss. [Chinese]

[38] Kester, Walt. "Taking the mystery out of the infamous formula," snr= 6.02 n+ 1.76 db," and why you should care." *Analog Devices Tutorial, MT-001 Rev. A* 10.08 (2009).

[39] Kai Zhao. Radar design and signal processing of automobile anti-collision system. Diss. [Chinese]

[40] Jensen, Arne, and Anders la Cour-Harbo. *Ripples in mathematics: the discrete wavelet transform*. Springer Science & Business Media, 2001.

[41] Mallat, Stephane G. "A theory for multiresolution signal decomposition: the wavelet representation." IEEE Transactions on Pattern Analysis & Machine Intelligence 7 (1989): 674-693.

[42] Percival, Donald B., and Andrew T. Walden. Wavelet methods for time series analysis. Vol. 4. Cambridge university press, 2006.

[43] Postolache, O., et al. "Multi-usage of microwave Doppler radar in pervasive healthcare systems for elderly." 2011 IEEE International Instrumentation and Measurement Technology Conference. IEEE, 2011.

[44] Stirman, Charles. Applications of Wavelets to Radar Data Processing. No. OA-11606. MARTIN MARIETTA ELECTRONICS AND MISSILES GROUP ORLANDO FL MISSILE SYSTEMS, 1991.

[45] Jing-yi, Lu, et al. "A new wavelet threshold function and denoising application." *Mathematical Problems in Engineering* 2016 (2016).

[46] Huimin, C. U. I., Zhao Ruimei, and H. O. U. Yanli. "Improved threshold denoising method based on wavelet transform." Physics procedia 33 (2012): 1354-1359.

[47] Rouveure, Raphaël, Patrice Faure, and Marie-Odile Monod. "PELICAN: Panoramic millimeter-wave radar for perception in mobile robotics applications, Part 1: Principles of FMCW radar and of 2D image construction." Robotics and Autonomous Systems 81 (2016): 1-16.

[48] Gunther, Jacob H. "Simultaneous DFT and IDFT of real N-point sequences." IEEE Signal Processing Letters 9.8 (2002): 245-246.

[49] Wang, Tien T. "The segmented chirp z-transform and its application in spectrum analysis." IEEE Transactions on instrumentation and measurement 39.2 (1990): 318-323.

[50] Rabiner, Lawrence R., Ronald W. Schafer, and Charles M. Rader. "The chirp z-transform algorithm and its application." Bell System Technical Journal 48.5 (1969): 1249-1292.

[51] Corinthios, Michael J. "A fast Z transformation algorithm for system identification." IEEE Transactions on Computers 100.1 (1977): 55-67.

[52] Kronauge, Matthias, Christoph Schroeder, and Hermann Rohling. "Radar target detection and Doppler ambiguity resolution." 11-th INTERNATIONAL RADAR

SYMPOSIUM. IEEE, 2010.
[53] Andres, Markus, et al. "Detection of slow moving targets using automotive radar sensors." 2012 The 7th German Microwave Conference. IEEE, 2012.
[54] Molchanov P, Gupta S, Kim K, et al. Short-range FMCW monopulse radar for hand-gesture sensing[C]//2015 IEEE Radar Conference (RadarCon). IEEE, 2015: 1491-1496
[55] Winkler, Volker. "Range Doppler detection for automotive FMCW radars." 2007 European Radar Conference. IEEE, 2007.
[56] Bouallègue, Soufiene, and Rabii Fessi. "Rapid control prototyping and PIL co-simulation of a quadrotor UAV based on NI myRIO-1900 board." coordinates 3 (2016): 3.
[57] Vo, Hong Hai, et al. "Development of real-time radiation monitoring system using embedded FPGA NI myRIO and INSPECTOR+." (2015).
[58] Caldeira, Tiago, Hamad Al Remeithi, and Ibrahim Al Raeesi. "MyRIO based mobile robot for rescue competitions." *2017 IEEE International Conference on Autonomous Robot Systems and Competitions (ICARSC)*. IEEE, 2017.

Appendix A – Scientific Articles

Article: **Short-Range Detection Scheme of FMCW Doppler Radar based on Wavelet Denoising with Adapted Threshold Function**. This article has been accepted and presented at IEEE ISSI 2019 international conference, August 29-30, Lisbon, Portugal and will be published in IEEEXplorer.

Organized by IEEE International Symposium on Sensing and Instrumentation in IoT Era (ISSI) Organizing Committee, IEEE Instrumentation and Measurement Society. The conference was held in Lisbon, Portugal. Lisbon is capital and the largest city of Portugal. It is a vibrant global city since 15th century with top class historical, educational and research establishments, modern architectures, as well as diverse mix of cultures, landscapes and tastes.

Short-Range Detection Scheme based on FMCW Doppler Radar and Wavelet Denoising with Adapted Threshold Function

Lin Ma
[1]Instituto de Telecomunicações, ISCTE- Instituto Universitário de Lisboa, Portugal
[2]Institute of Logistics Science & Engineering
Shanghai Maritime University
Shanghai, China
lmani@iscte-iul.pt

Octavian Postolache
Instituto de Telecomunicações
ISCTE-Instituto Universitário de Lisboa
Lisbon, Portugal
opostolache@lx.it.pt

Haiqing Yao
Institute of Logistics Science & Engineering
Shanghai Maritime University
Shanghai, China
haiqing8612@163.com

Yongsheng Yang
Institute of Logistics Science & Engineering
Shanghai Maritime University
Shanghai, China
yangys_smu@126.com

***Abstract*—Range detection is the key to solve localization, tracking, navigation and other applications. Several solutions, such as LIDAR range sensor, is commonly used to achieve range detection. Considering that the microwave Doppler radar has the advantages of being unaffected by humidity, temperature and light variation, so it is more suitable for complex environment. The paper proposed a Frequency Modulated Continuous Wave (FMCW) Doppler radar system to perform short range detection of the target. Several methods were considered to extract the range information. According to the principle of FMCW radar, beat signal can be analyzed. Due to the complexity of the working environment, the beat signal contains various noise jamming. In order to eliminate noise contained in the beat signal, wavelet denoising method with the adapted threshold function was considered. In the frequency domain analysis, traditional FFT causes fence effects. FFT and CZT joint algorithm is proposed to suppress the influence of fence effects and improves real-time performance. The experimental results based on above methods are included in the paper.**

Keywords*—*FMCW radar, microwave Doppler radar, range detection, wavelet denoising, CTZ

I. INTRODUCTION

Microwave Doppler radar is extensively applied in military applications and civil aviation. Compared with LIDAR range sensor, the microwave Doppler radar is suitable for complex environmental conditions (day and night, fog, rain and snow), because that the microwave has longer wavelength than other electromagnetic waves, such as infrared rays, so microwave has better penetration. Microwave Doppler radar provides robust target range information even in degraded visual conditions [1]. It can also operate from -20 to +60 degrees Celsius and its power is only 175mW. Therefore, microwave Doppler radar is favored by researchers. There are a lot of measurement systems based on microwave Doppler radar reported in the literature.

Siska Aulia et al. [2] proposed a method for range detection of static targets based on Fast Fourier Transform (FFT). M.O.Monod et al. [3] used a new intertwined linear waveform principle to detect range, therefore got excellent resolution and accuracy. Wei Liu et al. [4] used millimeter-wave radar combined with flight control unit to control altitude of Unmanned Air Vehicle (UAV) and the results indicated that the accuracy of radar sensor satisfied the main requirements. Volker Winkler et al. [5] achieved different range resolutions by generating different slope of modulated frequency. Hao-Hsien Ko et.al [6] proposed a modified method of range detection based on curve fitting through analyzed output signal of FMCW mixer, and range resolution improving by 20 times. Eugin Hyun et.al [7] proposed the method of target detection using FMCW radar. The power spectral density of the up- and down- beat frequency is used to suppress the ghost target and detect the lost target. Faiza Ali et.al [8] reported a 2-D range processing method for Frequency-Modulated Continuous-Wave (FMCW) radar signal, the use of this method is suitable for detection of moving target. Stephan Max et.al [9] used phase assessment to detect target, even under the circumstance of strong noise and clutter. Mario Pauli et.al [10] presented a signal processing method that combined frequency evaluation with phase evaluation of FMCW radar Intermediate Frequency (IF) signals, and the accurate location information indicated that the algorithm was effective.

In this paper, the range measurement using microwave doppler radar was considered. Therefore, the beat signal which contained range information, obtained from 24GHz K-Band microwave Doppler radar sensor IVS-162 (from InnoSenT) was processed to extract the range information. The first part introduces the advantages of microwave Doppler radar and the related works. The second part describes the measurement principles of microwave Doppler radar and FMCW for radar. The third part includes the Digital Signal Processing (DSP) of beat signal about Discrete Wavelet Transform (DWT) to denoising with the adapted threshold function. Next part presents FFT and CZT joint algorithm to thinning difference frequency. The content of last part is hardware description, and the experimental results followed by conclusions.

II. FMCW Radar

The FMCW radar can simultaneously measure the range, velocity, and motion direction of one or more targets. The frequency band of the FMCW radar is selected according to the actual application. For example, 24GHz-77GHz [11-12] is used in vehicle field, and the maximum detection range can reach to 200m [13]; the FMCW radar of 1GHz-12GHz is used in snow depth [14], its accuracy is up to 1.6cm; in addition, the frequency of 2.4GHz-24GHz is used to monitor weak variations such as respiratory conditions [15]. In this paper, 24GHz FMCW radar is used to detect the target about 3 meters to 20 meters.

A. Microwave Doppler Radar - Hardware

Microwave Doppler radar transmits signal by using one antenna, the other antenna receives reflected signal after signal meets obstacles. Fig.1 shows the Radio Frequency (RF) front end of microwave Doppler radar receiver. The Voltage Controlled Oscillator (VCO) receives modulated signal and outputs signals of different frequencies. After directional coupling, most of the signals are transmitted through the transmitted antenna, another small part is divided into two parts and output to the mixer as the local oscillator signal. The signal of the Q channel needs to be phase shifted by 90° before mixing. The obtained mixed signal is subjected to filtering and amplifying processing, and finally two Intermediate Frequency (IF) signals of IF1 and IF2 are obtained. The distance can be calculated according to the IF signal, that is, beat signal.

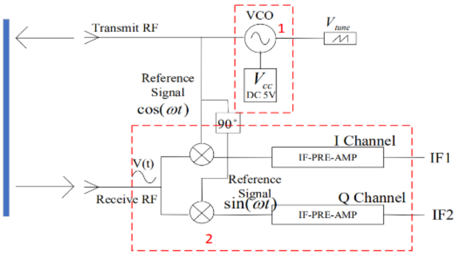

Fig.1 The Chart of RF front end

At most research domain, FMCW microwave Doppler radar is used to acquire the distance (range) between the radar and target characterized by high electrical conductivity. Therefore, the range can be calculated considering the time delay between transmitted and received signal.

B. FMCW Doppler Radar Measurement Method

For a static test scenario (static radar and static target), the transmitted signal which is modulated by Sawtooth wave has the period of $t_m = 1/f_m$, as is presented in Fig.2. The bandwidth ΔF depends on the modulated signal, and its central point is the transmitted center frequency f_0.

Range r_i can be expressed as time delay between transmitted signal and received signal, that is,

$$\Delta t = 2r_i/c \tag{1}$$

Among them, c is the light speed. Beat signal $S_b(t)$are represented as [16],

$$S_b(t) = k\sum_i a_t\, a_{ri}\cos(2\pi\left(2\Delta F\cdot f_m\frac{r_i}{c}\right)t+\emptyset_i \tag{2}$$

Where, a_t is the amplitude of transmitted signal, a_{ri} and $\emptyset_i$ are amplitude and phase of received signal, k is mixed coefficient. From (2), beat signal $S_b(t)$ is the sum of frequency component f_{bi} and $\emptyset_i$ phase from target i. For each specific target i, f_{bi},

$$f_{bi} = 2\Delta F\cdot f_m\frac{r_i}{c} \tag{3}$$

So the range of target i can be expressed as,

$$r_i = \frac{c\cdot f_{bi}}{2\Delta F\cdot f_m} \tag{4}$$

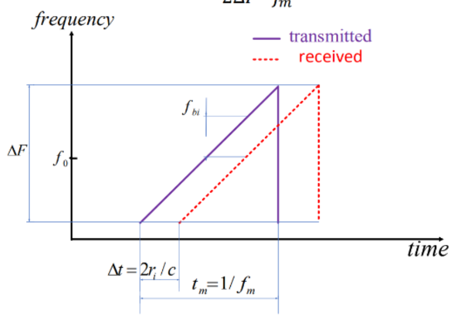

Fig.2 FMCW Principle

C. Range Measurement Resolution

Range resolution is defined as the ability to distinguish two rather near objects. From (4), frequency component is proportional to range of target i. In this case, assuming that range resolution is equal to frequency resolution, which is related to range resolution,

$$\delta f = \frac{1}{t_m} = f_m \tag{5}$$

So the range resolution δr is,

$$\delta r = \delta f\frac{c}{2\Delta F\cdot f_m} = \frac{c}{2\Delta F} \tag{6}$$

It can be observed in (6), the minimum detection range of radar only depends on bandwidth ΔF. Range resolution can be changed by adjusting the bandwidth. Higher range resolution can be obtained by increasing the bandwidth.

III. The Signal Processing of Noise

A. Noise Analysis of Beat Signal

Noise sources of FMCW radar mainly have internal systematic noise and external environmental noise. When the receiver and transmitter working simultaneously, the noise which is generated by the leakage of transmitted signal will cause the received signal to submerge in the leakage signal. Therefore, internal systematic noise normally refers to the leakage of modulated signal and is low frequency signal compared with useful beat signal. Generally, the high-pass filter is adopted to handling internal systematic noise, it can be effectively suppressed. External environmental noise usually contains thermal of antenna and industrial interference. Therefore, all the useful signal is submerged in the non-stationary and random noise. This part of noise expressed as White Gaussian noise.

B. Discrete Wavelet Transform

The Wavelet Transform (WT) is suitable for analyzing abrupt signal and non-stationary signal. In addition, WT has the characteristics of multi-resolution analysis and bandpass filter, and can be implemented by fast algorithm, so it is often used for filtering and denoising. The WT uses a mother wavelet function with fast decay and oscillation. Stretching and translating the mother wavelet to get a set of wavelet basis functions. The basic idea of wavelet transform is to use wavelet basis functions to represent or approximate the signal. When processing noisy signal using WT, it is necessary to discretize the wavelet and use the Discrete Wavelet Transform (DWT). The DWT is a batch method, which can analyse a finite-length time-domain signal at different frequency bands and different resolutions by successive decomposition into coarse approximation and detail information [17].

The Fig.3 indicates DWT decomposition process of the discrete-time signal (X). Among them, c_J is the detailed coefficients and d_J is the approximation coefficients. In return, approximate coefficients information is low frequency component, detailed coefficients information is high-frequency component. At the end of decomposition, no matter what decomposition levels it is, there has a wavelet decomposition tree, each layer has two branches, one is detail and another is approximation which has their own coefficients. Formula (7) is an example of 4-layer decomposition,

$$X = d_1 + d_2 + d_3 + d_4 + c_4 \qquad (7)$$

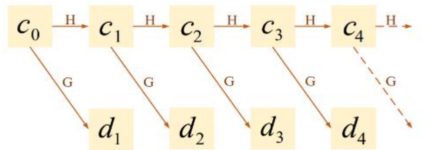

Fig.3 The Decomposition Process of DWT

Discrete beat noisy signal of FMCW radar is expressed by,

$$X_i = S_{bi} + n_i \qquad (8)$$

Where, X_i is measured signal including with white noise, S_{bi} is useful beat signal to extract range information, n_i is white noise, i is sampling order. However the white Gaussian noise is not continue in the time domain, therefore the wavelet coefficients have strong randomness after DWT, that is, the coefficients corresponding to the noise still satisfy the Gaussian distribution.

The processes of DWT are, at first, choose a suitable mother wavelet. There have common mother wavelets which can support DWT and suit for actual signal denoising, as showed in Table 1,

TABLE I. COMMON MOTHER WAVELET

Name	***Haar***	***Daubechies***	***Coiflets***	***Symlets***
Representation	haar	dbZ	coifZ	symZ

Wavelet basis functions are formed by scaling and translating transforms based on mother wavelets. Fig.4 presents examples of common wavelet basis function that are characterized by orthogonality.

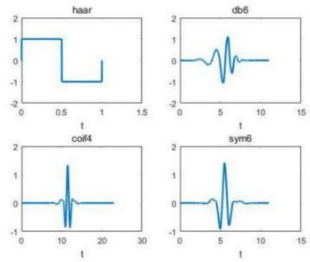

Fig.4 Examples of Wavelet Basis Function

In this case, wavelet basis function 'sym6' is considered according to [21], which can acquire maximum Signal-to-Noise Ratio (SNR) for FMCW radar signal.

Next step is to determine the number of decomposition layers J. In general, the larger J is, the easier it is to distinguish between signal and noise, and the better the denoising effect, but the larger the reconstruction error. FMCW beat signal is usually decomposed into 3-5 levels [18-19]. In the j^{th} level, the formula (9) is used to calculated wavelet coefficients of c_j and d_j by orthogonal DWT [20],

$$\begin{cases} c_{j,k} = \sum_{n=-\infty}^{+\infty} c_{j-1,n} h_{n-2k} \\ d_{j,k} = \sum_{n=-\infty}^{+\infty} c_{j-1,n} g_{n-2k} \end{cases} \qquad (9)$$

Where, h and g are orthogonal filter banks to each other. $c_{j,k}$ is the k^{th} detailed coefficient, $d_{j,k}$ is the k^{th} approximate coefficient. And $k = 1,2,\cdots,K$.

C. Wavelet denoising method with adapted threshold function

The key step is to select the appropriate threshold. Each wavelet coefficient $d_{j,k}$ is compared with threshold $thr(j)$. The threshold is,

$$\text{thr(j)} = \varepsilon\sqrt{\ln(K_j)} \qquad (10)$$

Where, j is present decomposition level, K_j is the j^{th} level length of wavelet coefficients, ε is standard deviation of signal, and ε needs to estimate from the noisy beat signal by using formula (11),

$$\varepsilon = median(|d_{j,k}|)/0.6745 \qquad (11)$$

Each $d_{j,k}$ compares with $thr(j)$ according to formula (12) to filter the Gaussian white noise in measured noisy beat signal.

$$\hat{d}_{j,k} = \begin{cases} \operatorname{sgn}(d_{j,k})\left(|d_{j,k}| - \dfrac{3\cdot thr(j)}{3 + e^{\sqrt{(\frac{d_{j,k}}{thr(j)})^2 - 1}}}\right), |d_{j,k}| \ge thr(j) \\ 0, |d_{j,k}| < thr(j) \end{cases} \qquad (12)$$

Finally, the signal S' is reconstructed, and the reconstructed signal is the denoised signal. The flow chart of wavelet denoising based on the adapted threshold function is shown in Fig.5.

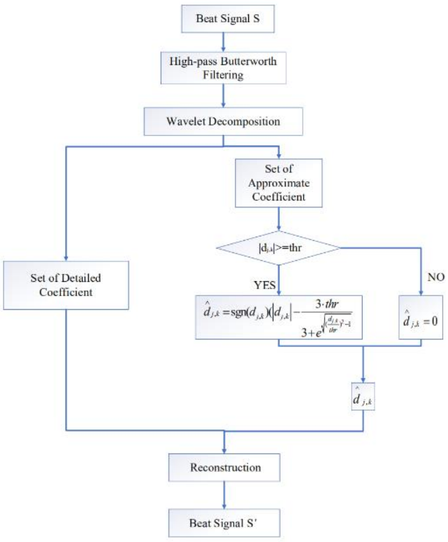

Fig.5 The Flow Chart of Wavelet Denoising based on Adapted Threshold Function

IV. FFT AND CZT JOINT ALGORITHM

Usually the DSP of beat signals requires FFT as a spectrum analyser. FFT is a fast calculation algorithm for Discrete Fourier Transform (DFT), transforms the time domain sampling of the beat signal into the frequency domain sampling to extract difference signal which contained range information. The spectrum of beat signal by using FFT produces sampling interval ΔR,

$$\Delta \mathrm{R} = \frac{f_s}{M} \tag{13}$$

Where, f_s is sampling frequency, M is sampling points of FFT.

The fence effect is due to M-point FFT is limited to M sample points, and the spectral value between the two-point sampling interval is indistinguishable. The fence effect produces an error Δr for the distance, can cause a magnitude loss of the spectral line corresponding to a target [21]. According to formula (4), the Δr can be calculated by,

$$\Delta r = \Delta R \cdot \frac{c}{2 \cdot \Delta F \cdot f_m} \tag{14}$$

Although increasing the points of FFT (normally, the sampling points number is 2^n, for example, 1024) can be used to decrease the Δr, but computation time will increase, resulting in real-time processing not be allowed.

In practical applications, only a certain segment of the discrete spectrum in the beat signal contains target information, so it is vain to refine all the spectrum. The CZT is an improvement of a Z-Transform [22], it can be used to calculate the transformation on any curve on the unit circle [23]. For i-point length time signal $S(i)$, the CZT of length N-point is defined as,

$$\mathrm{X}(z_r) = CZT[S(i)] = \sum_{i=0}^{I-1} S(i) z_r^{-i} = \sum_{i=0}^{I-1} S(i) A^{-i} W^{ir} \tag{15}$$

Where, $A = A_0 e^{j\theta_0}$, $W = W_0 e^{-j\varphi_0}$, θ_0 is the onset angular frequency, φ_0 is the sampling interval. When $A_0 = W_0 = 1$, it sample on the unit circle, formula (15) change to,

$$\mathrm{X(r)} = \sum_{i=0}^{I-1} x(i) \exp[-j(\theta_0 + \varphi_0 r) i] \tag{16}$$

There $\theta_0 = 2\pi f_x / f_s$, $\varphi_0 = 2\pi f_L / (N f_s)$. Among them, f_x is the starting frequency of analytical spectrum, f_L is the length of analytical spectrum. Thus the frequency resolution of CZT is $\Delta F' = f_L / N$.

The process of FFT and CZT joint algorithm is shown in Fig.6. Firstly, the beat signal is processed by M - point FFT. From spectrum, the m^{th} point is the peak corresponding to the target. The frequency of m^{th} point can be calculated by relation (17),

$$f_{m^{th}} = \frac{f_s}{M} \cdot m \tag{17}$$

The frequency values f_{m-1} and f_{m+1} of two adjacent point $(m-1)$ and $(m+1)$ is calculated. The maximum value m'^{th} and corresponding frequency value $f_{m'^{th}}$ can be counted by using N-point CZT during frequency interval $f_L = [f_{m-1}, f_{m+1}]$ which need to refine. The range information of target can be acquired form $f_{m'^{th}}$ and relation (4).

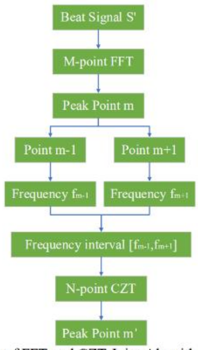

Fig.6 The Flow Chart of FFT and CZT Joint Algorithm

Theoretically, the FFT and CZT joint algorithm can not only improve the calculation accuracy, but also improve the real-time processing performance of whole the system [24-25].

V. EXPERIMENTAL RESULTS AND DISCUSSIONS

A. Experimental Setup

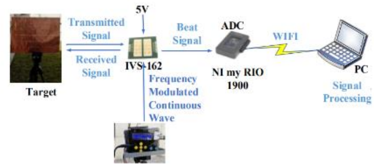

Fig.7 Laboratory Experimental setup block diagram

The hardware platform is shown in Fig.7. The arbitrary waveform generation module is used to generate Sawtooth waveform with modulation frequency of 500Hz. IVS-162 radar sensor transmits FMCW to target and generates beat signal. The beat signal transmits to the PC through Wi-Fi by using NI my RIO 1900. And the function of my RIO 1900 also has Analog-to-Digital (ADC). The experimental equipment is shown in Fig.8. And the main technical parameters are shown in Table 2.

Fig.8 The System Prototype

TABLE II. FMCW DOPPLER RADAR CHARACTERISTICS

Supply Voltage	V_{cc}	5.0V
Transmitted Frequency	f_0	24.000-24.125GHz
Bandwidth	ΔF	125MHz
Modulation Voltage	V_{tune}	5.0V
Modulation Frequency	f_m	500Hz
Full Beam Width @ -3dB	azimuth	45°
	elevation	38°
Sampling Frequency	f_s	5×10^4Hz
Range Resolution	δ_r	1.2m
Maximum Range	R_{max}	20m

The laboratory environment as shown in Fig.9. The measurement setup is tested in an open courtyard, and the target is a metal board, which has a stronger reflection of microwave. The whole system is placed about 1.7 meters above ground to avoid the interference from ground clutter.

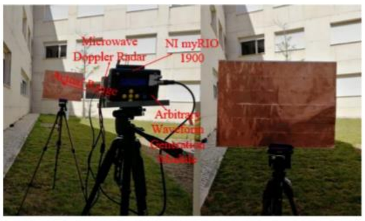

Fig.9 Range measurement Experimental setup

B. Experimental Results

Six tests were conducted, the ranges were 3m, 4m, 5m, 6m, 9m, 11m respectively. In tests, the target is a metal plate.

A 500Hz Butterworth high-pass filter was set to filter low-frequency noise such as modulated signal leakage in the beat signal. The wavelet denoising with adapted threshold function was used to filter high-frequency White Gaussian noise. The DWT used 'sym6' as wavelet basis function, the level of wavelet decomposition was 4.

In Fig.10 is presented the measured beat signal and the beat signal after wavelet denoising of target ranges of 6m and 11m. Comparing the signals can be underlined the capabilities of wavelet denoising with adapted threshold function applied algorithm that reduce the White Gaussian noise and improve the SNR of beat signal.

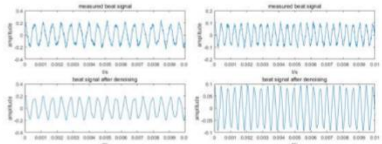

Fig.10 Measured Beat Signal and Denoising Beat Signal of 6m (Left) and 11m (Right) Range

After the noise was filtered out, the FFT and CZT joint algorithm is applied for the purer beat signal to acquire difference frequency of target which mentioned above. The FFT size is chosen as 1024, and CZT size is 256. The reason for 256-point CZT size is the fence effect has been reduced to 0.38Hz, the corresponding range accuracy can reach 0.9mm that is satisfying short-range detection. Larger CZT size can also lead to poor real-time performance. Using 1024-point FFT to acquire spectrum.

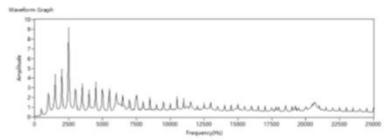

Fig.11 FFT Spectrum which the radar-target range is 6m

Fig.11 describes the FFT spectrum of 6m-range, that is, the distance between radar and target is 6m. There is a peak of 51st point. The frequency of 50th point is 2441.13Hz and 52nd point is 2538.64Hz. Processing frequency interval [2441.13, 2538.64] by using 256-point CZT.

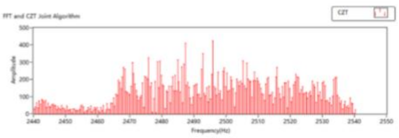

Fig.12 CZT Spectrum for a radar-target range of 6m

CZT spectrum as shown in Fig.12. The 153rd point is the peak of CZT.

The results of FFT and CZT joint algorithm of 11m as shown in Fig.13. Similarly, 94th point is a peak of FFT and frequency interval of 93th points and 95th points is [4541.02, 4638.67]. Within this interval, 106th point is a peak after 256-point CZT.

From Fig.11, Fig.12 and Fig.13, it is easy to observe that different ranges of target produce different peak locations in spectrum after 1024-point FFT. Therefore, the frequency interval needed to use 256-point CZT to refine has significant difference. According to formula (4), the range can be calculated. The experimental results can be seen in Table III. In the Table III can observed that all the values of Result 2 are closer to the real range than result 1, and the errors of Result 2 are 1%, 2.75%, 1.2%, 0.5%, 2.67% and 0.18% respectively.

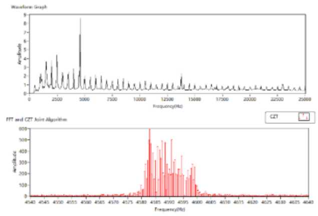

Fig.13 FFT and CZT joint Algorithm: FFT Spectrum and CZT Spectrum of 11m

TABLE III. RANGE MEASUREMENT EXPERIMENTAL RESULTS

	Real Range (m)	Result 1[a] (m)	Result 2[b] (m)	Result 3[c] (m)
Test 1	3.00	2.93	2.97	2.99
Test 2	4.00	3.82	3.89	3.95
Test 3	5.00	4.80	4.94	5.01
Test 4	6.00	5.86	5.97	5.99
Test 5	9.00	9.30	9.24	9.17
Test 6	11.00	11.25	11.02	10.99

a. Range only based on FFT

b. Range based on FFT and CZT Joint Algorithm, without Wavelet Denoisin

c. Range based on Wavelet Threshold Denoising and FFT and CZT Joint Algorithm

Because the spectrum after CZT reduces the fence effect, a more accurate frequency corresponding to the target can be identified. Therefore, the FFT and CZT Joint Algorithm is feasible in short-range detection system of FMCW Doppler radar. The most optimization results as shown in Result 3, the errors of range detection accuracy go down to 0.33%, 1.25%, 0.2%, 0.17%, 1.88% and 0.09% respectively. And correspond to the application of wavelet denoising based on adapted threshold function and FFT and CZT joint algorithm at the same time to calculate range of target, finally has a satisfactory effect.

VI. CONCLUSION

In this paper, a short-range ranging scheme based on wavelet denoising for FMCW microwave radar is designed. The adapted threshold function of DWT is proposed to process noisy beat signal. To improve real-time performance and ranging accuracy of system, FFT and CZT joint algorithm is applied in range calculating. The experimental results verify the feasibility of the above methods.

The scheme only implements single target ranging and it is not suitable for complex environments which have two or more targets. In the future work, the target recognition from known environment will be considered.

ACKNOWLEDGEMENTS

This work is supported by the Shanghai Science and Technology Commission (No. 19595810700, 18295801100, 175958810300) and Yunnan Science and Technology Program (No. 2018IB022).

REFERENCES

[1] Brakke, Thomas W., et al. "Microwave radar response to canopy moisture, leaf-area index, and dry weight of wheat, corn, and sorghum." Remote Sensing of Environment 11 (1981): 207-220.

[2] Aulia S , Suksmono A B , Munir A . Stationary and moving targets detection on FMCW radar using GNU radio-based software defined radio[C]// International Symposium on Intelligent Signal Processing & Communication Systems. IEEE, 2016.

[3] Monod M O, Faure P, Rouveure R. Intertwined linear frequency modulated radar and simulator for outdoor robotics applications[C]//Radar. 2009, 9: 06-12.

[4] Liu W, Yu C, Wang X, et al. The altitude hold algorithm of UAV based on millimeter wave radar sensors[C]//2017 9th International Conference on Intelligent Human-Machine Systems and Cybernetics (IHMSC). IEEE, 2017, 1: 436-439.

[5] Winkler V. Range Doppler detection for automotive FMCW radars[C]//2007 European Radar Conference. IEEE, 2007: 166-169.

[6] Ko H H, Cheng K W, Su H J. Range resolution improvement for FMCW radars[C]//2008 European Radar Conference. IEEE, 2008: 352-355.

[7] Hyun E, Lee J H. A meothod for multi-target range and velocity detection in automotive FMCW radar[C]//2009 12th International IEEE Conference on Intelligent Transportation Systems. IEEE, 2009: 1-5.

[8] Ali F, Vossiek M. Detection of weak moving targets based on 2-D range-Doppler FMCW radar Fourier processing[C]//German Microwave Conference Digest of Papers. IEEE, 2010: 214-217.

[9] Max S, Vossiek M, Gulden P. Fusion of FMCW secondary radar signal beat frequency and phase estimations for high precision distance measurement[C]//2008 European Radar Conference. IEEE,2008: 124-127.

[10] Pauli M, Ayhan S, Scherr S, et al. Range detection with micrometer precision using a high accuracy FMCW radar system[C]//International Multi-Conference on Systems, Sygnals & Devices. IEEE, 2012: 1-4.

[11] Winkler, Volker. "Range Doppler detection for automotive FMCW radars." 2007 European Radar Conference. IEEE, 2007.

[12] Folster, Florian, Hermann Rohling, and Urs Lubbert. "An automotive radar network based on 77 GHz FMCW sensors." IEEE International Radar Conference, 2005.. IEEE, 2005.

[13] Hyun, Eugin, and Jong-Hun Lee. "Method to improve range and velocity error using de-interleaving and frequency interpolation for automotive FMCW radars." International Journal of Signal Processing, Image Processing and Pattern Recognition 2.2 (2009): 11-21.

[14] Marshall, Hans-Peter, and Gary Koh. "FMCW radars for snow research." Cold Regions Science and Technology 52.2 (2008): 118-131.

[15] Anitori, Laura, Ardjan de Jong, and Frans Nennie. "FMCW radar for life-sign detection." 2009 IEEE Radar Conference. IEEE, 2009.

[16] Rouveure, Raphaël, Patrice Faure, and Marie-Odile Monod. "PELICAN: Panoramic millimeter-wave radar for perception in mobile robotics applications, Part 1: Principles of FMCW radar and of 2D image construction." Robotics and Autonomous Systems 81 (2016): 1-16.

[17] Paraschiv-Ionescu, Anisoara, et al. "Wavelet denoising for highly noisy source separation." 2002 IEEE International Symposium on Circuits and Systems. Proceedings (Cat. No. 02CH37353). Vol. 1. IEEE, 2002.

[18] Postolache, O., et al. "Multi-usage of microwave Doppler radar in pervasive healthcare systems for elderly." 2011 IEEE International Instrumentation and Measurement Technology Conference. IEEE, 2011.

[19] Stirman, Charles. Applications of Wavelets to Radar Data Processing. No. OA-11606. MARTIN MARIETTA ELECTRONICS AND MISSILES GROUP ORLANDO FL MISSILE SYSTEMS, 1991.

[20] Guo, Dai-fei, et al. "A study of wavelet thresholding denoising." WCC 2000-ICSP 2000. 2000 5th International Conference on Signal Processing Proceedings. 16th World Computer Congress 2000. Vol. 1. IEEE, 2000.

[21] Wang, Yuankai, Zelong Xiao, and Jianzhong Xu. "A novel threshold detection method for fmcw radar." (2015): 5-5.

[22] Lazaro, Antonio, David Girbau, and Ramon Villarino. "Analysis of vital signs monitoring using an IR-UWB radar." Progress In Electromagnetics Research 100 (2010): 265-284.

[23] Wang, Tien T. "The segmented chirp z-transform and its application in spectrum analysis." IEEE Transactions on instrumentation and measurement 39.2 (1990): 318-323.

[24] PengZhong. Design and Research of FMCW Radar Proximity Ranging System[D]. Wuhan University of Science and Technology, 2014.

[25] Xiangmei Gao.Key Technology of Software and Hardware of Intermediate Frequency Signal Processing in FMCW Radar Automobile Anti-collision System. Hefei Polytechnic University,2013

Appendix B – Technical Manual

ISCTE IUL
Instituto Universitário de Lisboa
Department of Information Science and Technology

Technical Manual

AGV-RAD: AGV Positioning System for Ports using Microwave Doppler Radar

Lin Ma

Supervisor:

Dr. Octavian Adrian Postolache, Associate Professor

ISCTE-IUL

Co-supervisor

Dr. Yongsheng Yang, Full Professor

Shanghai Maritime University

September 2019

Content

List of Figures

List of Tables

Technical Manual

This manual aims to describe feature of the system. Chapter I describes the hardware configuration and program of microwave Doppler radar sensor IVS-162. Chapter II explains the communication and the algorithm program of microwave radar system Nano SP25.

Chapter 1 – IVS-162

All technologies are based on the function of microwave Doppler radar sensor IVS-162, those are distance detection and speed detection.

2.1 Configuration

After connecting the PINs of the IVS-165 and the analog input interface of myRIO according to the regulations, as shown in Figure 1.1, it is necessary to set the corresponding sampling frequency for the radar signal.

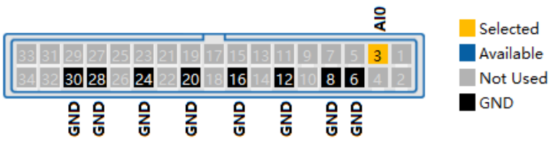

Figure 1.1- The Analog Input Interface of AI0

Use the Time Loop in myRIO Project, as shown in Figure 1.1, when the system needs multirate timing capabilities, precise timing, feedback on loop execution, timing characteristic that change dynamically, or several levels of execution priority. Therefore the Time Loop can use for set sampling frequency, and the Period is set as 20μs to satisfy 50kHz of sampling frequency.

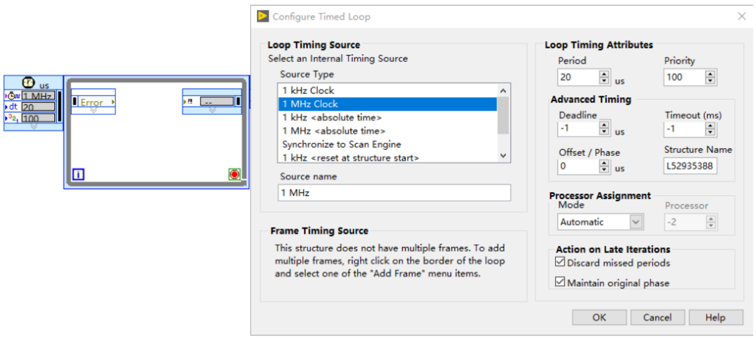

Figure 1.2- The Time Loop

2.2 Filtering

In general, microwave Doppler radar signals contain noise interference. Thus the filtering program is important, as shown in Figure 1.3. The Filtering can process low-frequency noise. And in Filtering Configuration, the Filtering Type is Highpass, the Cutoff Frequency is 100Hz, the Topology is Butterworth and its Order is 3.

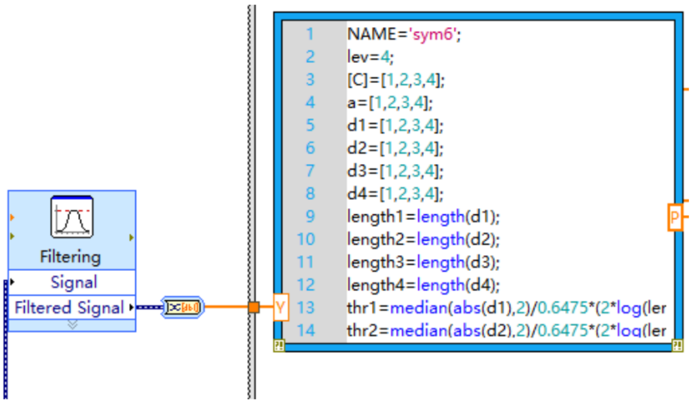

Figure 1.3- Noise Filtering

The characteristics of high-frequency noise have mutability and instability, the MATLAB Script is used in LabVIEW to achieve wavelet denoising with the adapted threshold function, and the complete program is,

```
NAME='sym6';
Lev=4;
[C,L]=wavedec (Y,Lev,NAME);
a=appcoef (C,L,NAME,lev);
d1=detcoef (C,L,4);
d2=detcoef (C,L,3);
d3=detcoef (C,L,2);
d4=detcoef (C,L,1);
length1=length (d1);
length2=length (d2);
length3=length (d3);
length4=length (d4);
thr1=median(abs(d1),2)/0.6475*(2*log(length1))^(1/2);
thr2=median(abs(d2),2)/0.6475*(2*log(length2))^(1/2);
```

```
thr3=median(abs(d3),2)/0.6475*(2*log(length3))^(1/2);
thr4=median(abs(d4),2)/0.6475*(2*log(length4))^(1/2);
for i1=1:1:length1
   if   abs(d1(i1))>=thr1
     d1(i1)=sign(d1(i1))*(abs(d1(i1))-thr1/exp((d1(i1)-thr1)^3));
     else   d1(i1)=0;
     end
end
for i2=1:1:length2
   if   abs(d2(i2))>=thr2
     d2(i2)=sign(d2(i2))*(abs(d2(i2))-thr2/exp((d2(i2)-thr2)^3));
     else   d2(i2)=0;
     end
end
for i3=1:1:length3
   if   abs(d3(i3))>=thr3
     d3(i3)=sign(d3(i3))*(abs(d3(i3))-thr3/exp((d3(i3)-thr3)^3));
     else   d3(i3)=0;
     end
end
for i4=1:1:length4
   if   abs(d4(i4))>=thr4
     d4(i4)=sign(d4(i4))*(abs(d4(i4))-thr4/exp((d4(i4)-thr4)^3));
     else   d4(i4)=0;
     end
end
h=[a d1 d2 d3 d4]
p=waverec (h,L,NAME);
```

The meanings of the functions called from the wavelet library of MATLAB are shown in Table 1.1.

Table 1.1- The Part of Wavelet Library

wavedec	1-D wavelet decomposition
appcoef	1-D approximation coefficients
detcoef	1-D detail coefficients
waverec	1-D wavelet reconstruction

Because the MATLAB Script needs one or more graphical Input and Output, therefore the Input is Y and the Output is p, their data type are both 1-D Arrange.

4

2.3 Frequency Estimate Algorithm

The program uses a sequential structure as a whole to meet different processing time needs. In the Figure 1.4 is the LabVIEW program about FFT and CZT joint algorithm, which can calculate the AGV distance. The signal source is ‘p’ that is the output of wavelet denoising.

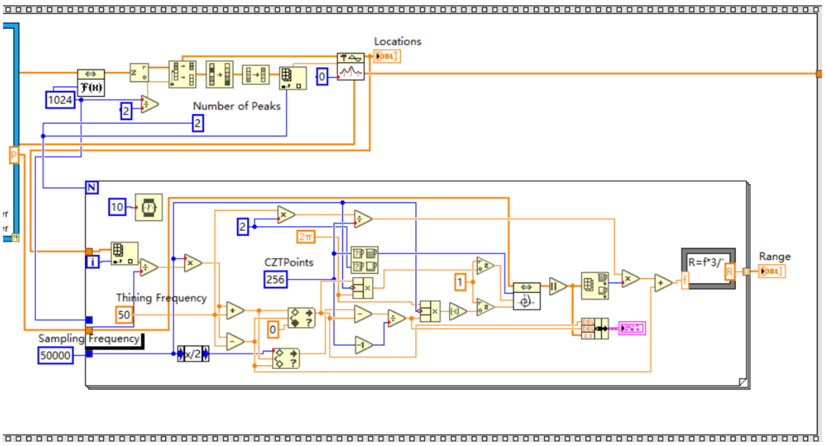

Figure 1.4- The LabVIEW Program of FFT and CZT Joint Algorithm

The design thought is, at first, the system detects the frequency peak location of FFT spectrum, then according to the above location, the frequency interval of radar signal can be found. At last, the CZT is used in this frequency interval.

In the Figure 1.5 is the LabVIEW program about 2D FFT, which can calculate the AGV speed.

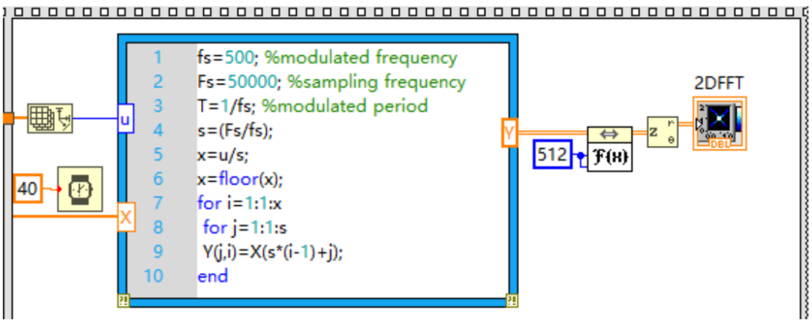

Figure 1.5- The LabVIEW Program of 2D FFT Algorithm

Since the algorithm can only process 2D signals, first convert the 1D signal into a 2D signal according to the sampling time. The MATLAB Script is used to convert because of its clear. The input u is the length of radar signal, X is the radar signal. And the output Y is 2D radar signal. The X-axis of 2D radar signal is fast time, the Y-axis is slow time.

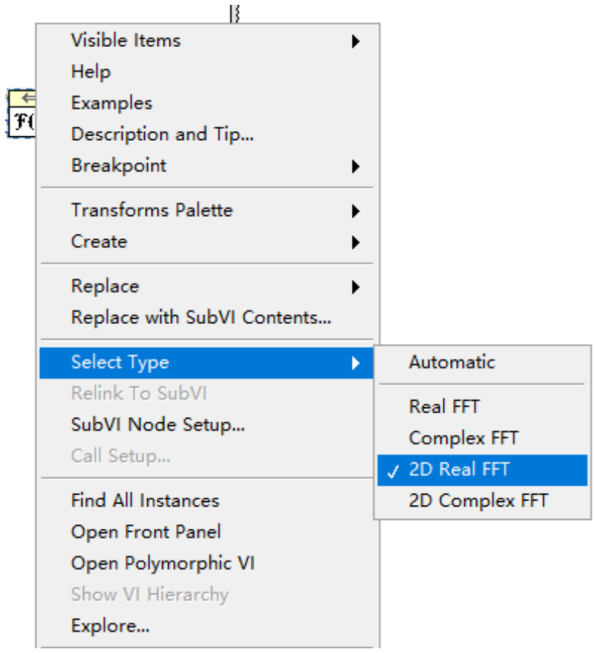

Figure 1.6- Select Type for FFT in LabVIEW

As shown in Figure 1.6, in LabVIEW, FFT Control can select different types according to different requirements of users.

Chapter 2 – SP25

2.1 Configuration

Since SP25 requires TTL to USB conversion, myRIO's TX and RX interfaces are used.

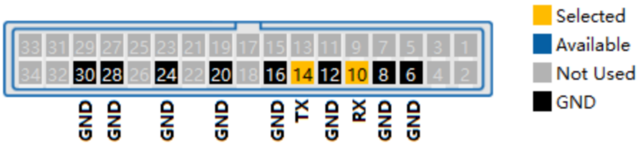

Figure 2.1- The TX and RX Interface

Table 2.1- The Configuration of myRIO

Node Name	UART
Channel	A/UART(ASRL1::INSTR)
Mode	Read (Read all available)
Communication	
Baud rate	115200
Data bite	8
Parity	None
Stop bits	1.0

2.2 Message Reading

The LabVIEW of message reading is shown in Figure 2.2.

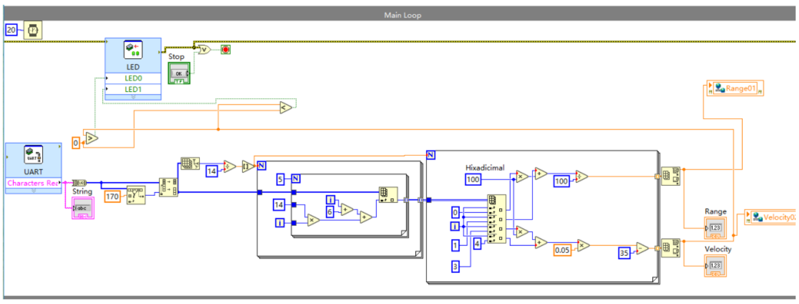

Figure 2.2- The Program of SP25 Message Reading

The idea of the design process is,

(1) Because the SP25 data update rate is 50Hz, in order to ensure that the message is not dropped when reading the message, set the 20ms Timer to the system.

(2) Convert the hexadecimal of the message to decimal by using ‘String To Byte Array’;

(3) Search for the decimal starting sequence ‘170’ of the message to ensure that the system can read the correct distance and speed sequence locations;

(4) Calculate the actual distance and speed values according to the equation,

$$Range=(RangeHValue*256+RangeLValue)*0.01 \tag{2-1}$$

$$Verlocity=(VerlHValue*256+VerlValue)*0.05-35 \tag{2-2}$$

(5) The actual distance and speed values are set as shared variables for another myRIO-1900 to read via Wi-Fi and process the data.

2.3 Data Fusion

According to the positioning algorithm, the positioning system needs two distance values and two speed values of AGV generated from two different myRIO-1900, therefore the system needs data fusion. The LabVIEW program for positioning algorithm is shown in Figure 2.3.

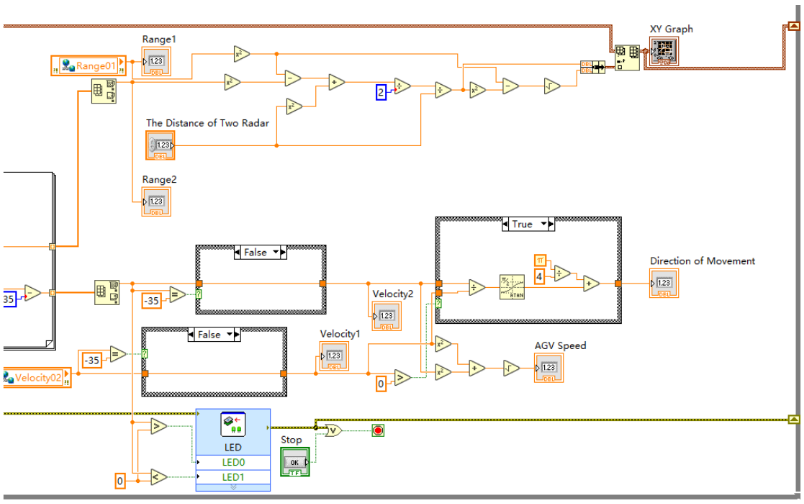

Figure 2.3- The LabVEW Program of System Data Fusion

It means, for the area to be tested, two radar systems should be fixed in tow corners of the area. The direction of the radar antenna is the same as the angle bisector definition, which can ensure cover all the detected area. According to the real-time ranges r_1, r_2 and velocity v_1, v_2, the positioning coordinate *[X, Y]* can be calculated from below equations,

$$X = \frac{r_1^2 - r_2^2 + R^2}{2R} \quad (2\text{-}3)$$

$$Y = \sqrt{r_1^2 - (\frac{r_1^2 - r_2^2 + R^2}{2R})^2} \quad (2\text{-}4)$$

Because the velocity detected by the radar is straight with respect to the direction of the antenna. The velocity of the target (AGV) is,

$$v_0 = \sqrt{v_1^2 + v_2^2} \quad (2\text{-}5)$$

In addition, the real target (AGV) velocity is related to the sign of velocity components v_1 and v_2. The direction of the target (AGV) movement can be described as follows:

If $v_1 > 0$, no matter the sign of v_2 is, the real velocity direction of the target (AGV) is,

$$\theta = \frac{\pi}{4} + arctan\frac{v_2}{v_1}, \theta \epsilon[-\pi, \pi] \quad (2\text{-}6)$$

If $v_1 < 0$, no matter the sign of v_2 is, the real velocity direction of the target (AGV) is,

$$\theta = -\frac{3\pi}{4} + arctan\frac{v_2}{v_1}, \theta \epsilon[-\pi, \pi] \quad (2\text{-}7)$$

2.4 Errors Handling

The goal of this section is to improve the noise in the path.

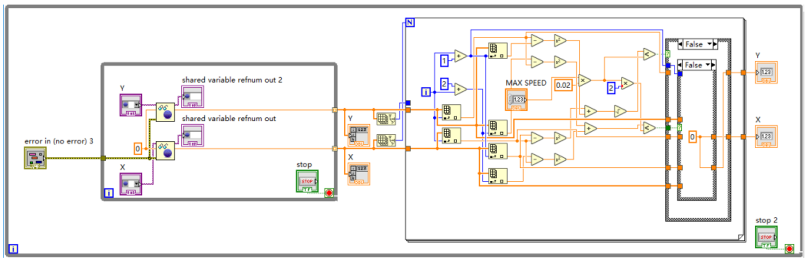

Figure 2.4- The LabVIEW Program of Error Handling

The meaning of this program is,

(1) Read the shared variables [X, Y] generated from positioning system;

(2) Detect the position $[X_0,Y_0]$ at time 0, the position $[X_1,Y_1]$ at time 1 and the position $[X_2,Y_2]$ at time 2, determine if the distance between them is within the specified threshold;

(3) If a point is outside the range of depreciation, it is removed from the generated path.